THE ROLE OF ATM IN THE REGULATION OF CARDIOMYOCYTE GLUCOSE UTILIZATION UNDER NORMAL AND INSULIN RESISTANT CONDITIONS

by

Mignon Albertha van Vuuren

Thesis presented in fulfilment of the requirements for the degree Master of Science in Medical Sciences in the Faculty of Medicine and Health Science at Stellenbosch University

Supervisor: Prof Barbara Huisamen

March 2016

DECLARATION

By submitting this thesis/dissertation electronically, I declare that the entirety of the work contained therein is my own, original work, that I am the sole author thereof (save to the extent explicitly otherwise stated), that reproduction and publication thereof by Stellenbosch University will not infringe any third party rights and that I have not previously in its entirety or in part submitted it for obtaining any qualification.

Date: .....March 2016.....

ABSTRACT

Introduction: Ataxia-telangiectasia (A-T) is an autosomal, recessive disorder that progressively affects multiple organs. A-T is caused by mutations in the Atm gene (ataxia-telangiectasia mutated gene), resulting in lack/inactivation of the ATM protein. These patients display a high incidence of insulin resistance or full-blown type 2 diabetes (T2D) and are therefore more prone to develop ischaemic heart disease. According to literature, ATM expression may be altered by obesity and therefore we investigated its expression and impact in the heart in the context of obesity-induced insulin resistance.

Aim: To determine the importance of ATM in glucose uptake in cardiomyocytes prepared from control vs. obesity-induced insulin resistant animals.

Objectives: (i) To determine ATM levels in rat models of obesity-induced insulin resistance and characterize a suitable model for the study. (ii) To manipulate the ATM protein in isolated cardiomyocytes from both control and insulin resistant animals using suitable activators or inhibitors of ATM followed by the measurement of 2-Deoxy-D-^{3}[H] glucose (2DG) uptake levels, expression and activation of intermediates of the insulin signalling pathway (IRS1, PI3K, PTEN, PKB, AS160, GSK-3β, AMPK) and GLUT4 expression.

Methods: Male Wistar rats were fed a high fat diet (HFD) for 16 weeks to induce obesity and insulin resistance and compared to chow-fed controls. Body weight, intra-peritoneal (IP) fat weight, fasting glucose and insulin levels were determined. Ventricular cardiomyocytes were prepared by collagenase perfusion digestion whereafter 2DG uptake was measured in response to treatment with specific activators/inhibitors of ATM. The specific ATM inhibitor, KU 60019, was used to manipulate the activity of the protein while the expression of proteins in the insulin signalling pathway was determined by Western blotting.

Results: (i) No differences in body weight were observed. (ii) HFD animals presented with higher IP fat weight (33.7±2.4 vs. 19.1±1.5 g; $p<0.001$), basal glucose (5.4±0.16 vs. 4.71±0.05 mmol/L; $p<0.001$) and insulin (14.6±2.0 vs. 6.7±2.2 mIU/ml; $p<0.05$) levels vs. controls. (iii) KU 60019 inhibited insulin-stimulated 2DG uptake in the control and HFD cardiomyocytes from 26.8±3.93 and 28.38±1.27 to 13.1±2.4 ($p<0.01$) and 18.6±2.8 ($p<0.05$) pmol/mg prot/30min respectively. (iv) HFD downregulated T-ATM expression by 50% (1±0.1 vs. 0.5±0.1 ADU; $p<0.001$); T-PI3K by 30% (1±0.02 vs. 0.7±0.2 ADU; $p<0.01$); T-PKB by 40% (1±0.03 vs. 0.6±0.08 ADU; $p<0.01$); T-GSK-3β by 10% (1±0.02 vs. 0.9±0.05 ADU; $p<0.01$); T-AMPK by 30% (1±0.03 vs. 0.7±0.09 ADU; $p<0.05$) and P-AS160 by 30% (1±0.08 vs. 0.7±0.2 ADU; $p<0.001$). (v) HFD increased the phosphorylation of IRS1 with 100% at Ser307 (1±0.3 vs. 2.2±0.1 ADU; $p<0.05$) vs. controls. (vi)

KU 60019 inhibited insulin-stimulated phosphorylation of ATM in the HFD animals ($p<0.05$). (vii) The inhibitory effect of KU 60019 on P-PI3K (p85) and P-PKB in both the control and HFD animals was significant ($p<0.05$ & $p=0.001$ respectively). (viii) In addition, by comparing results with younger animals, we observed age-related effects in insulin-sensitivity of cardiomyocytes.

Conclusion: HFD was coupled to the development of insulin resistance, as these animals presented with higher IP fat weight, basal glucose and insulin levels and also downregulation of multiple metabolic signalling proteins and insulin sensitivity in the heart. Older control animals were also more resistant to the action of insulin than young animals. KU 60019 inhibited insulin-stimulated 2DG uptake, placing ATM in the pathway whereby insulin stimulates glucose uptake in the heart. KU 60019 significantly attenuated baseline PI3K activity and insulin-stimulated activation of ATM and PKB but did not affect AMPK/GLUT4 levels. Thus downregulation of ATM expression in obesity may be central to the development of myocardial insulin resistance.

Keywords: Obesity, insulin resistance, ATM, KU 60019, cardiovascular

OPSOMMING

Inleiding: Ataxia-telangiectasia (A-T) is ‘n outosomale resessiewe siektetoestand wat verskeie organe progressief affekteer. Hierdie siektetoestand ontstaan weens mutasies in die Atm geen (ataxia-telangiectasia ge-muteerde geen), wat veroorsaak dat die ATM proteïen baie laag uitgedruk word of onaktief bly. A-T individue is meer vatbaar vir die ontwikkeling van insulien-weerstandigheid asook diabetes tipe 2 (T2D) wat gevolglik hulle risiko vir iskemiese hartsiektes verhoog. Volgens vorige studies kan vetsug tot verlaagde ATM uitdrukking bydra. Weens laasgenoemde, het ons die uitdrukking/aktivering van ATM in die konteks van ‘n vetsug-geïnduseerde insulien-weerstandige model in die hart ondersoek.

Doelstelling: Om die belang van ATM in glukose opname te bepaal in kontrole en vetsug-geïnduseerde insulin-weerstandige kardiomiosiete.

Objektiewes: (i) Om ATM vlakke te bepaal in vetsug-geïnduseerde insulien-weerstandige rotte en sodoende ‘n geskikte model vir die studie te kies. (ii) Om ATM in geïsoleerde ventrikulêre kardiomiosiete van beide kontrole en vet diere met geskikte aktiveerders/inhibitore van ATM te manipuleer, waarna 2-Deoksi-D-^{3}[H] glukose (2DG) opnames, die uitdrukking/aktivering van proteïene van die insulien-seintransduksie-pad (IRS1, PI3K, PTEN, PKB, AS160, GSK-3β, AMPK) en GLUT4 uitdrukking, bepaal sal word.

Metodes: Manlike Wistar rotte is gebruik. Die helfte van hierdie rotte is ‘n hoë vet dieet (HFD) vir 16 weke gevoer om vetsug/insulien-weerstandigheid te induseer, teenoor die kontrole diere wat slegs standaard rotkos ontvang het. Die liggaamsgewig, intra-peritoneale (IP) vet, vastende glukose- en insulien-vlakke is bepaal. Ventrikulêre kardiomiosiete van beide diergroepe is voorberei deur die harte met kollagenase te perfuseer waarna 2DG opname gemeet is t.o.v die behandeling met spesifieke aktiveerders/inhibitore van ATM. Die spesifieke ATM inhibitor, KU 60019 is gebruik om ATM aktiwiteit te inhibeer. Die uitdrukking/aktivering van insulien-seintransduksie proteïene is deur Westerse klad tegnieke bepaal.

Resultate: (i) Daar was geen verskille in die liggaamsgewig tussen die diergroepe nie. (ii) HFD diere het hoër IP vet-massa (33.7±2.4 vs. 19.1±1.5 g; $p<0.001$), basale glukose vlakke (5.4±0.16 vs. 4.71±0.05 mmol/L; $p<0.001$) en insulien-vlakke (14.6±2.0 vs. 6.7±2.2 mIU/ml; $p<0.05$) teenoor die kontrole diere gehad. (iii) KU 60019 het die insulien-gemedieerde 2DG opname respons in die kontrole en HFD diere onderskeidelik onderdruk vanaf 26.8±3.93 en 28.38±1.27 tot 13.1±2.4 ($p<0.01$) en 18.6±2.8 ($p<0.05$) pmol/mg prot/30min. (iv) HFD het T-ATM uitdrukking met 50% verlaag (1±0.1 vs. 0.5±0.1 ADU; $p<0.001$); T-PI3K met 30% (1±0.02 vs. 0.7±0.2 ADU; $p<0.01$), T-PKB met 40% (1±0.03 vs. 0.6±0.08 ADU; $p<0.01$), T-GSK-3β met 10% (1±0.02 vs.

0.9±0.05 ADU; p<0.01), T-AMPK met 30% (1±0.03 vs. 0.7±0.09 ADU; p<0.05 en P-AS160 met 30% (1±0.08 vs. 0.7±0.2; p<0.001) teenoor die kontroles. (v) HFD het IRS1 fosforilering(Ser307) met 100% verhoog (1±0.3 vs. 2.2±0.1 ADU; p<0.05) vs. die kontroles. (vi) KU 60019 het die insulien-gestimuleerde fosforilering van ATM in die HFD diere onderdruk (p<0.05). (vii) Die inhibitoriese effek van KU 60019 op P-PI3K en P-PKB in beide diergroepe was beduidend (p<0.05 & p=0.001 onderskeidelik). (viii) Deur resultate met jonger diere te vergelyk, is duidelike ouderdomsgeïnduseerde effekte op die insuliensensitiwiteit van kardiomiosiete waargeneem.

Gevolgtrekking: Die HFD het IP vet, basale glukose en insulien vlakke verhoog, asook verskeie metaboliese seintransduksie proteïne en insulien sensitiwiteit in die hart afgereguleer. KU 60019 het insulien-gestimuleerde 2DG opname geïnhibeer, wat bewys dat ATM deel vorm van die pad waardeur insulien glukose-opname in die hart stimuleer. KU 60019 het die aktivering van basale PI3K afgereguleer sowel as die insulien-gestimuleerde aktivering van ATM en PKB, met geen effek op AMPK en GLUT4 vlakke nie. Dus mag die afregulering van ATM uitdrukking in vetsugtigheid sentraal staan in die ontwikkeling van miokardiale insulienweerstandigheid.

Sleutelwoorde: Vetsug, insulien-weerstandigheid, ATM, KU 60019, kardiovaskulêr

ACKNOWLEDGEMENTS

- Firstly, I would like to acknowledge the Department of Medical Physiology for the privilege to partake in this research project, and my Professor, Barbara Huisamen, for her guidance, advice, continuous support and encouragement thorough out my research project.

- A special thanks to all my colleagues in the Department of Medical Physiology, especially for Yolandi Espach and Sybrand Smit for their wonderful friendship, patience and encouragement.

- Thank you to my parents (Alfonso and Brenda van Vuuren), my brother (Alfonso George van Vuuren) and the rest of my family and friends for their continuous support and love.

- A special thanks to the Harry Crossley Foundation, the National Research Foundation and the University of Stellenbosch for funding throughout my MSc studies.

- Lastly I would like to thank my Heavenly Father for giving me the ability to complete my master's degree.

DISCLOSURE OF INTEREST

Signed on the …….. day of ……. 2015 at…….

…… ……..……...

(Prof. B. Huisamen) (Mignon van Vuuren)

TABLE OF CONTENTS

LIST OF FIGURES

LIST OF TABLES

LIST OF ABBREVIATIONS

µl	Microliter
2DG	2-Deoxy-D-^{3}[H] glucose
2-ME	2-mercaptoethanol
4EBP1	Eukaryotic translation initiation factor 4E-binding protein 1
Abl	Abelson murine leukemia
AcCoA	Acetyl-coenzyme A
AGEs	Advanced glycation end products
AICAR	5-Aminoimidazole-4-carboxamide ribonucleotide
AMP	Adenosine monophosphate
AMPK	AMP-activated protein kinase
ANOVA	Analysis of Variance
ApoE	Apolipoprotein E
AS160	Akt substrate of 160 kDa
A-T	Ataxia telangiectasia
BcR	Breakpoint cluster region
BDM	2,3-butanedione monoxime
BMI	Body mass index
BSA	Bovine serum albumin
bTC-1	Betacellulin-1
bTC-7	Betacellulin-7

C3G	Guanine nucleotide exchange factor
CD36	Cluster of differentiation 36
CHD	Coronary heart disease
CHF	Chronic heart failure
Chk-1	Checkpoint kinases-1
Chk-2	Checkpoint kinases-2
Ci	Curies
CK2	Casein kinase II
COOH	Carboxyl
CPT1	Carnitine palmitoyl-transferase 1
Crk	Adapter molecule crk
Csk	C-Src kinase
CTGF	Connective tissue growth factor
CVD	Cardiovascular disease
dH_2O	Distilled water
DNA	Deoxyribonucleic acid
DNA-PKc	DNA-dependant protein kinase c
DPM	Disintegrations per minute
ECL	Enhanced chemiluminescence
eIF-4E	Eukaryotic translation initiation factor 4E
ELISA	Enzyme-linked immunosorbent assay

ERK	Extracellular signal-regulated kinase
FAT/CD36	Fatty acid translocase CD36
FFA	Free fatty acid
FOXO1	Forkhead box protein O1
Fru-2,6-P_2	Fuctose 2,6-bisphosphate
Fyn	Proto-oncogene tyrosine-protein kinase Fyn
g	Grams
G6Pase	Glucose 6-phosphatase
GIPC1	Gα-interacting protein C terminus 1
GLUT1	Glucose transporter 1
GLUT4	Glucose transporter 4
Grb2	Growth factor receptor-bound protein 2
GS	Glycogen synthase
GSK-3β	Glycogen synthase kinase-3β
H2AX	Histone 2A gene
HDL	High density lipoprotein
HFD	High fat diet
HGP	Hepatic glucose production
HRP	Horse Radish Peroxidase
IC50	Half maximal inhibitory concentration
ICAM-1	Intercellular adhesion molecule-1

IDE	Insulin degrading enzyme
IGF1R	Insulin-like growth factor 1 receptor
IGFBP	Serum IGF-binding protein
IGF-I	Insulin-like growth factor- I
IGT	Impaired glucose tolerance
IL-6	Interleukin-6
IP fat	Intra-peritoneal fat
IR	Insulin receptor
IRS	Insulin receptor substrate
IRS	IR substrates
JNK	c-Jun N-terminal kinase
kDa	Kilo Dalton
kg	Kilogram
Ki	Inhibitor constant
KO	Knockout
KRLB	Kinase regulatory loop binding
LCFA	Long-chain fatty acid
LDL	Low density lipoprotein
LDLR	Low density lipoprotein receptor
LKB1	Liver kinase B1
m	Meter

M	Molar
MAP	Mitogen-activated protein
MAPK	Mitogen-activated protein kinase
MCD	Malonyl-coenzyme A decarboxylase
McoA	Malonyl-coenzyme A
MEK	Mitogen-activated protein kinase kinase
mg	Milligram
MHC	Myosin heavy chain
min	Minutes
ml	Millilitre
MLCK	Myosin light chain kinase
mm	Millimetre
MMP-2	Matrix metalloproteinase- 2
mRNA	Messenger ribonucleic acid
mTOR	Mammalian target of rapamycin
NADPH	Nicotinamide adenine dinucleotide phosphate
Nck	Non-catalytic region of tyrosine kinase adaptor protein
nM	Nano Molar
Nm	Nanometres
NO	Nitric oxide
O_2	Oxygen

ºC	Degree Celsius
OGTT	Oral glucose tolerance test
OS	Osteogenic sarcoma
OS	Oxidative stress
OxLDL	Oxidized low density lipoproteins
PAI-1	Plasminogen activator inhibitor-1
PDH	Pyruvate dehydrogenase
PDK	Phosphoinositide-dependent kinase
PDK4	Pyruvate dehydrogenase kinase 4
PFK-1	Phosphofructo-1-kinase
PFK-2	6-phosphofructo-2-kinase
PH	Pleckstrin homology domain
PI3K	Phosphoinositide 3-kinase
PI4KA	Phosphatidylinositol-4-OH kinase
PIKKs	Phosphatidylinositol 3-kinase-related kinases
PIP2	Phosphoinositide 3,4-bisphosphate
PIP3	Phosphoinositide (3,4,5) trisphosphate
PKB	Protein kinase B
PKC	Protein kinase C
PLCγ	Phospholipase Cγ
pmol	picomol

PP1	Protein phosphatase 1
PP4-6	Protein phosphatase 4-6
PPAR-α	Peroxisome proliferator-activated receptor- alpha
PSCK9	Proprotein convertase subtilisin/kexin type 9
PTB	Phosphotyrosine-binding
PTEN	Phosphatase and tensin homolog
PTPase	Protein tyrosine phosphatase
PVDF	Polyvinylidene fluoride
QC	Quality control
RHEB	Ras homolog enriched in brain
RNS	Reactive nitrogen species
ROS	Reactive oxygen specie
rpm	Revolutions per minute
SDS-PAGE	Sodium dodecyl sulfate–polyacrylamide gel electrophoresis
sec	Seconds
SEM	Standard Error of the Mean
SH2	Src homology 2
SHC	SHC-transforming protein 1
SHIP	SH2 domain-containing inositol 5'-phosphatase
SOS	Son of sevenless homolog 1
SREBP-1c	Sterol regulatory element binding protein-1c

T2D	Type 2 Diabetes mellitus
TBC4	Domain family member 4
TBS	Tris-buffered saline
TLR4	Toll-like receptor 4
TMB	3,3',5,5'-Tetramethylbenzidine
TNF-α	Tumor Necrosis Factor- alpha
TSC1	Tuberous sclerosis 1
VAMP2	Vesicle-associated membrane protein 2
VCAM-1	Vascular cell adhesion molecule-1
WHO	World health organization
WM	Wortmannin
WT	Wild type
YXXM	Tyrosine-XX-Methionine
ZMP	AICAR monophosphate
β-AR	β-adrenergic receptor

CHAPTER 1: LITERATURE REVIEW

1. Insulin resistant conditions

Insulin resistance is a pathological condition in which muscle, liver and fat cells fail to properly respond to the hormone insulin. According to previous studies, obesity, especially the excess fat around the waist, is the primary cause of insulin resistance, imbalanced cholesterol, cardiovascular diseases (CVDs) and high blood pressure, due to several hormones and substances produced in the belly fat (National Institute of Diabetes and Digestive and Kidney Diseases - http://www.niddk.nih.gov).

1.1. Definition and overview of obesity and its role in insulin resistance

Obesity is defined as the accumulation of abnormal and excessive fat, mainly caused by the imbalance between energy intake and energy expenditure. The adipose tissue will consequently increase in the number of cells (hyperplasia) and the size of the cells (hypertrophy) to store the excess energy in the form of fat (Goedecke et al, 2006).

According to the World Health Organization (WHO), a Body Mass Index (BMI) greater than or equal to 25 is considered as overweight whereas a BMI greater than or equal to 30 is considered as obese. The BMI, measured in kilograms (kg)/meter $(m)^2$, is defined as a person's weight in kg divided by the square of his height in m (www.who.int/en/). The BMI is useful as it can be used for both males and females; however it is not accurate when used on its own.

According to 2015 updated WHO findings, the prevalence of obesity has more than doubled between 1980 and 2014. Data indicated that more than 1.9 billion adults, 18 years and older, were overweight in 2014. 600 million of these adults were classified as obese. In total, 13% of the world's whole population was obese (15% women and 11% men), and this is still markedly increasing to such an extent as to be classified as a global epidemic.

In countries undergoing epidemiological transition, including South Africa (Goedecke et al, 2006), obesity mainly develops because of high carbohydrate consumption, as it is the main source of food due to low income levels in these areas.

In 2014, four out of 10 men (40%) and seven out of 10 women (70%) in South Africa were overweight or obese, thus causing South Africa to have the highest obesity rate in the sub-Saharan Africa (Baleta & Mitchell, 2014). Of the 70% of women, 28% were overweight, whereas 42% were already suffering from obesity (Baleta & Mitchell, 2014).

The association between insulin resistance, visceral fat and the metabolic syndrome is due to the enhanced lipolytic activity of visceral fat cells which causes increased free fatty acid (FFA) release into the portal (hepatic insulin resistance) and systemic (muscle insulin resistance) circulation (Defronzo, 2004). Insulin resistance results in increased blood glucose levels compensated for by insulin secretion from pancreatic β-cells. Increased demand on the pancreas coupled to high FFA levels is causative in β-cell failure and a subsequent inability to maintain euglycaemia, resulting in type 2 diabetes mellitus (T2D). Furthermore, the increased FFAs also lowers high density lipoprotein (HDL) levels and increases blood pressure and triglyceride levels respectively. Together, all of these changes result in the development of cardiovascular diseases including atherosclerosis, ischemic heart disease and stroke (National Institute of Diabetes and Digestive and Kidney Diseases - http://www.niddk.nih.gov).

2. Physiological mechanisms of insulin action

2.1. Overview of insulin action

The insulin signal transduction pathway plays an important role in regulating blood glucose levels. This biochemical pathway can be affected by fed versus fasting states, certain hormones (Diabetes Education online, 2007-2016 - www.http://dtc.ucsf.edu) as well as stress levels (Livestrong, 2015 - www.livestrong.com). Carbohydrate consumption causes a subsequent rise in the blood glucose concentration. The β-cells, located in the pancreas, sense this increase and are consequently stimulated to secrete the hormone, insulin (Wilcox, 2005).

The tyrosine kinase insulin receptor (IR) *(Figure 1.1)*, located on the cell surface of the plasma membrane of insulin sensitive peripheral cells, consists of two extracellular α-subunits (~135 kilo Dalton (kDa)) and two transmembrane β-subunits (~95 kDa) (Yanagita et al, 2013). Once the secreted insulin molecule binds to the α-subunit, it results in the autophosphorylation of the β-subunit tyrosine residues. Consequently proteins containing phosphotyrosine-binding (PTB) as well as Src homology 2 (SH2) domains will be recruited

as these proteins have the ability to identify the phosphorylated tyrosine receptor residues (Yanagita et al, 2013).

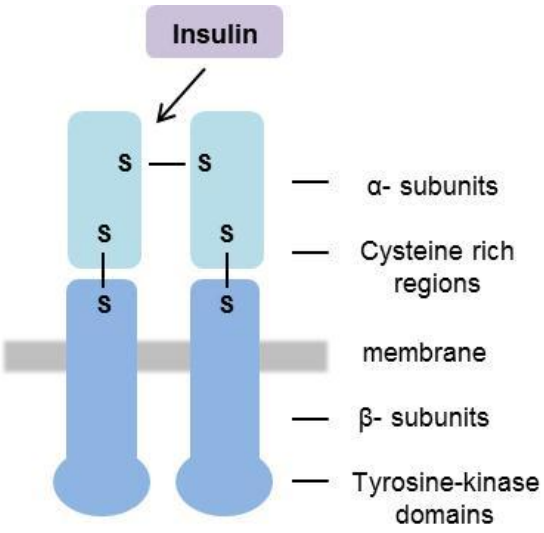

Figure 1.1: *The insulin receptor*

According to previous research, the IR substrates (IRS)-1/2 as well as SHC are the two scaffold proteins which are most likely to be recruited to the IR. Once these scaffold proteins are recruited, they link the activated IR to two parallel downstream signal transduction pathways including the: phosphoinositide 3-kinase (PI3K)/ phosphoinositide-dependent kinase 1 (PDK-1)/ Protein kinase B (PKB) pathway as well as the Ras/ Extracellular signal-regulated kinase (ERK) pathway (van der Heide et al, 2006; Wada et al, 2005).

To date, there are four IRS molecules identified: IRS1, IRS2, IRS3 and IRS4. All of these molecules can act as a docking protein between the IR and several intracellular signalling molecules containing a SH2 domain. These molecules are especially important in regulating not only insulin signalling, but also several basic cellular functions such as metabolism, growth and survival (Sesti et al, 2001). In the next section, the link between the four different IRS molecules and insulin signalling respectively will be discussed.

(i) IRS1

The IRS1 molecule contains 21 assumed tyrosine phosphorylation sites. Several of these sites are believed to be located in amino acid sequence motifs, which give IRS1 the ability to bind to SH2 domain proteins, including the p85 regulatory subunit of PI3K, Growth factor receptor-bound protein 2 (Grb2), Adapter molecule crk (Crk), C-Src kinase (Csk), Proto-

oncogene tyrosine-protein kinase Fyn (Fyn), protein tyrosine phosphatase (PTPase) SHP-2, non-catalytic region of tyrosine kinase adaptor protein 1 (Nck) and phospholipase Cγ (PLC) (White, 1997). Furthermore, IRS1 also contains 30 serine/threonine phosphorylation sites in motifs. These motifs are recognized by several kinases including protein kinase C (PKC), PKB, casein kinase II (CK2) and mitogen-activated protein (MAP) kinases (White, 1997; Sun et al, 1991).

In response to insulin binding, IRS1 is believed to be the main docking protein responsible for the activation of PI3K (Rondinone et al, 1997).

Several studies performed on different tissues in human and mouse respectively indicated that IRS1 plays an important role in mediating both mitogenic as well as metabolic effects of insulin in the peripheral tissues (muscle, adipose) (Sesti et al, 2001). It was also discovered that IRS1 plays a key role in regulating insulin secretion in pancreatic β-cells in mice. Once IRS1 was supressed, the islets were incapable to secrete sufficient amounts of insulin in response to increased glucose levels (Kulkarni et al, 1999).

(ii) IRS2

The IRS2 protein is functionally and structurally similar to the IRS1 protein, however the IRS2 protein is believed to be 100 residues longer than IRS1 (Sun et al, 1995).

As IRS1, the IRS2 protein also contains tyrosine phosphorylation sites (22 potential sites). When the amino acid sequences of IRS1 and IRS2 were compared, 43% of the sequences were similar, whereas the Pleckstrin homology domain (PH) (65%) and PTB (75%) domains exhibited a higher degree of similarity respectively (Sesti et al, 2001).

Interestingly, IRS2 contains a unique middle region in its structure, which gives it the ability to bind specifically with the kinase regulatory loop binding (KRLB) domain of the IR β-subunit (Sawka-Verhelle et al, 1996). This unique middle amino acid region is absent in IRS1, which makes IRS2 signalling specific.

The distribution of IRS1 and IRS2 in the fat cell was found to differ causing each one of these proteins to have different activation and deactivation kinetics. The IRS1 protein was twofold more concentrated in the intracellular membrane compartment when compared to the cytosol of 3T3-L adipocytes, whereas IRS2 was twofold more concentrated in the cytosol than in the intracellular membrane compartment (Inoue et al, 1998).

According to previous studies, the IRS2 protein, in comparison to IRS1, becomes dephosphorylated very speedily and also activates PI3K more rapidly. These differences in the activation kinetics play an important role in especially the insulin signalling pathway (Ogihara et al, 1997; Inoue et al, 1998).

Furthermore, the differences in distribution also affect the interaction of these proteins respectively with downstream effectors containing the SH2 domain (Shuppin et al, 1998; Sun et al, 1997; Giovannone et al, 2000). Both IRS1 and IRS2 binds to: PI3K, Crk, phospholipase Cγ, Fyn and Grb2, however only IRS1 binds to SHP-2 (White, 1997; Sun et al, 1997).

(iii) IRS3

IRS3, originally associated with only the adipose tissue is interestingly also expressed in the heart, kidney, liver, ovaries, fibroblasts, lung, betacellulin-1 (bTC-1) and betacellulin-7 (bTC-7) insulinoma cells (Giovannone et al, 2000; Sciacchitano & Taylor, 1997).

IRS3 is primarily located in the plasma membrane where it senses insulin (Anai et al, 1998), however in humans no IRS3 proteins are expressed (Sesti et al, 2001).

The IRS3 protein (in rat adipocytes), is 700-800 amino acid residues shorter than IRS1 and IRS2, however its PH domain, PTB domain and carboxyl (COOH)-terminal domain is similar to IRS1 (Sesti et al, 2001).

When the PH domain of IRS3 in rats was compared to IRS1 and IRS2, a similarity in the sequence identity of 50% (IRS1) and 45% (IRS2) respectively was observed. Furthermore, the PTB domain of IRS3 in rats displayed a similarity sequence identity of 48% (IRS1) and 53% (IRS2) (Lavan et al, 1997). The COOH-terminal domain of IRS3 contains less (13) tyrosine phosphorylation sites when compared to IRS1 (30) and IRS2 (22).

Furthermore, as IRS1 and IRS2, IRS3 also has the ability to potently bind to PI3K, SHC-transforming protein 1 (Shc), SHP-2 and Nck, but slightly less potent to PLC and Grb2 (Xu et al, 1999). When IRS3 was overexpressed in rat adipocytes, a robust increase in Glucose transporter 4 (GLUT4) vesicle translocation was observed, with or without insulin stimulation (Zhou et al, 1999).

Interestingly, when rat adipocytes were exposed to insulin, the p85 regulatory subunit of PI3K associated more rapidly with IRS3 than IRS1 and IRS2 (Smith-Hall et al, 1997).

(iv) IRS4

IRS4, the last IRS protein, was originally only observed at very low levels in human embryonic kidney 293 cells (Giovannone et al, 2000; Fantin et al, 1999; Uchida et al, 2000). Interestingly IRS4 was recently also observed in several human tissues and cell lines including the ovary, pituitary thyroid, fibroblasts, IM-9 lymphoblastoid cells, prostate, A-431 epidermoid carcinoma cells, U-2 osteogenic sarcoma (OS), Hep-2 larynx carcinoma cells, and several murine tissues including the brain, heart, skeletal muscle, bTC-1 and bTC-7 insulinoma cell lines, kidney, hypothalamus, liver, but not in the lung or spleen (Giovannone et al, 2000; Fantin et al, 1999; Uchida et al, 2000). At subcellular level, IRS4 is believed to be the most abundant in the plasma membrane (Tsuruzoe et al, 2001).

As the other IRS members, IRS4 also consists of a PH domain, a PTB domain and a COOH-terminal domain (Lavan et al, 1997). When the sequence identity of IRS4 was compared to IRS1 and IRS2, a similarity of only 27% and 29% respectively was observed (Sesti et al, 2001). The IRS4 protein however shares a high degree of ancestry (homology) with the IRS1, IRS2 and IRS3 protein domains.

Similar to the other IRS proteins, IRS4 also contains potential tyrosine phosphorylation sites (12), where 7 of these sites are associated with the YXXM (Tyrosine- XX- Methionine where X is any amino acid) motif and therefore has the ability to bind to the SH2 domain of the p85 regulatory subunit of PI3K. Furthermore, IRS4 also consists of two more potential tyrosine phosphorylation sites that lie in motifs that are known to bind to the SH2 domain of Grb2 and the NH2-terminal domain of either PLC or SHP-2 (Sesti et al, 2001).

Up to date, a definite role for IRS4 has not yet been established, but several possible functions include: regulation of pathways involved in cell differentiation, increasing GLUT4 vesicle translocation in the adipose tissue (Zhou et al, 1999) and increasing cell proliferation by stimulating the capability of insulin-like growth factor-1 (IGF-I) and insulin in fibroblasts and hematopoietic cells (Fantin et al, 1999; Qu et al, 1999). In previous studies, the overexpression of IRS4 resulted in the downregulation of IRS1 and IRS2 phosphorylation indicating that IRS4 probably acts as a negative regulator of IGF-1 signalling (Uchida et al, 2000). More recent studies indicated that IRS3 and IRS4 might act as IRS1 and IRS2 suppressors at numerous steps (Tsuruzoe et al, 2001).

When IRS3 and IRS4 were simultaneously overexpressed, a reduction in IRS2 messenger ribonucleic acid (mRNA) and in the association of IRS1 and IRS2 with PI3K was observed

(Tsuruzoe et al, 2001). The overexpression of only IRS3 resulted in downregulated IGF-I-stimulated tyrosine phosphorylation of IRS1 (Tsuruzoe et al, 2001).

From the above it is evident that the IRS proteins affect one another, and work together in combination to control several mechanisms in response to insulin.

In the next section, the two best-studied insulin responsive pathways, including the PI3K-dependent and the PI3K-independent pathway respectively, are described.

2.2. Insulin stimulation and signalling in the peripheral tissue

2.2.1. PI3K-dependent pathway

PI3K is a heterodimer tyrosine regulated kinase composed of a 110 kDa catalytic subunit (p110) and an 85 kDa regulatory/adapter subunit (p85). The p85 regulatory subunit consists of two SH2 domains (separated by an inter-SH2 domain), a SH3 domain and a proline rich breakpoint cluster region (BcR) homology domain (Dhand et al, 1994; Holt et al, 1994; Klippel et al, 1994).

The p110 catalytic subunit has a catalytic domain, a p85-interacting region (binds at the SH2 domains of p85), a homologous phosphatidylinositol-4-OH kinase (PI4K) region and a Ras-binding domain (Zvelebil et al, 1996; Dhand et al, 1994).

The association of the SH2 domains of the p85 subunit with the pTyr of IRS1 allows the association of the p110 subunit with the p85 subunit to form the enzyme PI3K.

The activation of PI3K is crucial for insulin-stimulated glucose uptake *(Figure 1.2)*. PI3K is a lipid kinase containing phospholipids that forms part of the plasma membrane. This enzyme transfers phosphate molecules to the 3 position hydroxyl group of the phosphoinositol ring lipids, consequently resulting in phosphoinositide 3,4-bisphosphate (PtIns(3,4)P2 and phosphoinositide (3,4,5) trisphosphate (PtIns(3,4,5)P3 formation. These 3-phosphorylated lipids create docking sites in the membrane that acts as rafts where proteins containing PH domains, such as PDK1, PKB and mammalian target of rapamycin (mTOR) c2 can associate/activate (Scheid & Woodgett, 2003). PKB is phosphorylated on its Thr308 residue by PDK1 and on its Ser473 residue by mTORc2 amongst others. Ser473 phosphorylation is usually seen as the final event to activate PKB.

Once PKB is active, the **PH domain** results in the activation of two different pathways: (i) Rab pathway and (ii) glycogen synthase kinase 3β (GSK-3β) pathway. In the first pathway (i) PKB phosphorylates the domain family member 4 (TBC4), also known as Akt substrate of 160 kDa (AS160), which results in the inhibition of the AS160 associated GTPase-activating domain. Thus AS160 becomes less active and relieves its inhibitory effect on Rab. The Rab protein is converted from its GDP bound form to a GTP bound state. In addition, activated Rab stimulates GLUT4 vesicle translocation to the membrane for glucose uptake (Bevan, 2009; Cell Signaling (2013) - www.cellsignal.com).

Furthermore, PKB can (ii) directly phosphorylate GSK-3β, resulting in inactive GSK-3β which no longer inhibits glycogen synthase (GS). Consequently, glycogen synthesis is induced to convert glucose to glycogen molecules (Bevan, 2009).

The **catalytic domain** of PKB also results in the activation of two different pathways including: (i) Forkhead box protein O1 (FOXO) pathway and (ii) mTOR pathway (Cell Signalling (2013) - www.cellsignal.com).

(i) FOXO1 is localized in the nucleus where it plays an important role in glucose 6-phosphatase (G6Pase) transcription. When PKB in the liver is activated in response to insulin stimulation, it translocates to the nucleus and phosphorylates FOXO1 at Ser256, Ser319 and Thr24 thereby initiating this protein to move out of the nucleus for degradation purposes. In response to this degradation, G6Pase transcription will be downregulated resulting in reduced glucose production in the liver (Nakae et al, 2001).

(ii) PKB furthermore phosphorylates tuberous sclerosis 1 (TSC1) causing the Ras homolog enriched in brain (RHEB) protein to change from its inactive to active form. Consequently, mTOR will be activated to induce protein synthesis via the eukaryotic translation initiation factor 4E-binding protein 1 (4EBP1) and $p70^{s6k}$ (Bevan, 2009).

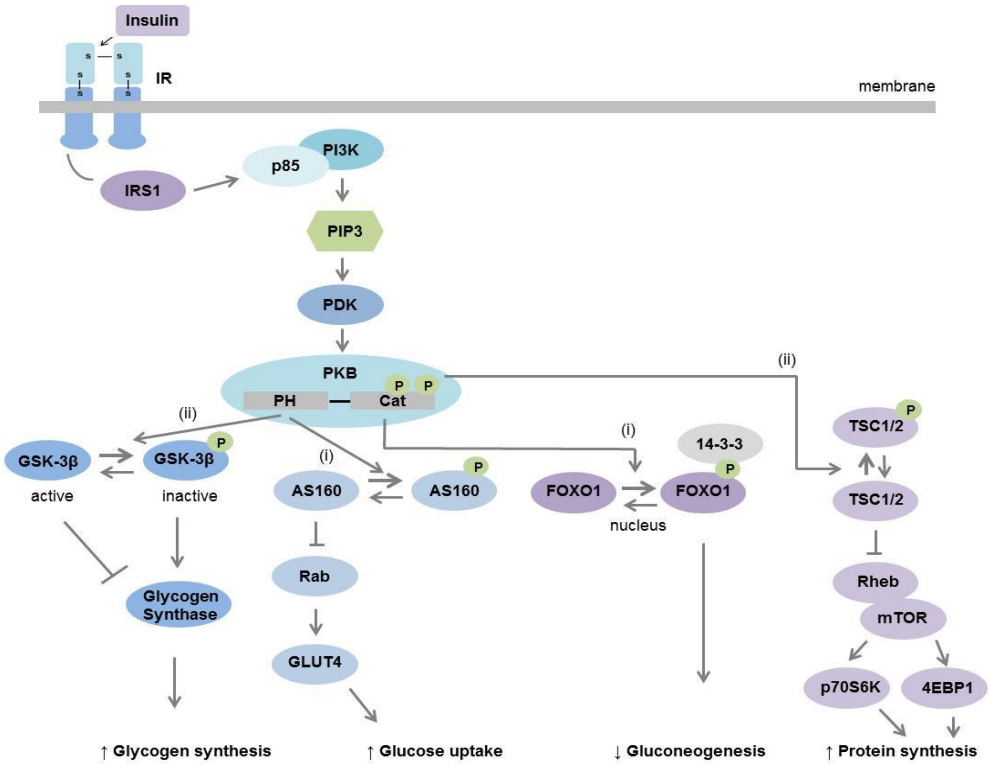

Figure 1.2: *The PI3K-dependent pathway*

2.2.2. PI3K-independent pathway

PI3K-independent signalling *(Figure 1.3)* includes the activation of two different pathways in response to insulin (Bevan, 2009).

In the first pathway (i) GLUT4 vesicle translocation is induced without the activation of PI3K. This pathway basically entails the activation of the IR in response to insulin secreted from the pancreas. Once the tyrosine residues of the IR are phosphorylated, the Cbl-CAP complex is phosphorylated and in response translocated to lipid rafts in the plasma membrane (Bevan, 2009). Following this, Cbl activates the Crk protein which is associated with Guanine nucleotide exchange factor (C3G).

Active C3G phosphorylates the GDP bound protein, TC10. Consequently GDP will be dissociated, and TC10 will bind to GTP. The active TC10 protein promotes GLUT4 vesicle translocation to the plasma membrane; however the mechanism of action is still unclear (Chiang et al, 2001).

The second pathway will only be briefly described as it is beyond the scope of this thesis.

In this pathway (ii), the SH2 domain of IRS1 binds to Grb2. The phosphorylated Grb2 protein consequently has the ability to bind to the Son of sevenless homolog 1 (SOS) protein. Once the SOS protein is activated, the GDP bound Ras is converted to a GTP bound Ras, resulting in the initiation of a phosphorylation cascade including Raf, Mitogen-activated protein kinase kinase (MEK) and ERK. Stimulated ERK results in gene transcription and regulation of various signalling pathways (Bevan, 2009).

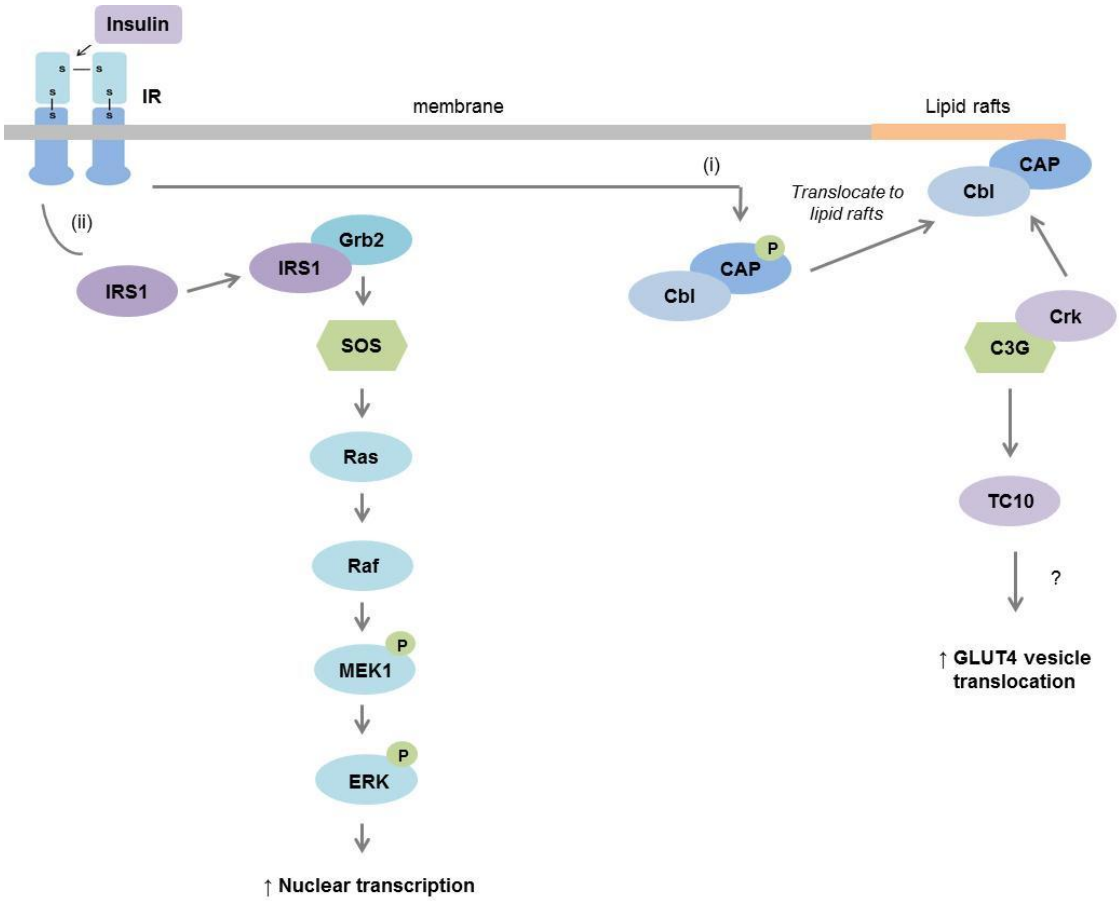

Figure 1.3: *The PI3K-independent pathway*

It is however important to note that the effects of insulin vary depending on the tissue involved. The different tissues described in section 2.3 include: adipose, skeletal muscle, heart and the liver.

2.3. Tissue specific insulin signalling in the context of glucose uptake in: (i) adipose tissue, (ii) skeletal muscle, (iii) heart and (iv) the liver:

2.3.1. Insulin signalling in the adipose tissue

Once insulin is secreted from the β-cells in the pancreas, it activates the relevant signalling pathways in adipocytes via the IR as described in Chapter 1, Section 2.2.1 and increase GLUT4 vesicle translocation for glucose uptake. Consequently the sterol regulatory element binding protein-1c (SREBP-1c) is also activated and lipogenesis is induced to store energy in the form of fat (Rask-Madsen & Kahn, 2012).

2.3.2. Insulin signalling in the skeletal muscle

Secreted insulin binds to the IR on the cell surface of the myocyte. The signal is transmitted intracellularly to IRS1 as described in Chapter 1, Section 2.2. Once phosphorylated, PI3K and PKB respectively undergo phosphorylation. PKB induces the translocation of GLUT4 vesicles to the plasma membrane, consequently increasing glucose uptake in the cell (Rask-Madsen & Kahn, 2012). PKB also initiates glycogen synthesis via the activation of GS (Pessin & Saltiel, 2000) and protein synthesis via the activation of mTOR/ 4EBP1/ $p70^{s6k}$ (Rask-Madsen & Kahn, 2012).

2.3.3. Insulin signalling in the heart

As described in Chapter 1, Section 2.2, insulin once again enters the heart tissue via the IR. Consequently, the PI3K-dependent pathway is activated resulting in GLUT4 vesicle translocation for glucose uptake. Furthermore, insulin also activates cardiac 6-phosphofructo-2-kinase (PFK-2) via the PI3K/PDK-dependent pathway (Mouton et al, 2007; Lefebvre et al, 1996; Bertrand et al, 1999; Pozuelo et al, 2003; Deprez et al, 2000).

This PFK-2 enzyme specifically synthesizes fructose 2,6-bisphosphate (Fru-2,6-P_2) (Rider & Hue, 1984), which, in addition, activates the main glycolytic regulator enzyme, phosphofructo-1-kinase (PFK-1). As an end result, glucose will be degraded into pyruvate. The direct activation of PFK-2 is however not yet identified (Mouton et al, 2007; Bertrand et al, 1999).

As glucose enters the heart tissue, insulin simultaneously also stimulates the translocation of fatty acid translocase (FAT/CD36) transporters to the plasma membrane via the PI3K pathway (Luiken et al, 2002). Subsequently long-chain fatty acid (LCFA)

uptake (Glatz et al, 2006; Coort et al, 2007) is initiated resulting in intracellular lipid storage (Dyck et al, 2001).

2.3.4. Insulin signalling in the liver

Once insulin enters the hepatocyte via the IR, it activates three different pathways. In the first pathway (i), PKB and FOXO are respectively phosphorylated and the glucose output by the liver is consequently decreased via the downregulation of G6Pase transcription. In the second pathway (ii), myosin heavy chain (MHC) and proprotein convertase subtilisin/kexin type 9 (PSCK9) are phosphorylated, resulting in increased protein synthesis. In the third pathway (iii), SREBP-1c results in the initiation of lipogenesis (Rask-Madsen & Kahn, 2012).

2.4. Termination of the insulin pathway

Insulin signalling is attenuated via the phosphatase SH2 domain-containing inositol 5'-phosphatase (SHIP) and a tensin homolog phosphatase (PTEN). Both these phosphatases dephosphorylate and consequently degrade PIP3 to PIP2 (Lazar & Saltiel, 2006). The PTPase SHP2 can also directly dephosphorylate IRS1 to prevent the activation of PI3K. Lastly, insulin signalling is further attenuated when insulin is degraded by the insulin degrading enzyme (IDE) and when the insulin-IR complex is internalized into endosomes (Bevan, 2009). During endocytosis, insulin molecules will be degraded whereas the IR's are recycled to the plasma membrane.

2.5. Activators and inhibitors of the PI3K-dependent pathway *(used in the current study)*

2.5.1. Insulin

The activation of the PI3K-dependent pathway in response to insulin is described in Chapter 1, Section 2.2.1.

2.5.2. Wortmannin (WM)

WM is a specific, covalent PI3K inhibitor. The structure consists of a highly reactive 20 carbon ring which is responsible for the inhibition of the PI3K. Due to WM's low half maximal inhibitory concentration (IC50) value (5nM) in vitro, it is considered as the most potent PI3K inhibitor. When used at low concentrations, WM is believed to have equal

inhibitory potency for PI3Ks class I, II and III. When used at a higher concentration, WM also has the ability to inhibit other PI3K related enzymes including: the Ataxia telangiectasia Mutated (ATM)- related deoxyribonucleic acid (DNA)-dependent protein kinase (DNA-PKc), mTOR, Mitogen-activated protein kinase (MAPK), myosin light chain kinase (MLCK) as well as some of the PI4KAs (Ferby et al, 1996; Vanhaesebroeck et al, 2001; Wymann et al, 1996). According to Sarkaria et al (1998), WM can also inhibit ATM with an IC50 of 150 nM.

3. The link between obesity and insulin resistance

More individuals are globally diagnosed with T2D as a consequence of obesity and insulin resistance. Insulin sensitivity can however be influenced by the fat distribution in the body. According to research, individuals with high levels of visceral fat (upper body fat) are more susceptible to develop insulin resistance than individuals with lower body fat (Defronzo, 2004). This association between increased visceral fat and insulin resistance development can be attributed to the enhanced lipolytic activity observed in visceral fat cells, which initiates the release of FFA into circulation (systemic and portal) (Defronzo, 2004).

3.1. Inflammatory response in adipocytes

Obesity is associated with adipocytes which increase in size (hypertrophy) and number (hyperplasia) to store excess nutrients in the form of fat.

According to Virtue (2010), hypertrophied adipocytes induce the activation of several chemokines. The chemokines recruit macrophages which, in response, secrete pro-inflammatory cytokines e.g. tumor necrosis factor- alpha (TNF-α) and Interleukin-6 (IL6). Once inflammation is induced, it results in the development of insulin resistance in the mature adipocytes (Virtue, 2010). Insulin resistant adipocytes release more FFAs which initiates further recruitment and activation of macrophages. Activated macrophages inhibit pre-adipocyte formation, consequently causing the mature adipocytes to become more insulin resistant, inducing more FFA release and additional macrophage activation (Virtue, 2010).

3.2. FFA release

Obesity is in addition, associated with enhanced lipolytic activity in the visceral fat cells which causes a subsequent rise in the amount of FFA released into the portal and systemic

circulation (Defronzo, 2004). This acute rise in the amount of circulating FFA in pre-diabetic individuals stimulates insulin secretion. However in these individuals, the amount of insulin secreted is not sufficient to compensate for the FFA-induced insulin resistance (Boden, 2008). Consequently, hepatic- and muscle insulin resistance can develop in turn (Defronzo, 2004).

3.3. Oxidative stress

Oxidative stress (OS) refers to the imbalance between the production of reactive oxygen species (ROS) and antioxidant defences to detoxify/neutralize these species (Rains & Jain, 2011). According to Rain & Jain (2011) oxidative stress is a contributor to the (i) onset of diabetes, (ii) progression of diabetes and (iii) complications associated with diabetes, including insulin resistance and β-cell dysfunction.

As mentioned in Chapter 1, Section 3.1, obesity is associated with increased proinflammatory cytokine production, including TNF-α and IL-6 (Fernandez et al, 2011). Both these cytokines stimulate ROS and reactive nitrogen species (RNS) production via monocytes and macrophages. Furthermore, TNF-α also inhibits the activity of polymerase chain reaction (PCR), consequently increasing the interaction of electrons with oxygen, resulting in superoxide anions formation (Fonseca-Alaniz et al, 2007). In addition, the adipose tissue also secretes angiotensin II, which results in the stimulation of Nicotinamide adenine dinucleotide phosphate (NADPH) oxidase activity. NADPH oxidase is a major contributor for ROS production in adipocytes (Morrow, 2003).

4. Link between insulin resistance and T2D

T2D is a metabolic disorder that is associated with high circulating blood glucose levels (hyperglycemia), resulting in insulin resistance in the liver and muscle tissue respectively. Insulin resistance in the liver is characterized by faulty suppression of hepatic glucose production (HGP) and increased lipoprotein uptake, whereas insulin resistance in the muscle is associated with impaired glucose uptake via GLUT4 and declining glycogen synthesis (Defronzo, 2004).

When insulin resistant, insulin secretion from the β-cells in the pancreas increases to maintain normal circulating glucose levels. However as insulin resistance in the liver and the muscle worsens, the release of insulin becomes disrupted. This disruption results in declining early phase insulin secretion followed by excessive late phase insulin secretion. This observation of

irregular insulin secretion is considered as the onset of impaired glucose tolerance (IGT) (Defronzo, 2004).

IGT results in T2D when the pancreas is not capable to secrete the optimal amount of insulin needed. Consequently, insulin secretion sharply declines as the glucose concentration continues to rise (Defronzo, 2004).

5. Insulin resistance, T2D and CVD

The disturbance of insulin signalling plays a central role in the development of the metabolic syndrome. Due to these disruptions, one is more prone to develop CVDs and vascular complications as a result of the inflammatory, hyperglycemic, hypertensive and dislipidemic environment created by T2D (Rask-Madsen & Kahn, 2012).

In the next section, the link between cardiovascular complications and insulin resistance in the (5.1) endothelial tissue, (5.2) macrophages and (5.3) cardiac tissue is respectively described:

5.1. Insulin resistance in the endothelial tissue

Previous studies (Kubota et al, 2011; Kim et al, 2007) observed that in diet-induced obese rats, insulin was not able to activate PKB and nitric oxide (NO) synthase in aortic tissue indicating insulin resistance. Insulin resistance is associated with increased leukocyte adhesion to the endothelium, increased expression of the vascular cell adhesion molecule-1 (VCAM-1) and impaired NO-mediated vasorelaxation (Rask-Madsen et al, 2010).

The downregulation of VCAM-1 in response to insulin stimulation is not blocked by NO-synthase inhibitors, confirming that insulin signalling independent of NO is responsible for VCAM-1 expression (Rask-Madsen & Kahn, 2012). Furthermore, insulin resistance in the endothelial tissue results in increased vascular wall inflammation and atherosclerosis. Insulin resistance in the endothelial cells develop through: (i) the activation of toll-like receptor 4 (TLR4) in response to increased FFA levels (Kim et al, 2007), (ii) the downregulation of the IRS proteins (Kubota et al, 2011) and also (iii) the elevated TNF-α and other pro-inflammatory cytokines released from the adipose tissue (Rask-Madsen et al, 2003).

Mechanism: Once insulin binds to its receptors on the endothelial cells, it activates PKB. Following this, PKB translocates to the nucleus and consequently phosphorylates FOXO1. (Nakae et al, 2001; Rask-Madsen et al, 2012).

When FOXO1 is phosphorylated, it downregulates VCAM-1 expression (Rask-Madsen & Kahn, 2012) and decrease leukocyte adhesion to the endothelium. Insulin resistance is however coupled to upregulated VCAM-1 expression and leukocyte adhesion to the endothelium resulting in cardiovascular damage (Rask-Madsen et al, 2003). Thus, the phosphorylation of FOXO1 in endothelial cells can prevent atherosclerosis development in individuals suffering from the metabolic syndrome (Rask-Madsen & Kahn, 2012).

5.2. Insulin resistance in macrophages

Insulin resistance in macrophages causes a subsequent rise in cluster of differentiation 36 (CD36) expression which results in increased LDL uptake (Han et al, 2006) and pro-inflammatory cytokine inhibition (Baumgartl et al, 2006). CD36 is a glycoprotein which endocytose oxidized low density lipoproteins (OxLDL) (Collot-Teixeira et al, 2007). Consequently, these insulin resistant macrophages will undergo increased apoptosis (Han et al, 2006) causing the formation of a necrotic core in the atherosclerotic plaques. Once the plaques rupture, the necrotic core is exposed to circulating blood and raises the susceptibility to develop thrombosis, transitory cerebral ischemia, unstable angina pectoris, myocardial infarction and stroke (Moore & Tabas, 2011).

5.3. Insulin resistance in the cardiac tissue

Obesity is associated with changes in the myocardial metabolism such as: higher fatty acid oxidation and lower glucose oxidation rates (Mazumder et al, 2004). This switch is due to the increased FFA production and release into circulation during obesity.

Furthermore obese animals tend to have higher expression of the β isoform of the MHC. The expression of this isoform is especially upregulated during remodelling in cardiac failure (Rask-Madsen & Kahn, 2012), consequently resulting in downregulated contractile properties and increased disease progression (Kiriazis & Kranias, 2000; Fatkin et al, 2000).

Insulin resistance in the cardiac muscle is associated with reduced cardiomyocyte volume, decreased GLUT4 expression, decreased GLUT1 expression (Rask-Madsen & Kahn, 2012) as well as the excessive β-oxidation of FFA in the mitochondria (Koves et al, 2008). These

changes, especially in metabolic substrate inflexibility and increased oxidant production in the mitochondria, can cause the development of heart failure (Rask-Madsen & Kahn, 2012).

The insulin-like growth factor-1 receptor (IGF1R) compensates to a small extent for insulin signalling in insulin resistant cardiomyocytes. However, once the IGF1R becomes unresponsive due to the loss of insulin sensitivity, fatty acid β-oxidation in the mitochondria is increased and the expression of the contractile proteins is downregulated (Rask-Madsen & Kahn, 2012). As a result, heart failure and cardiomyopathy will develop (Laustsen et al, 2007).

5.4. Coronary heart disease (CHD)

CHD is generally caused by atherosclerosis which refers to plaque build-up in the arterial walls. According to the American Heart Association, plaque consists of fatty substances, cholesterol, calcium, cellular waste products, and the clotting material, fibrin. Plaque formation results in: arterial wall narrowing; restriction of oxygenated blood supply to the heart consequently causing angina pectoris (chest pain); heart attack (myocardial infarction) and shortness of breath amongst others (Singh, 2014).

Over time, plaque in the arteries can harden causing the coronary arteries to narrow and reduce oxygen-rich blood flow to the heart to a further extent. The plaque can also rupture resulting in the formation of a blood clot, which can partially or completely block the blood flow thorough the coronary artery (Mayo Clinic Health - www.mayoclinic.org).

The most common coronary heart disease risk factors include: obesity, T2D, hypertension, high circulating blood lipids, smoking, a lack of exercise and stress (Singh, 2014). According to Kivimäki et al (2012), smoking contributes to 36% of CHD development followed by obesity which is associated with 20% of the cases.

5.4.1. Heart failure

Heart failure, also known as chronic heart failure (CHF), is a condition where the heart is unable to pump a sufficient amount of blood to meet the body's needs (Dorland's Medical Dictionary; Medical Dictionary, 2011; Mayo Clinic, 2009). In individuals suffering from heart failure, the heart is either unable to be filled with enough blood, or unable to provide enough blood to the rest of the body (National Clinical Guideline Centre (2010) – www.ncgc.ac.uk).

Heart failure is associated with the development of weaker heart pumping as the condition progresses over time. Heart failure can affect both sides of the heart. Right-side heart failure is associated with the inability of the heart to pump blood to the lungs for oxygen exchange whereas left-side heart failure refers to the inability of the heart to pump oxygenated blood to the whole body. Individuals suffering from heart failure develop symptoms such as leg, feet and ankle swelling; shortness of breath; and excessive fatigue (McDonagh, 2011).

5.4.2. Diabetic cardiomyopathy

Diabetic cardiomyopathy, a term originally introduced by Rubler and collogues in 1972, is a condition where T2D affects the cardiac function and structure independently of CHD and hypertension. Since the first identification of cardiomyopathy, it was further divided in to two main types: (i) primary cardiomyopathy and (ii) secondary cardiomyopathy.

(i) Primary cardiomyopathy refers to a defect in the heart tissue itself which subsequently aggravates the cardiac function. (ii) Secondary cardiomyopathy develops due to systemic syndromes which affects cardiac performance (Elliott et al, 2008).

Cardiomyopathy can either lead to diastolic heart failure (preserved ejection fraction), or to systolic heart failure (reduced ejection fraction) (Paulus et al, 2007). The proposed mechanisms to explain these changes in the cardiac tissue include myocardial fibrosis and myocyte hypertrophy (Trachanas et al, 2014).

Mechanism: Diabetes is associated with hyperglycemia and increased FFA production. Under hyperglycemic conditions, PKC and advanced glycation end products (AGEs) are upregulated, resulting in the development of fibrosis. Hyperglycemia can also lead to glucotoxicity due to increased ROS production (Boudina & Abel, 2007). In addition, pathways like the hexosamine biosynthetic pathway (HBP) may be activated, resulting in biochemical changes with possible detrimental effects including cell death.

Increased FFAs activate the peroxisome proliferator-activated receptor alpha (PPAR-α) signalling pathway, which in turn, increases the transcription of several genes associated with fatty acid oxidation. PPAR-α increases pyruvate dehydrogenase kinase 4 (PDK4) expression, which downregulates pyruvate dehydrogenase (PDH) activity, consequently resulting in lactic acid accumulation and low glucose oxidation. In addition, PPAR-α activates malonyl-coenzyme A decarboxylase (MCD), thus restricting the conversion of acetyl-coenzyme A (AcCoA) to malonyl-coenzyme A (McoA). Downregulated McoA

levels lead to the activation of carnitine palmitoyl-transferase 1 (CPT1) in the mitochondria, which in response further initiates fatty acid oxidation (Boudina & Abel, 2007). Once fatty acid oxidation in the mitochondria is increased, mitochondrial uncoupling and ROS generation from the electron transport chain, increase. Excessive ROS production in combination with high fatty acid levels result in lipotoxicity (Boudina & Abel, 2007).

Glucotoxicity, fibrosis, mitochondrial uncoupling and lioptoxicity are all potential contributors to the development of a diabetic cardiomyopathy (Boudina & Abel, 2007).

6. Overview on A-T and ATM

6.1. A-T

Ataxia telangiectasia (A-T) is a rare autosomal recessive disorder that progressively affects multiple organs causing severe disability. Ataxia, which refers to a lack of voluntary coordination and telangiectasia, to small dilated blood vessels, are both characteristics of the disease. A-T is caused by mutations in the Atm gene which consequently results in unstable and truncated ATM protein variants (Zhang et al, 1997). According to the National Ataxia Foundation (www.ataxia.org), the most common types of mutations that occur in the Atm gene are: frame shifting (25%), splicing (35%) and nonsensing (25%).

6.2. Symptoms of A-T

A-T emerges in the first 2 decades of life (Valentin-Vega et al, 2012). The first symptoms can usually be observed in early childhood when children begin to walk. Unlike normal children of their age, these children wobble when they are walking, sitting or standing still. During late pre-school and early school A-T causes a gradual and continual loss of certain types of cells in the cerebellum of the brain. Consequently these children develop difficulty with coordination and movement such as: oculomotor apraxia (difficulty in eye movement), swallowing complications, and inaccurate/unclear speech (National Ataxia Foundation - www.ataxia.org).

The appearance of small dilated blood vessels covering the white of the eyes, the bridge of the nose, or the ears are all characteristics of A-T suffering individuals. Furthermore, A-T also weakens the immune system, causing A-T children to become more susceptible to

developing respiratory tract infections, including: sinusitis, pneumonia, ear infections and bronchitis (National Ataxia Foundation - www.ataxia.org).

In addition, A-T prevents DNA repair, due to a lack of ATM protein which is responsible for recognising DNA breaks. As a result, these individuals are more prone to develop cancer, usually as lymphoma or leukemia (National Ataxia Foundation - www.ataxia.org).

Previous studies linked ATM to the development of atherosclerosis in ApoE-/- mice (Sheneider et al, 2006). According to Mercer et al (2010), ATM haploinsufficiency results in the development of atherosclerosis in response to both the direct effects on the vessel wall, and the indirect metabolic effects.

Lastly, ATM deficiency is closely related to the development of insulin resistance and ischemic heart disease. Individuals suffering from this disease have a very high (up to 49%) incidence of T2D and were found to die approximately 11 years earlier due to ischemic heart disease when compared to non-disease carriers (Su & Swift, 2000; Swift & Chase, 1983).

6.3. The ATM protein

ATM is a 370 kDa serine/threonine protein kinase which contains an open reading frame of 3056 amino acids (Abraham, 2001). ATM is believed to be closely related to the large protein family of Phosphatidylinositol 3-kinase-related kinases (PIKKs) as it displays the same homologies (Abraham, 2001). Proteins in the PI3K pathway play an important role especially in regulating cellular growth, proliferation, metabolism, protein synthesis and transcription (Cell Signalling (2014) – www.cellsignal.com). The ATM protein also has other sequences in its structure including: nuclear localization signals, HEAT rod-like helical structures for intracellular transport and a leucine zipper domain for the binding of DNA motifs. These sequences are characteristic in several nuclear and cytoplasmic proteins associated with protein trafficking (Yang et al, 2011).

6.4. Functions of ATM

According to Shiloh and Kastan (2001), less than 10% of the ATM protein functions can be attributed to its amino acid sequence, thus implying that more than 90% of this protein's additional functions are still not yet identified. This kinase was traditionally believed to be located only in the nucleus where it responds to genotoxic stress; however increasing evidence suggested that it might also be present and have significant functions in the mitochondria or in the cytosol of the cell (Abraham, 2001).

In the next section, the functions of ATM in the nucleus, mitochondria and cytosol of the cell are described respectively:

6.4.1. Nuclear ATM

Nuclear ATM *(Figure 1.4)* is recruited and activated by DNA double-strand breaks (Abraham, 2001). When activated, ATM consequently phosphorylates numerous proteins which in turn initiate the activation of the DNA damage response network (DNA repair, cell cycle arrest or apoptosis). Activated proteins include the cell cycle arrest checkpoint kinases (Chk-1 and Chk-2), tumor suppressor gene p53 and histone 2A gene (H2AX) (Canman et al, 1998; Banin, 1998).

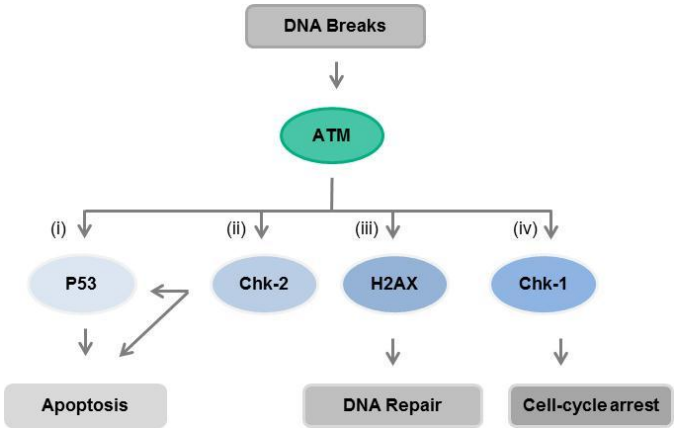

Figure 1.4: *The activation of nuclear ATM via DNA breaks*

6.4.2. Mitochondrial ATM

The smallest portion of ATM is localized to the mitochondria and is activated in response to mitochondrial dysfunction (Valentin-Vega et al, 2012).

In thymocytes, a lack in mitochondrial ATM, as in individuals suffering from A-T, leads to the development of intrinsic mitochondrial abnormalities, including: increased ROS production, abnormal mitochondrial behaviour, increased cellular respiratory capacity and a reduction in mitophagy (Valentin-Vega et. al, 2012). It is suggested that ATM in the mitochondria plays a key role in regulating mitochondrial homeostasis (Valentin-Vega et al, 2012).

6.4.3. Cytosolic ATM

The cytoplasmic functions of ATM are not yet fully determined. According to several studies, cytoplasmic ATM is predominantly found in neuronal or neuron-like cells (Oka & Takashima, 1998; Barlow et al, 2000; Boehrs et al, 2007). A study done by Lim et al (1998), also suggested that cytoplasmic ATM is present in proliferating cells where it associates with a protein, b-adaptin, which is involved in vesicle trafficking.

Importantly, especially with regards to our study, cytoplasmic ATM is also alleged to be involved in insulin signalling pathways, although the mechanism of action is still unclear (Yang & Kastan, 2000; Viniegra et al, 2005; Halaby et al, 2008).

6.5. ATM and insulin signalling

The association between ATM and insulin signalling is to date, not yet clearly established. The activity of ATM kinase was reportedly increased 3-fold in response to insulin stimulation. Furthermore, this observation was specifically seen in rat 3T3-L1 cells that had differentiated into adipocytes (Yang & Kastan, 2000).

Insulin is assumed to phosphorylate the cytoplasmic translation repressor protein, 4EBP1 (also called PHAS-I) via an ATM-dependent pathway *(Figure 1.5).* Under normal conditions, 4EBP1 is bound to the eukaryotic translation initiation factor-4E (eIF-4E), thereby inhibiting it. When 4EBP1 is phosphorylated in response to ATM, it dissociates from eIF-4E, consequently initiating mRNA translation (i). Studies done by Yang and Kastan (2000) indicated that, in response to insulin stimulation, 4EBP1 is phosphorylated at specifically Thr36 and Thr45 residues via the PI3K/PKB/mTOR pathway or at Ser111 via ATM. In addition, ATM seemed to be only partially required for 4EBP1 release, which might also be interacting with the mTOR pathway to initiate the dissociation of 4EBP1 and eIF-4E efficiently (Yang & Kastan, 2000).

According to more recent studies, the activation of ATM in response to insulin stimulation also (ii) phosphorylates PKB at Ser473, via an unknown phosphatase (Viniegra et al, 2005; Halaby et al, 2008). Once PKB is phosphorylated, it initiates multiple important physiological processes including: glucose uptake, protein translation, cell proliferation and also cell survival (Yang et al, 2011). However this mechanism is still vague and according to Yang et al (2011), it might be a good starting point to investigate the unknown functions associated with specifically cytoplasmic ATM and the A-T disease.

Phosphorylated PKB in response, phosphorylates the (a) Tsc2-Tsc1 complex and (b) the AS160 protein. As mentioned in Chapter 1, Section 2.2.1, once the Tsc2-Tsc1 complex is phosphorylated, Rheb is stimulated, resulting in the activation of mTOR. Following this, mTOR can diverge into two different pathways to induce protein synthesis including: the activation of the 4EBP1 consequently resulting in the dissociation of eIF-4E or, the activation of $p70^{s6k}$ (Bevan, 2009). PKB can also directly phosphorylate AS160, resulting in the association of AS160 at Thr642 with 14-3-3. Once bound to 14-3-3, a Rab binding domain is created which in turn converts Rab-GDP to Rab-GTP. In addition, GLUT4 vesicle translocation to the plasma membrane is initiated for optimal glucose uptake (Bevan, 2009).

Furthermore, insulin stimulated activation of ATM also (iii) phosphorylates Liver kinase B1 (LKB1), which in turn activates AMP-activated protein kinase (AMPK). LKB1 is an important kinase regulating (a) growth control (tumour suppressor) and (b) also cell polarity (Shackelford & Shaw, 2009). In addition, AS160 can also be phosphorylated via AMPK, which in turn also activates the translocation of GLUT4 vesicles to the plasma membrane (Cell Signalling (2013) - www.cellsignal.com).

From the above, it is evident that ATM may play an important role in regulating insulin signalling via 4EBP1, PKB or LKB1 activation respectively, although these pathways have not been fully determined yet and has not been shown to be active in this context in the heart.

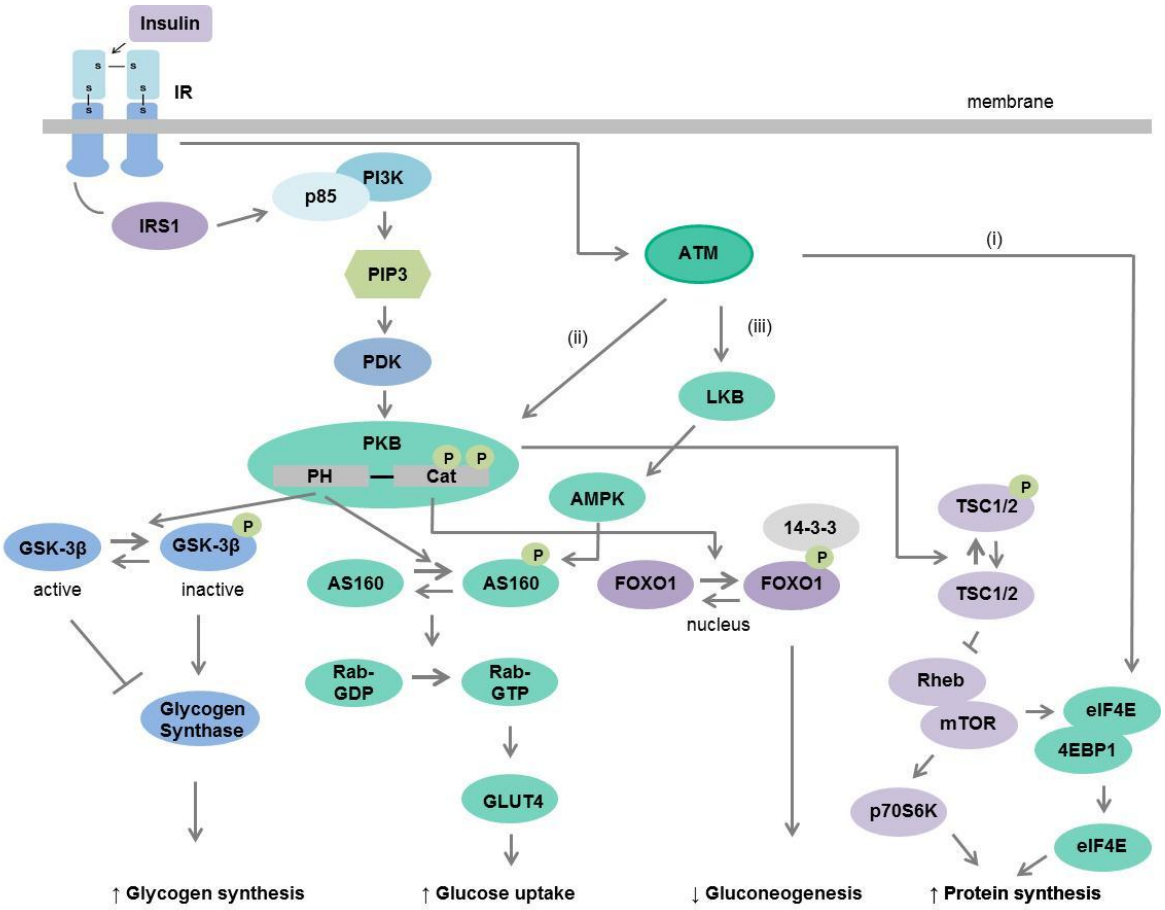

Figure 1.5: *ATM and insulin signalling*

6.6. ATM and insulin resistance

A-T individuals display several symptoms associated with insulin resistance, including: glucose intolerance, hyperinsulinemia and hyperglycemia (Yang et al, 2011) which can subsequently lead to the development of insulin resistance and T2D.

According to a study done by Schalch et al (1970), it was reported that 59% of A-T suffering individuals developed T2D. Since A-T individuals most likely die before T2D is fully diagnosed (Yang et al, 2011), the exact percentage of diabetic A-T individuals is difficult to determine.

Recently, the effect of ATM deficiency on insulin resistance was investigated in apolipoprotein E (ApoE) null background mice. This atherosclerotic mouse model was cross-bred with Atm -/- and Atm +/- mice respectively (Schneider et al, 2006) whereafter they were fed a high fat diet (HFD) (Halaby et al, 2008) to induce insulin resistance. They found that ATM deficiency increased glucose intolerance, atherosclerosis and insulin

resistance (Schneider et al, 2006), thus indicating that ATM plays a crucial role in regulating insulin signalling.

According to several other studies, individuals suffering from A-T also present with: lower IGF1R expression (Peretz et al, 2001), significantly increased circulating IGF-1 serum levels, and slightly increased serum IGF-binding protein (IGFBP)-3 levels (Busiguina et al, 2000). In line with this finding, they also observed that A-T individuals have higher insulin levels in their blood, which can exacerbate the development of insulin resistance.

When rats were fed a HFD to induce insulin resistance, it was observed that the expression of ATM dramatically decreased in skeletal muscle. Insulin-stimulated phosphorylation of PKB at Ser473 and Thr308 in the muscle tissue was also attenuated, when compared to chow-fed controls (Halaby et al, 2008).

Thus, one can propose that downregulated ATM levels, as seen in obese animals, are directly involved in the development of insulin resistance via the downregulation of PKB activation and consequently also GLUT4 translocation (Halaby et al, 2008).

Since Ser473 is not an S/T-Q motif, ATM cannot directly phosphorylate PKB at this site (Kim et al, 1999; Golding et al, 2009). According to Golding et al (2009), it is speculated that ATM increased PKB phosphorylation by some unknown okadaic acid-sensitive phosphatase, like Protein phosphatase 1 (PP1) or Protein phosphatase 4-6 (PP4-6).

Furthermore, ATM appears to indirectly regulate glucose homeostasis and the functions of insulin through a p53-dependent pathway (Ambrose & Gatti, 2013). Once ATM is activated, it phosphorylates the tumour suppressor p53, at Ser18 in mice (or Ser15 in human). In doing so, the transcriptional activity of p53 is activated. The inhibition of p53 Ser18 in mice resulted in the development of glucose intolerance and insulin resistance (Armata et al, 2010). In light of the above, it can be suggested that ATM phosphorylation of p53 plays an important role in not only regulating cellular ROS levels but also controlling glucose homeostasis (Ambrose & Gatti, 2013).

Taken together, insulin resistance in A-T individuals may develop due the either the lack of ATM to activate PKB at Ser473 or Thr 308 via some unknown ocadaic acid phosphatase, or to phosphorylate the tumour suppressor p53 at Ser15/18.

6.7. Activators & Inhibitors of ATM

6.7.1 Activators

ATM activators include: (i) Insulin, (ii) Metformin and (iii) Chloroquine.

Note: Only insulin was used as an activator of ATM (described in Chapter 1, Section 6.5) in this study, therefore activation with Metformin and Chloroquine will not be discussed in detail.

(ii) Metformin

Metformin is a well-known first-choice treatment for T2D (Nathan et al, 2009) as it has the ability to lower fasting glucose levels.

Metformin surprisingly also activates ATM, however very little is known about the mechanism (Vazquez-Martin et al, 2011). According to a study done by Birnbaum & Shaw (2011), ATM becomes phosphorylated in response to metformin treatment. The activated ATM protein consequently results in the activation of AMPK directly or via LKB1, which in response, increases GLUT4 vesicle translocation and glucose uptake (Cell Signalling (2014) – www.cellsignal.com).

(iii) Chloroquine

Chloroquine is a well-known medication used for the treatment of malaria (Halaby et al, 2013) and is currently also believed to improve insulin sensitivity and glucose tolerance potential (Emami et al, 1999; Halaby et al, 2013). According to Esposito & Sinden (1987) and Sogo et al, (1984) chloroquine has the ability to unwind the DNA double helix, resulting in restricted binding to nucleosomal linker regions; however the nucleosomes are not disrupted by chloroquine. As a result, alterations in the rotation angle between the adjacent nucleosomes occur, thereby affecting the higher-order chromatin structure formation (Krajewski, 2005).

Recently is has been discovered that chloroquine might also be a potent stimulator of ATM. The exact mechanism of action is still unclear, however according to Kruit (2008) active ATM in response to chloroquine inhibits the c-Jun N-terminal kinase (JNK) pathway. Inactive JNK lowers the risk of developing atherosclerosis and insulin

resistance (Kruit, 2008). It is also possible that the unwinding of DNA may trigger ATM activity.

6.7.2 Inhibitors

(i) KU 55933/60019

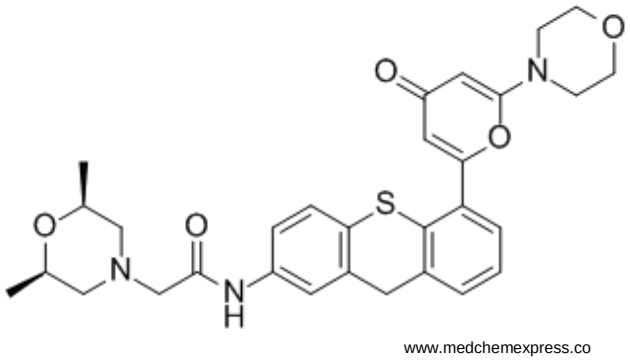

Figure 1.6: *KU 60019 structure*

KU 55933/60019 are both specific ATM kinase inhibitors. According to recent studies, KU 55933 has the ability to radiosensitize human cancer cells. KU 60019 *(Figure 1.6)* shares the same pharmacological, structural and biological effects as KU 55933, although the KU 60019 analogue is improved to be 10 fold more effective to inhibit ATM phosphorylation in radiation-induced human glioma cells (Golding et al, 2009). In the same study done by Golding et al (2009), they tested the effect of 1 µM KU 60019 on 229 kinases and observed that KU 60019 had no or a very little effect on these kinases; therefore they concluded that KU 60019 is specific to ATM inhibition. Furthermore the Ki 1 nano Molar (nM) and IC50 (6.3 nM) values of KU 60019 are manipulated to be more than half of those of KU 55933.

*The **half maximal inhibitory concentration (IC50)** value is an important measurement to determine the effectiveness of a substance to inhibit a specific biological process or biological component (Pharmacelsus®). **The inhibitor constant, Ki**, indicates the potency of an inhibitor, thus the concentration required to produce half maximum inhibition (Enzyme inhibitors - http://www.ucl.ac.uk).*

KU 60019 mechanism: According to ApexBio Technology® (2013), KU 60019 inhibits ATM kinase directly; however the exact mechanism is still unknown but possibly the initial autophosphorylation event of activation of the kinase is inhibited as KU 60019 leads to lower phosphorylated levels of ATM at Ser1981 (Bakkenist & Kastan, 2003).

According to Golding et al (2009), the more water-soluble KU 60019 effectively radiosensitized human glioma cells. A-T fibroblasts were not radiosensitized via KU 60019 which might be an indication that ATM kinase is target specific. KU 60019 also reduced the phosphorylation of basal Ser473 PKB, thus speculating that ATM might activate a protein phosphatase that dephosphorylates PKB (Golding et al, 2009).

Furthermore, KU 60019 inhibits the migration and invasion (in vitro) of glioma cells which could be an indication that glioma growth/motility is controlled by ATM via PKB. It is also suggested that KU 60019 interferes with prosurvival signalling pathways as it had no further radiosensitizing effects on PKB and MEK inhibited treated cells (Golding et al, 2009).

Thus in summary, KU 60019 reduces ATM phosphorylation at Ser1981 and PKB phosphorylation at Ser473, inhibits the DNA damage response mechanism and, radiosensitizes and inhibits the migration and invasion of certain cells (Golding et al, 2009).

6.8. Link between ATM & CVD

CVDs refer to several disorders of the heart and blood vessels. According to the WHO (2015), CVDs are the main cause of death globally. In 2012, a projected 17.5 million individuals died from CVDs globally, whereas the greater number of these deaths was due to stroke (6.7 million) and coronary heart disease (7.4 million).

Cardiomyocyte apoptosis regulates both functional and structural aspects of the heart, mainly during remodelling and/or growth (Foster et al, 2011).

Once the β-adrenergic receptor (β-AR) in the heart is stimulated in response to isoprenaline or noradrenaline, the ventricular contraction in the heart increases due to increased calcium release (Yano et al, 2005). However overstimulation of these receptors results in cardiomyocyte apoptosis initiation through numerous pathways. One of the pathways results in the activation of JNK and stabilization of p53, both of which are targets of ATM. Another β-AR target is PKB, which is part of the anti-apoptotic pathway (Freemantle et al, 1999).

Although the mechanism of how ATM affects the cardiovascular system is still vague, Foster et al (2011) demonstrated that ATM KO mice structurally displayed a reduction in

septal wall thickness and functioning of the left ventricular parameters. ATM KO mice also exhibited increased cardiac hypertrophy and fibrosis.

Cardiac hypertrophy is an adaptive response and refers to thickening of the heart muscle (myocardium) consequently reducing the ventricular space. It is mainly caused by hypertension or heart valve stenosis (Nature (2015) – www.nature.com).

Fibrosis refers to the development of fibrous connective tissue as a response mechanism to repair injured or damaged tissue. Fibrosis arises especially when the heart is damaged as a result of myocardial infarction, which consequently results in the stiffening of the heart muscle and valves. This decrease in flexibility can increase the risk of heart failure and valvular dysfunction (Robertson, 2014).

ATM KO mice furthermore displayed upregulated connective tissue growth factor (CTGF), plasminogen activator inhibitor-1 (PAI-1) and matrix metalloproteinase (MMP)-2. CTCF is believed to induce fibrosis in the heart tissue whereas PAI-1 is a risk factor for thrombosis and atherosclerosis development. MMP-2 levels are normally upregulated in response to heart failure and results in cardiac rupture (Foster et al, 2011).

In ATM heterozygous KO animals, apoptosis is triggered in response to β-AR stimulation, whereas in ATM wild type (WT) animals β-AR-triggered apoptosis is prevented (Foster et al, 2011). In addition, ATM expression increased upon β-AR stimulation, which consequently inhibited ventricular fibrosis and remodeling. Thus, a decrease in cardiac ATM expression results in increased myocyte apoptosis (Gorr et al, 2012), causing fibrosis and hypertrophy. Foster et al (2011) furthermore claimed that myocyte apoptosis in ATM deficient animals is due to the decreasing activity of PKB, rather than through the JNK/p53 pathway.

From the above it is evident that the complete mechanism and link between ATM and the heart is not yet fully understood. It is however clear that ATM is crucial for the activation of the anti-apoptotic PKB pathway to prevent the development of cardiovascular diseases.

7. Motivation for the study

In 2014, 40% men and 70% women were already suffering from being overweight or obese in South Africa (Baleta & Mitchell, 2014) mostly due to high levels of carbohydrate consumption as

a result of poor financial support (Goedecke et al, 2006). Obesity is associated with the development of insulin resistance, which, in turn, is positively correlated with the risk of CVD development. In 2014, the International Diabetes Federation stated that 22.7 million South Africans are suffering from diabetes. Diabetic cardiomyopathy is a condition where T2D affects the cardiac function and structure independently of CHD and hypertension (Rubler et al, 1972).

A-T patients display a very high incidence of insulin resistance or T2D (Yang et al, 2011) and are also more susceptible to ischaemic heart disease. Furthermore, ATM expression was a found to be downregulated in obese/insulin resistant animals (Halaby et al, 2008).

ATM is expressed in the heart but it is currently unknown whether it is involved in insulin signalling in the heart, or whether it is in any way involved in the development of a cardiomyopathy.

Up to date it is not yet established where in the insulin signalling cascade this protein may fit in and what pathways it may affect or not. Previous studies linked ATM to glucose uptake, the activation of AMPK (Shackelford & Shaw, 2009) and PKB (Viniegra et al, 2005), and the development of atherosclerosis in ApoE-/- mice (Sheneider et al, 2006); however none of these have been investigated in the heart.

If the relationship claims between ATM and insulin resistance is validated by the present study, ATM can be an effective and alternative therapeutic target to treat the increasing amount of South Africans suffering from obesity-induced T2D.

8. Aim and Objectives

Aim: To determine the importance of ATM in glucose uptake in cardiomyocytes prepared from control vs. obesity-induced insulin resistant animals.

Objective 1: To determine ATM levels in rat models of obesity-induced insulin resistance and characterized a suitable model for the study.

Objective 2: To manipulate the ATM protein in isolated cardiomyocytes from both obese, insulin resistant rats and their age-matched control groups with suitable activators or inhibitors of ATM and measure 2DG uptake, expression and activation of intermediates of the insulin signalling pathway (IRS1, PI3K, PTEN, PKB, AS160, AMPK, GSK-3β) and GLUT4 expression.

We only investigated cytosolic ATM, and not ATM present in the nucleus or in the mitochondria.

CHAPTER 2: MATERIALS AND METHODS

1. Animals

40 Male Wistar rats of the same age and initial weights of 190 ± 10 grams (g) were used in this study. The animals were divided randomly into two groups. Group one was fed a HFD containing 11.5 % fat while group two, the age-matched controls received normal rat chow (4.8 % fat) for a period of 16 weeks. The animals had free access to food and water and kept on a 12-hour day/night cycle in the Central Research Facility of the Faculty of Health Sciences of the University of Stellenbosch.

The study was registered at the Committee for the use of animals in research of the University of Stellenbosch (Number SU-ACUM12-00040) and conducted under the revised South African National Standard for the Care and Use of Animals for Scientific Purposes (South African Bureau of Standards, SANS 10386, 2008).

2. Diet compositions

The Table below *(Table 2.1)* indicates the two different diet compositions which were fed to the animals over the 16 week period. The HFD was prepared by adding Holsum cooking fat to the diet-induced obese (DIO) diet (Salie et al, 2014). The DIO diet consisted of standard rat chow as described by Pickavance et al (1999) with additional sucrose and condensed milk (Ruduwaan et al, 2014). We only used the HFD in our study to induce obesity related insulin resistance.

Table 2.1: *Different diet compositions (Control vs. HFD)*

	Fat (g/100g)	Cholesterol (mg/100g)	% Protein	% Carbohydrates	Sugar (g/100g)	kJ/100g
Control	4.8	3	17.1	34.6	6.6	1272
HFD	11.5	13	8.3	42	24.4	1354

3. Oral Glucose Tolerance Test (OGTT) & Glucose measurement

OGTT's are used as a central marker in the determination of insulin sensitivity. In this study, OGTT's were performed in week 15 after the animals were fasted overnight. For ethical purposes, the animals were injected with 0.1 microliter (µl) Eutha-naze (53 mg/kg Sodium

pentobarbital) to create an anaesthetic environment throughout the procedure. Using a glucometer, the basal glucose level for each rat was taken by collecting a drop of blood after a tail prick. This was followed by gavaging 1 milligram (mg)/kg sucrose to each animal, where after their blood glucose levels were monitored constantly for 2 hours. The blood glucose level for each rat was measured at 3 minutes (min), 5 min, 10 min, 15 min, 20 min, 25 min, 30 min, 45 min, 60 min, 90 min and 120 min respectively using a glucometer and a drop of blood from the same tail prick. The animals were left to recuperate from the metabolic insult for a week before experimentation.

4. Biometric measurements and sacrificing of animals

After 16 weeks, the body weight of each animal was determined just before sacrificing. The animals were sacrificed by injecting them with 0.5 µl Eutha-naze (265mg/kg Sodium pentobarbital). A foot-pinch test (pedal reflex) was performed to be assured that the animals showed no response before opening the chest cavity and removing the heart. Following this, the intra-peritoneal fat (IP fat) of each animal was removed and weighed.

5. Biochemical analysis

5.1. Blood collection

Blood collection entailed the withdrawal of 1 millilitre (ml) blood directly from the carotid artery from control and HFD anaesthetized overnight fasted animals respectively at the time of the OGTT in week 15. The blood of each animal was transferred to a SGVac gel tube and left on ice for 20 min. Following this, the blood samples were centrifuged at 3000 revolutions per minute (rpm) for 10 min.

The blood serum was removed and stored at -80 degree Celsius (ºC). The remaining blood (white blood cells, platelets, red blood cells) was discarded.

5.2. Insulin assay

For the determination of insulin levels, a commercially available EMD Millipore Corporation Enzyme-linked immunosorbent assay (ELISA) was used. All the reagents were pre-warmed to room temperature (25ºC). Control and HFD serum samples were analysed in duplicate for the determination of insulin levels. This non-radioactive quantification assay contained an

anti-rat insulin antibody coated 96-well microplate and all relevant reagents were supplied by the assay kit.

The required number of wells for all the blank, standard, quality control (QC) and serum samples were washed 3 times with 300 µl 10X diluted Wash buffer, where after the residual fluid in the wells were decanted. Following this, 10 µl Assay buffer (0.05 Molar (M) phosphosaline, pH 7.4, containing 0.025 M EDTA, 0.08% Na-azide and 1% Bovine serum albumin (BSA)) was added to each blank and sample well and 10 µl Matrix solution (charcoal stripped pooled mouse serum) was added to the blank, standard and QC wells.

Following this, the standards (10 µl/ml, 5 µl/ml, 2 µl/ml, 1 µl/ml, 0.5 µl/ml, 0.2 µl/ml, 0 µl/ml) were prepared in duplicate. In the order of ascending concentration 10 µl of each standard was pipetted into the respective wells and 10 µl of the two QC samples were added to their appropriate wells. Following this, 10 µl serum of both the control and HFD animals were added sequentially in duplicate to the remaining wells.

80 µl rat pre-titered biotinylated anti-insulin Detection antibody was added to all the standards (including the blank and QC samples) and the serum samples followed by an incubation period of 2 hours at room temperature on slow rotator (400-500 rpm). During these 2 hours, insulin present in the standard and serum samples bound to the wells. All the fluid was decanted and the wells were washed thoroughly with 300 µl 10X Wash Buffer. 100 µl pre-titered Streptavidin- Horse Radish Peroxidase (HRP)-conjugate in buffer was pipetted to each well and incubated for 30 min at room temperature to visualize the target molecule, insulin. After washing the wells again 3 times with 300 µl 10X Wash Buffer, 100 µl 3,3',5,5'-Tetramethylbenzidine (TMB) One-Step Substrate Reagent was added to each well and incubated for 15 min at room temperature. TMB is a specific reagent which has the ability to act as a hydrogen donor in response to the reduction of hydrogen peroxide to water by HRP enzymes. Consequently the resulting diimine causes a blue colour development in proportion to the amount of insulin bound. 100 µl 0.3 M Stop Solution was pipetted into each well. This sulphuric acid solution changed the blue colour to a yellow colour. The intensity of the colour was immediately measured within 5 min on a microplate reader at 450 nanometres (nm) and 590 nm respectively.

A 4-parameter logistic equation dose-response curve was set up by plotting the absorbance unit of 450 nm less that of 590 nm, on the Y-axis against the rat insulin standard concentrations on the X-axis. The increase in absorbance is directly proportional to the amount of insulin measured in the unknown serum samples; therefore the curve was set up by known standard insulin concentrations where after it was used as a reference for the

determination of the samples of interest. An online ELISA analysis program (http://www.elisaanalysis.com) was used to set up the curve and calculate the insulin levels of the control and HFD serum samples. The assay was only accepted if the QC values fell within the calculated QC range (EMD Millipore Corporation).

5.3. HOMA IR index calculation

The Homeostasis model assessment of insulin resistance (HOMA IR) index was an assessment method used to quantify insulin resistance in the different groups. The HOMA IR index was calculated using the following formula:

HOMA IR index = Basal glucose levels (mmol/L) x Fasting insulin levels (mIU/ml)/22.5.

6. Ventricular cardiomyocyte preparation

Adult ventricular cardiomyocytes from the control and HFD animals were prepared in our laboratory by collagenase perfusion, essentially as described by Fischer et al (1991) and subsequently modified in our laboratory (Huisamen et al, 2001). The collagenase used in this study, was previously tested in our laboratory to give a yield of ~ 80% rod-shape myocytes (Huisamen et al, 2008).

After 16 weeks, animals were fully anaesthetized as described in Chapter 2, Section 4, whereafter their hearts were removed and placed in ice-cold Krebs-Henseleit buffer (119 mM NaCl; 24.9 mM $NaHCO_3$; 4.74 mM KCl; 1.19 mM KH_2PO_4; 0.6 mM $MgSO_4.7H_2O$; 0.59 mM Na_2SO_4; 1.25 mM $CaCl_2.12H_2O$ and 10 mM glucose). The isolated hearts were cannulated via the aorta onto the perfusion system, whereupon it was retrogradely perfused with a Ca^{2+} free HEPES buffer ("Solution A" containing: 6 mM KCl; 1 mM $NaHPO_4$; 0.2 mM NaH_2PO_4; 1.4 mM $MgSO_4$; 128 mM NaCl; 10 mM HEPES; 5.5 mM D-glucose and 2 mM pyruvate, pH 7.4) at 37ºC for 5 min.

<u>Why Ca^{2+} free buffer?</u> According to Zimmerman et al (1967), Ca^{2+} depletion leads to minimal ultrastructural changes in cells, however when Ca^{2+} is reintroduced, it results in the hypercontraction of the cells. Previous studies (Muir, 1967; Yates & Dhalla, 1975; Ashraf, 1979; Frank et al, 1982) indicated that during Ca^{2+} free circumstances, the intercalated discs in the muscle tissue are becoming partly separated due to the dissociation of the cadherin complexes. Furthermore, the glycocalyx covering the plasma membrane also vanishes in response to downregulated Ca^{2+} conditions. These conditions therefore allow dissociation of myocytes from

each other. If Ca^{2+} is rapidly reintroduced in the uncoupled adjacent cells, it results in contractile activation, which disrupts the weakened cell-cell contact sites. The cells will therefore rupture and terminal Ca^{2+} overload will result in hypercontracture (Piper, 2000).

The hearts were continuously gassed with 100% oxygen (O_2) throughout the perfusion procedure. Following this, the hearts were perfused for 15 min (37℃) in a re-circulating manner with a HEPES digestion buffer ("Solution B" containing: "Solution A" + 0.7% fatty acid free BSA + 1 mg/ml Worthington Collagenase Type II + 18 mM 2,3-butanedione monoxime (BDM)).

BDM is an ATPase inhibitor preventing the activation of the myosin protein and crossbridge formation for contraction.

To prevent Ca^{2+} overload, Ca^{2+} levels were increased slowly by the addition of 50 µl $CaCl_2$ (100 µM) after exactly 20 min and 25 min of the total perfusion time. As soon as the perfusate changed from a dripping to a continuously free flowing state, the heart was fully digested. The digested hearts were detached from the perfusion system, followed by the removal of the ventricles from the atria and connective tissues.

The ventricular tissues were torn apart and incubated in 50 ml post-digestion buffer ("Solution C" containing: 50% of "Solution A" + 50% of "Solution B" + 1% BSA + 1% fatty acid free BSA + 0.2 mM $CaCl_2$) for a period of 15 min under 100% O_2 in a shaking water bath (180 strokes/min at 37ºC). After 15 min of incubation, $CaCl_2$ was added respectively on 15 min, 16 min, 17 min, 18 min and 19 min to the ventricular heart tissue to reach a final concentration of 1.25 mM (4 x 100 µl $CaCl_2$ and 1 x 125 µl of a 100 mM $CaCl_2$ solution). The tissue was then filtered through a 200 x 200 µm nylon mesh and gently centrifuged at 100 rpm for 3 min. The supernatant was aspirated and the pellet was resuspended in 35 ml Solution D ("Solution D" containing: "Solution A" + 2% fatty acid free BSA + 1.25 mM $CaCl_2$) for 5 min. This resuspension step was important to assure that the cells settle under gravity through the 2% BSA solution into a loose cell pellet. As only the viable cardiomyocytes will settle, the supernatant, containing the dead/dying cells, was once again aspirated. The cell pellet was resuspended in 15 ml fresh Solution D, where after which it was left on a slow rotator (30 rpm), under O_2, at room temperature for 1 hour to stabilize. After stabilization, the cells were allowed to settle under gravity for 5 min. The supernatant was gently aspirated and the cells were resuspended in 6 ml Solution E ("Solution E" containing: "Solution A" minus D-glucose and pyruvate + 2.0% fatty acid free BSA + 1.25 mM $CaCl_2$), and spun down at 100 rpm for 3 min. This washing step was repeated 3 times (the supernatant was discarded after every wash) with 6 ml fresh Solution E. After the last wash, the pellet was suspended in a suitable volume of Solution E. The volume depended on the number of conditions to be tested

for the determination of (a) 2DG uptake and (b) Western blotting experiments as described in Chapter 2, Section 7 and Section 8 respectively.

The HEPES, BDM, D-glucose as well as the Na-pyruvate were purchased from Sigma-Aldrich (St Louis, MO), the Worthington Collagenase Type II was obtained from Worthington Biochemical Corporation (Lakewood, NJ) and both BSA's were purchased from Roche (Cape Town).

7. 2DG uptake by cardiomyocytes

2DG refers to a glucose molecule which can be taken up but not metabolized, because it has a hydrogen molecule instead of a 2-hydroxyl group at position C2 of its structure *(Figure 2.1).*

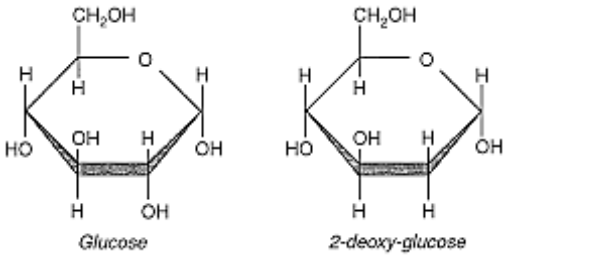

Figure 2.1: *Glucose vs. 2DG structure*

2DG uptake by the cardiomyocytes was measured at different insulin concentrations (Chapter 2, Section 7.1) and with different activators (Chapter 2, Section 7.2) in combination with inhibitors as described below:

Note: The insulin dosage response experiment as described in Chapter 2, Section 7.1 was conducted on young control (250 g weight animals), age-matched control and HFD animals.

7.1. 2DG uptake at different insulin concentrations

500 µl cardiomyocytes (approximately 0.5 mg protein), as prepared in Chapter 2, Section 6, was suspended in different volumes oxygenated Solution E for each variable (Basal, Phloretin, 1 nM insulin (INS 1), 10 nM insulin (INS 10), 100 nM insulin (INS 100)). 50 µl Phloretin (final concentration 400 µM) was added to the Phloretin samples only for the measurement of non-carrier mediated glucose uptake *(Table 2.2).*

(i) Insulin was serially diluted before experimentation:

INS 100: *450 µl Solution E + 50 µl insulin stock [10 µM to 1µM]*

INS 10: *450 µl Solution E + 50 µl 1 µM [to 100 nM insulin]*

INS 1: *450 µl Solution E + 50 µl 100 nM [to 10 nM insulin]*

(ii) The 2DG and Phloretin were prepared as follow:

2DG: *290 µl Deoxy-glucose (45.6 mM stock solution) + 10 µl radioactive (tritiated) Deoxy-glucose*

Phloretin: *450 µl Solution E + 50 µl Phloretin stock [64 mM stock solution in DMSO]*

Insulin, Deoxy-glucose and Phloretin were purchased from Sigma-Aldrich (St Louis, MO), radiolabelled 2DG was purchased from PerkinElmer South Africa (Pty) Ltd.

Table 2.2: *Assay for the determination of 2DG uptake at different insulin concentration (INS 1, 10, 100)*

	Solution E	Myocytes	Insulin	2DG	Phloretin
Basal	175 µl	500 µl		25 µl	50 µl
Phloretin	175 µl	500 µl		25 µl	50 µl
1 nM Insulin	100 µl	500 µl	75 µl	25 µl	50 µl
10 nM Insulin	100 µl	500 µl	75 µl	25 µl	50 µl
100 nM Insulin	100 µl	500 µl	75 µl	25 µl	50 µl

All the cells were incubated at 37℃ in a shaking water bath (180 strokes/ min), where 75 µl INS 1, INS 10 and INS 100 as prepared in Chapter 2, Section 7.1(i) were respectively added after 5 min to the corresponding insulin samples *(Figure 2.2).* After 20 min, glucose uptake was initiated by the addition of 25 µl 2DG as prepared in Chapter 2, Section 7.1(ii) (1.5 µCuries(Ci)/ml; final 2DG concentration 1.8 µM) to all of the samples. At this low concentration of 2DG, the kinetics of uptake of 2DG is equivalent to that of glucose and can therefore be used as a measure of glucose movement into the cell. At higher concentrations, this presumption is not valid, because 2DG at higher concentrations slows the glycolytic process and therefore glucose uptake. 2DG glucose uptake was also shown to be linear under these conditions for up to 60min (Fischer et al, 1991).

After 30 min, glucose uptake was terminated by the addition of 50 µl Phloretin (400 µM) to all the samples (except the Phloretin samples).

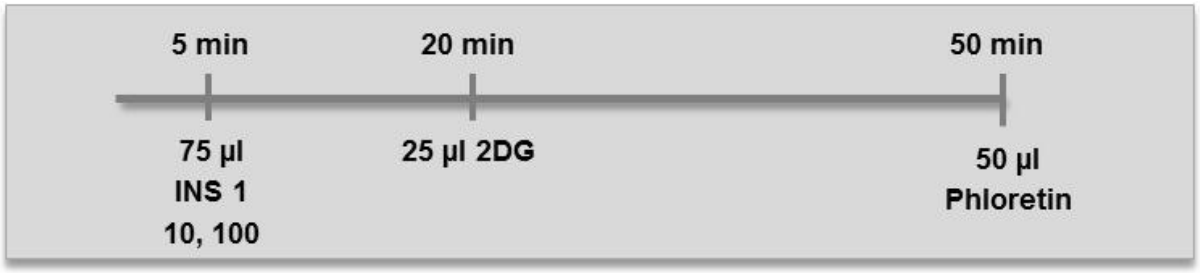

Figure 2.2: *2DG uptake protocol in response to insulin stimulation (INS 1, 10, 100 nM)*

The cells were transferred into Eppendorf tubes and spun down at 14 500 rpm for 90 seconds (sec). The pellets were washed twice with 450 µl HEPES buffer and dissolved in 1 N NaOH. After the pellets were dissolved, an equal volume of distilled water (dH_2O) was added to render a concentration of 0.5 NaOH where after the samples were used for (a) Lowry (Lowry et al, 1951) protein determination and (b) counting of accumulated radio-activity using a scintillation counter.

(a) Lowry protein determination

The Lowry method is a well-known colorimetric assay which entails the interaction of the proteins in the samples with an alkaline copper tartrate (Na-K-Tartrate-CuSO4) and Folin Ciocalteus reagent. Colour development can be visualized when the protein and copper complex in the alkaline buffer is formed, and secondly when a reduction reaction caused by Folin Ciocalteus leads to a spectral shift from 405 nm to 750 nm (Lowry et al, 1951).

BSA standards were prepared as follow from a BSA solution with known concentration determined spectrophotometrically by determining the OD at 280 nm and using the albumin extinction coefficient of 1.51:

Standard 1: 1 ml undiluted BSA in 200 ml 0.5 NaOH.

Standard 2: 2 ml undiluted BSA in 200 ml 0.5 NaOH.

Standard 3: 2 ml undiluted BSA in 100 ml 0.5 NaOH.

The concentration of these standards were then also determined accurately.

In the assay, 50 µl of 0.5 N NaOH was added to the first Luckham tube and served as a blank. Following this, 50 µl of each three BSA standards and samples (in triplicate) were pipetted into the rest of the Luckham tubes. Next, 1 ml Na-K-Tartrate-$CuSO_4$ containing: 0.5 ml 2% Na-K-Tartrate, 0.5 ml 1% $CuSO_4.5H_2O$ and 49 ml 2% Na_2CO_3, was added to each

tube with time intervals of 10 sec between tubes. After 10 min of the first addition of Na-K-Tartrate-$CuSO_4$, 100 µl Folin C (2 ml Folin-Ciocalteu in 4 ml dH_2O) was added to each tube with time intervals of 10 sec between tubes. After every addition, the tubes were vortexed. The tubes were left on the bench for 30 min for optimal reaction, whereafter the OD values were read at 750 nm in a spectrophotometer. A standard curve was set up in Excel by plotting the OD absorbance values on the Y-axis and the standard protein concentration values (mg/ml) on the X-axis. Using the standard curve, the total amount of protein (mg/ml) in each sample was determined.

(b) 2DG uptake

To determine the amount of radioactivity associated with the cells, 100 µl of each sample in duplicate was added to 3 ml scintillation fluid. We also respectively prepared a blank tube containing only scintillation fluid and a radioactive total counts tube containing 25 µl 2DG (as prepared in Chapter 2, Section 7.1(ii)) and scintillation fluid. All the samples were kept overnight in a sealed dark area to minimize chemiluminescence produced by adding the alkaline solution to the scintillation fluid. The total radioactivity was counted in a scintillation counter (Beckman®) beforehand to determine the specific activity of the 2DG solution. Following this, all samples were counted in disintegrations per minute (DPM). Using the total protein values (mg/ml) calculated from the Lowry method, and the DPM values from the scintillation counter, 2DG uptake was calculated and expressed in picomol (pmol) 2DG/mg protein/30min. Lastly, the the average of the Phloretin samples in pmol 2DG/mg protein/30min was subtracted from each sample to correct for background data. Phloretin inhibits all carrier mediated (GLUT1 and GLUT4) glucose uptake, but there is always residual glucose entering the cell, especially through the fructose transporters (Fischer et al, 1991).

INS 10 was used for the following experiments due to its optimal glucose uptake stimulatory capacity. However INS 10 is still a physiological concentration and it will allow any additive responses to be visible, whereas INS 100 is a pharmacological concentration, and it will elicit a maximal response that will mask any additive effect of the substrates used.

7.2. 2DG uptake determination with activators and inhibitors

The same procedure as described in Chapter 2, Section 7.1 was followed for 2DG uptake determination, but in combination with activator INS 10 and inhibitors WM (100 nM) and KU 60019 (3µM) *(Table 2.3).* Phloretin was once again added to the Phloretin samples only before experimentation in the water bath started.

(i) Preparation of activators and inhibitors:

INS 10 and Phloretin as prepared in Chapter 2, Section 7.1(i) and (ii) respectively, was used.

WM (100 nM): *9990 µl Solution E + 10 µl WM stock [2mM]*

KU 60019 (3µM): *990 µl Solution E + 10 µl KU 60019 stock [9mM]*

WM was obtained from Sigma-Aldrich (St Louis, MO) and KU 60019 was obtained from Selleck Chem.

Table 2.3: *Assay for the determination of 2DG uptake with different activator and inhibitors*

	Solution E	Myocytes	WM & KU	Insulin	2DG	Phloretin
Control	175 µl	500 µl			25 µl	50 µl
Phloretin	175 µl	500 µl		25 µl	25 µl	50 µl
INS 10	175 µl	500 µl		75 µl	25 µl	50 µl
WM	162.5 µl	500 µl	37.5 µl		25 µl	50 µl
WM & INS 10	100 µl	500 µl	37.5 µl	75 µl	25 µl	50 µl
KU 60019	175 µl	500 µl	25 µl		25 µl	50 µl
KU 60019 & INS 10	100 µl	500 µl	25 µl	75 µl	25 µl	50 µl

After 5 min of incubation at 37℃ in a water bath (180 strokes/ min) the two inhibitors (WM or KU 60019) were added to the specific cardiomyocytes, followed by the addition of INS 10 to the insulin samples (INS 10, WM & INS 10, KU60019 & INS 10) after an additional 15 min *(Figure 2.3)*. 2GD (as prepared in Chapter 2, Section 7.2(i)) was added at 35 min to initiate glucose uptake in the cells followed by the addition of Phloretin (as prepared in Chapter 2, Section 7.1(ii)) at 65 min to terminate the process.

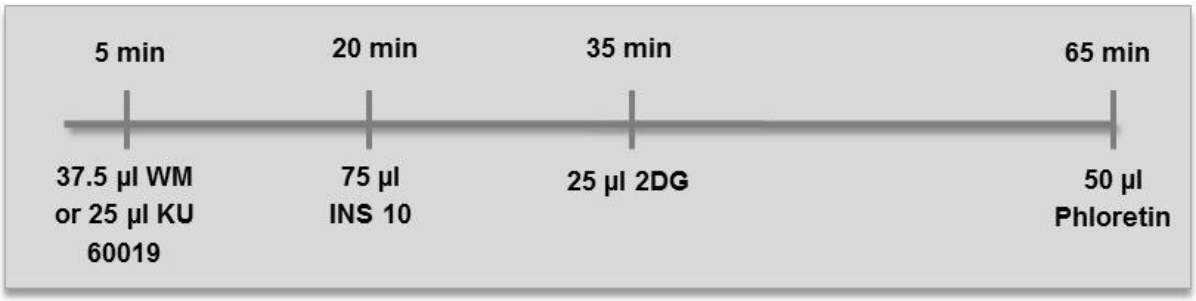

Figure 2.3: *2DG uptake protocol with different activators/inhibitors*

As described in Chapter 2, Section 7.1 the cells were spun down in Eppendorf tubes, washed, and the pellets dissolved in 1N NaOH. The samples were then used for Lowry (Lowry et al, 1951) protein and radiolabel determination and 2DG expressed in pmol 2DG/mg protein/30 min. Lastly, the the average of the Phloretin samples in pmol 2DG/mg

protein/30min was subtracted from each sample to correct for background non-carrier mediated 2DG uptake.

8. Western Blotting

Western blotting was conducted on cardiomyocytes from both the control and HFD animals to determine the expression and activation of certain proteins in the insulin signalling pathway. After the animals were sacrificed, as described in Chapter 2, Section 4, cardiomyocytes were prepared as described in Chapter 2, Section 6. The cardiomyocytes were then manipulated with INS 10, WM and KU 60019 respectively as presented in *Figure 2.3*; however at 35 min, Phloretin was added instead of 2DG as described in Chapter 2, Section 7.1 & 7.2. After the addition of Phloretin, the cells were directly placed on ice to stop all further reactions and spun down at 14 500 rpm for 90 sec. The supernatant was removed and the cells were washed twice with 450 µl HEPES buffer. The pellets were used for lysate preparation as described in the following Section.

8.1. Sample preparation (lysate)

For lysate preparation, the proteins of interest were extracted by the addition of 100 µl lysis buffer to each cell pellet (two volumes of lysis buffer for one volume of cells). The lysis buffer contained: 2 mM Tris-HCl (pH 7.5), 1 mM EGTA, 1 mM EDTA, 150 mM NaCl, 1 mM β-glycerophosphate, 2.5 mM tertasodiumpyrophosphate, 1 mM Na_3VO_4, 1% Triton X-100, 10 µg/ml leupeptin, 10 µg/ml aprotinin and 50 µg/ml PMSF.

Following this, 0.15 millimetre (mm) zirconium oxide beads purchased from Next Advance, were added to each sample (amount of beads added were equal to the pellet size). The samples were homogenized at speed 8 in the Bullet Blender™ for 4 min, where after it was left on ice for 20 min to allow for optimal reaction with the lysis buffer.

After 20 min, the samples were centrifuged at 15 000 rpm for 20 min (4℃). The supernatant of each sample was pipetted in to Eppendorf tubes. Using the Bradford method (Bradford, 1976), the amount of protein in each sample was determined as follows:

The supernatant of each sample was diluted (a) 1:10 (45 µl dH_2O and 5 µl supernatant). The samples were further diluted (b) 1:20 (5 µl of the diluted supernatant (a) and 95 µl dH_2O).

The Bradford assay was set up as indicated below:

- The standards in duplicate:
  - 0 (100 µl dH_2O)
  - 5 (5 µl diluted BSA & 95 µl dH_2O)
  - 10 (10 µl diluted BSA & 90 µl dH_2O)
  - 20 (20 µl diluted BSA & 80 µl dH_2O)
  - 40 (40 µl diluted BSA & 60 µl dH_2O)
  - 60 (60 µl diluted BSA & 40 µl dH_2O)
  - 80 (80 µl diluted BSA & 20 µl dH_2O)

  (Note: 1:4 Diluted BSA = 100 µl BSA stock solution & 400 µl dH_2O)

- Diluted samples in duplicate (b): 5 µl of diluted sample (a) & 95 µl dH_2O

The Bradford solution, containing: 0.6 mM Coomassie Brilliant Blue G-250, 95% ethanol and 50% (v/v) phosphoric acid was diluted 1:5 with dH_2O followed by filtration through a double layer of Whatman filter paper. 900 µl of this diluted Bradford reagent was added to the standards and duplicated samples. The colour changed from a red colour to a blue colour under acidic conditions in the standards and duplicate samples, where after the absorbance was measured at 595 nm in a spectrophotometer. Under the assay conditions, the Coomassie blue bound to protein with a colour development linear to protein concentration at low protein levels.

The standard curve was set up by calculating the mean of the duplicate standard values (mean OD values) using Excel. The protein (µg) values were plotted on the X-axis against the mean OD values on the Y-axis. Using the standard curve, the amount of protein, lysis buffer and Laemmli sample buffer (Laemmli, 1970), that must be added to each sample, to ensure that an equal amount of protein per volume unit used was calculated.

850 µl Laemmli sample buffer (4% SDS, 20% glycerol, 10% 2-mercaptothanol (2-ME), 0.0004% bromophenol blue and 0.125 M Tris-HCl) was diluted with 150 µl 2-ME before it was added to the lysates. After the lysates were prepared using the calculated values, the samples were boiled for 5 min and the aliquots were stored at -80°C.

8.2. Protein separation

Once again, all the stored samples were boiled for 5 min followed by 5 min of centrifuging at 5000 rpm. An equal amount of protein of each sample was loaded per well in the gel using a Hamilton syringe purchased from Sigma-Aldrich (St Louis, MO).

Sample loading:

Positive control: A lysate from a 7-8 week old untreated control rat heart was prepared to serve as the positive control in the study. The same positive control was loaded on to each gel to enable data from one blot to be compared to any other blot. All the samples were always normalized to this positive control. The control and HFD gels were loaded as follow:

Control: Marker, Positive control, 2 x Controls, 2 x INS 10, 2 x WM, 2 x INS 10 + WM, 2 x KU 60019, 2 x INS 10 + KU 60019.

HFD: Marker, Positive control, 1 x Control, 2 x HFD Controls, 2 x INS 10, 2 x WM, 2 x INS 10 + WM, 2 x KU 60019, 2 x INS 10 + KU 60019.

To compare the HFD blots with the control blots, a basal age-matched control sample was loaded on to the HFD blot. Thus, the HFD values could be calculated as a ratio to the control value.

Three different gel preparation techniques were used in the study due to the incorporation of new stain-free techniques in our laboratory and also due to ATM and IRS1 having large molecular sizes of 370 kDa and 180 kDa respectively.

(i) Standard gel preparation

Different percentages of polyacrylamide running gels (7.5%, 10% & 12%) with 4% stacking gels were prepared for the separation of the proteins in the samples as indicated in *Table 2.4*. To identify the molecular weights of the proteins of interest, 5 µl of the protein ladder, obtained from Thermo Scientific was loaded as a marker in the first well of the polyacrylamide gel. The boiled and centrifuged samples were loaded in the following wells and the gel compartment tank was filled with running buffer. The running buffer contained: 50 mM Tris, 384 mM glycine and 1% SDS, pH 8.3. The polyacrylamide gels were subjected to sodium dodecyl sulfate–polyacrylamide gel electrophoresis (SDS-PAGE) for 10 min at 100V, 200mA followed by 50 min at 200V, 200mA. After 60 min, the separated proteins within the polyacrylamide gels were transferred for 1 hour at 200V, 200 mA, to polyvinylidene fluoride

(PVDF) membranes (Immobilon™ P, Millipore), in a transfer buffer filled tank. The transfer buffer contained: 25 mM Tris, 192 mM glycine and 20% methanol, pH 8.3.

Once the transfer period was finished, the membranes were placed in fresh methanol for 30 sec and left to air dry for 15 min. The dry membranes were then immersed in reversible Ponceau red staining (5% Ponceau Red in acetic acid) for 2 min to visualize whether the proteins did transfer from the polyacrylamide gels to the membranes.

The membranes were washed thoroughly with a TBS-Tween solution (Tris-buffered saline (TBS) + 0.1% Tween 20) for 30 min (3 x 10 min) on a lab rotator V1.00.

(ii) Stain-free gel preparation

(a) TGX Stain-Free polyacrylamide gels (7.5%, 10% & 12 %) obtained from Bio-Rad, were prepared by adding the two pre-mixed solutions (for the running and stacking gel respectively) to each other according to the manufacturer's instructions.

(b) Alternatively, stain-free polyacrylamide gels were prepared as described in the Chapter 2, Section 8.2(i), however 50 µl 2,2-Trichloroethanol purchased from Sigma-Aldrich (St Louis, MO), was added to the mixture and 50 µl less water, creating a stain-free gel.

When the gels were set after 40 min, the same sample loading and running procedure as described in Chapter 2, Section 8.2(i) was followed. After the proteins were separated in the polyacrylamide gels, the gels were activated using the Bio-Rad ChemiDoc™ MP System. During the activation time, one can visualize whether the proteins separated equally on the gels. The stain-free polyacrylamide gels were also transferred to PVDF membranes. Once the transfer period was finished, the membranes were scanned to ensure that the proteins did transfer from the gels to the membranes. Scanning was carried out using the Bio-Rad ChemiDoc™ MP System.

The information of the amount of transferred proteins per lane was stored on the Bio-Rad ChemiDoc™ MP System for normalization purposes.

(iii) Precast gels

Bio-Rad Mini-PROTEAN® TGX Stain-Free™ Precast gradient gels purchased from Bio-Rad were used for the determination of Total (T)-ATM, Phospho (P)-ATM, T-IRS1 and P-IRS1. The same sample loading protocol was followed as described in Chapter 2, Section 8.2; however a specific HiMark™ Pre-Stained Protein ladder purchased at Novex®, Thermo

Scientific was loaded in the first well. The HiMark™ ladder range between 30-460 kDa and is therefore specifically designed for proteins with high molecular weights.

After loading the samples, the gel compartment tank was once again filled with running buffer. To compensate for the big ATM (370 kDa) and IRS1 (180 kDa) proteins, the stain-free precast gels were subjected for 90 min to SDS-PAGE at 200V, 200mA. After the proteins were separated on the stain-free precast gels, the gels were activated using the Bio-Rad ChemiDoc™ MP System to visualize whether the proteins separated equally on the gels.

Proteins on the stain-free precast gels were transferred to PVDF membranes for 90 min at 200V, 200mA. The transfer buffer, containing half the amount of methanol than previously described, was specially prepared for optimal transfer of the big ATM and IRS1 proteins. After the transfer period, the membranes were scanned to ensure that the proteins did transfer from the gels to the membranes. Scanning was once again carried out using the Bio-Rad ChemiDoc™ MP System and the data was stored on the system for normalization purposes.

8.3. Immunodetection of protein

The membranes where incubated for 2 hours at room temperature in 50 ml 5% milk (5 g fat free milk powder purchased from Elite, dissolved in 100 ml TBS-Tween solution). This step was to ensure non-specific site blocking. When the blocking period was finished, the membranes were washed with the TBS-Tween solution for 30 min (3 x 10 min) on the lab rotator V1.00. These membranes were individually subjected to primary antibodies directed against: T-IRS1 and P-IRS1 (Ser307), T-PI3K and P-PI3K p85 (Tyr458)/p55 (Tyr199), T-PTEN and P-PTEN (Ser380/Thr382/Tyr383), T-ATM and P-ATM (Ser1981), T-PKB and P-PKB (Ser473), T-AS160 and P-AS160 (Thr642), T-GSK-3β and P- GSK-3β (Ser9), T-AMPK and P-AMPK (Thr172), and GLUT4 respectively where after it was left to incubate at 4℃ overnight. The antibodies were diluted in TBS-Tween or in primary SignalBoost™ Immunoreaction Enhancer. SignalBoost™ was used to enhance the signal of certain antibodies e.g. IRS1, ATM and GLUT4.

All the antibodies were rabbit monoclonal antibodies, except for GLUT4 which was a mouse monoclonal antibody.

Table 2.4: *Western Blot analysis*

Protein	Molecular Size (kDa)	% Running gels	% Stacking gels	Primary Antibody dilutions	Secondary Antibody dilutions	Exposure Method
IRS-1	180	Precast 4-15 %		7.5 µl/5ml primary SignalBoost™	2.5 µl/10ml TBS-Tween	Dark Room
PI3K	85	12 %	4 %	7.5µl/5ml TBS-Tween	2.5 µl/10ml 2.5 % milk	ChemiDoc™ MP System
PTEN	54	10 %	4 %	7.5µl/5ml TBS-Tween	2.5µl/10ml 2.5 % milk	ChemiDoc™ MP System
ATM	370	Precast 4-15 %		7.5µl/5ml primary SignalBoost™	2µl/5ml secondary SignalBoost™	Dark Room
PKB	56	10 %	4 %	7.5µl/5ml TBS-Tween	2.5 µl/10ml TBS-Tween	ChemiDoc™ MP System
AS160	160	7.5 %	4 %	7.5µl/5ml TBS-Tween	2.5 µl/10ml 2.5 % milk	ChemiDoc™ MP System
GSK-3β	47	10 %	4 %	7.5µl/5ml TBS-Tween	2.5 µl/10ml TBS-Tween	ChemiDoc™ MP System
AMPK	62	10 %	4 %	7.5µl/5ml TBS-Tween	2.5 µl/10ml 2.5 % milk	ChemiDoc™ MP System
GLUT 4	45-54	10 %	4 %	7.5µl/5ml primary SignalBoost™	2.5 µl/10ml TBS-Tween	ChemiDoc™ MP System

After incubation, the membranes were washed in TBS-Tween solution for 30 min (3 x 10 min) on the lab rotator V1.00. An Anti-rabbit immunoglobulin G, HRP- conjugated secondary antibody (from donkey), purchased from Cell Signaling Technology, Inc, was diluted according to *Table 2.4* for all the antibodies except GLUT4. The GLUT4 incubated membranes were probed in diluted Anti-mouse immunoglobulin G, HRP- conjugated secondary antibody also purchased from Cell Signaling Technology, Inc. The secondary antibody for ATM was diluted in secondary SignalBoost™ Immunoreaction Enhancer to enhance the secondary signal.

Membranes were immersed in these diluted secondary antibodies for 1 hour. During this time, the secondary antibody bound to the primary antibody to eventually initiate the signal. The membranes were washed again in TBS-Tween solution for 30 min (3 x 10 min) on the lab rotator V1.00 to remove the excess secondary antibody.

To visualize the proteins of interest on the membranes, Clarity™ enhanced chemiluminescence (ECL), purchased from Bio-Rad, was added to each membrane and left to incubate for 5 min.

Following this, the membranes were exposed either (i) in the Dark Room or (ii) using the Bio-Rad ChemiDoc™ MP System.

(i) Dark Room

The ATM and IRS1 membranes were exposed to an autoradiography film (Amersham™ Hyperfilm™ ECL). During the exposure time, the HRP (secondary antibody) reacts with the specific detection reagent in the ECL which results in a light emission. This signal is captured on the radiography film which is then developed and fixed. After thorough washing with water, the radiography films were allowed to dry where after they were laser-scanned for densitometry. Once scanned the band intensities were quantified using the program UN-SCAN-IT ^{TM} (version 5.1, Silkscience) image analysis.

(ii) Bio-Rad ChemiDoc™ MP System

The stain-free membranes were exposed in the Bio-Rad ChemiDoc™ MP System. The exposure time as well as the number of images one would like to take was set beforehand and visualised throughout the procedure. If the bands were coloured red, the blot was overexposed and not used for analysis purposes. The best images were saved for normalisation of the density of the individual bands against the total amount of protein per lane transferred to the PVDF membrane that was previously stored.

8.4. Stripping of the membranes

All the total probed membranes were stripped and re-probed/reblotted with the specific phospho antibodies. The stripping procedure included: incubation of the membranes 2 x 5 min in dH_2O, 1 x 5 min in 0.2 M NaOH and again 2 x 5 min in distilled water. After stripping, the membranes were blocked in 5% milk, and the same procedures as described in Chapter 2, Section 8.3 followed.

9. Statistical analysis

All the data were statistically analysed using GraphPad Prism 5. All values were expressed as Mean ± Standard Error of the Mean (SEM). One-way Analysis of Variance (ANOVA), followed by a Bonferroni post-hoc test was performed to determine the differences in response to different treatments on both the control and HFD animals. A Two-way ANOVA with repeated measures was performed to determine significant differences obtained for the OGTT analysis.

Furthermore, a Two-way ANOVA was performed on P-ATM, P-PI3K and P-PKB from both the control and HFD animals to specifically determine the effect of KU 60019 on baseline P-PI3K levels and insulin stimulated phosphorylation of ATM and PKB. A p-value of < 0.05 was regarded as significant.

CHAPTER 3: RESULTS

Over a period of 16 weeks, half of the animals received a HFD (containing 40% fat) to induce insulin resistance compared to group two, the age-matched controls. Using both these animal models, the relationship between ATM and insulin signalling/ insulin resistance was investigated.

1. Biometric data:

1.1. Body weight, IP fat weight, Fasting blood glucose levels, Insulin and HOMA IR index

Table 3.1: *Biometric data*

	Body weight (grams)	IP fat weight (grams)	Fasting Blood glucose levels (mmol/L)	Insulin (mIU/ml)	HOMA IR index
Control	430.66 ± 15.48 (n = 25)	19.06 ± 1.52 (n = 25)	4.71 ± 0.05 (n = 10)	6.68 ± 2.21 (n = 6)	1.55 ± 0.70 (n = 6)
HFD	462.84 ± 10.32 (n = 25)	33.68 ± 2.42 (n = 25) ***	5.4 ± 0.15 (n = 10) ***	14.58 ± 2.04 (n = 5) *	4.68 ± 0.87 (n = 5) *

HOMA IR index; n = 25 per group for the Body weight and IP fat weight; n = 10 for Fasting blood glucose levels; n = 6 for control Insulin and HOMA IR index levels, n = 5 for HFD insulin and HOMA IR index levels. The data are expressed as Mean ± SEM (p < 0.05; *** p < 0.001 HFD vs. control).*

1.2. Body Weight

The Body weight of the control (430.66 ± 15.48 g) and HFD (462.84 ± 10.32 g) animals showed no significant differences. Therefore, consumption of the HFD did not increase the overall body weight gain of these animals; n = 25 per group *(Table 3.1; Figure 3.1).*

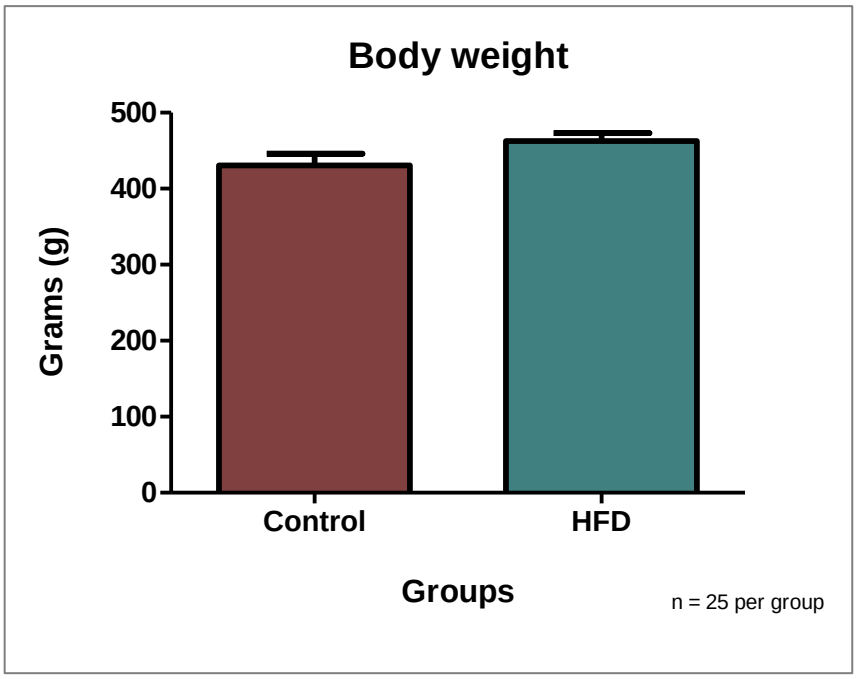

Figure 3.1: *Body weight (g) of the control vs. the HFD animals measured after 16 weeks*

1.3. IP fat weight

After 16 weeks, the HFD animals gained significantly more IP fat than the control animals (33.68 ± 2.42 g vs. 19.06 ± 1.51 g; $p < 0.001$ (HFD vs. control); n = 25 per group *(Table 3.1; Figure 3.2).*

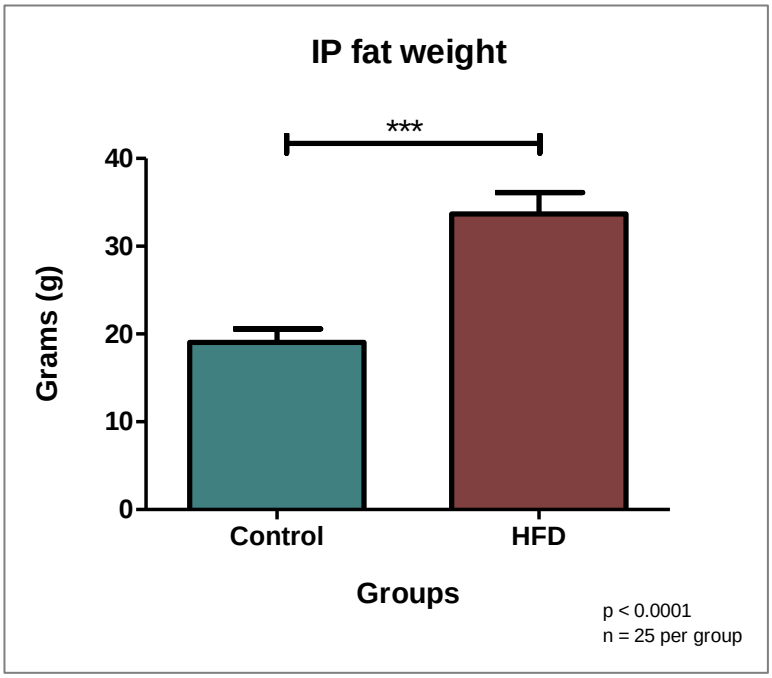

Figure 3.2: *IP fat weight (g) of the control vs. the HFD animals measured after 16 weeks*

1.4. OGTT

In week 15, a group of animals was fasted overnight to determine their glucose tolerance by performing an OGTT. The baseline glucose levels (0 min) of the control and HFD animals differed significantly (4.72 ± 0.05 vs. 5.72 ± 0.16 mmol/L; $p < 0.001$) *(Table 3.2, Figure 3.3)*. When 1g/kg sucrose was orally administered to the animals, the HFD animals presented with significantly higher glucose levels from 3 min to 45 min when compared to the control animals. There were no significant differences between the groups at 60 min and 90 min respectively; however after 120 min the HFD animals once again displayed a significantly higher blood glucose concentration when compared to the control animals (4.67 ± 0.19 vs. 5.44 ± 0.20; $p < 0.05$); n = 9 for the control group, n = 5 for the HFD group.

Table 3.2: *OGTT (mmol/L plasma glucose) values in the control and HFD animals*

OGTT		
Time (min)	Control	HFD
	Mean ± SEM	
0	4.72 ± 0.05	5.72 ± 0.16 ***
3	5.16 ± 0.26	6.66 ± 0.22 **
5	5.08 ± 0.16	7.46 ± 0.37 ***
10	6.31 ± 0.20	8.06 ± 0.46 **
15	6.74 ± 0.19	8.40 ± 0.33 ***
20	6.83 ± 0.28	8.18 ± 0.45 *
25	6.74 ± 0.25	8.10 ± 0.39 *
30	6.31 ± 0.34	7.66 ± 0.40 *
45	5.44 ± 0.40	7.20 ± 0.34 *
60	5.36 ± 0.44	6.60 ± 0.20
90	5.18 ± 0.36	5.56 ± 0.26
120	4.67 ± 0.19	5.44 ± 0.20 *

OGTT data is expressed as Mean ± SEM. n = 9 for the control animals; n = 5 for the HFD animals ($p < 0.05$; ** $p < 0.01$; *** $p < 0.001$ HFD vs. control). A Two-way ANOVA with repeated measures was performed to determine significant differences.*

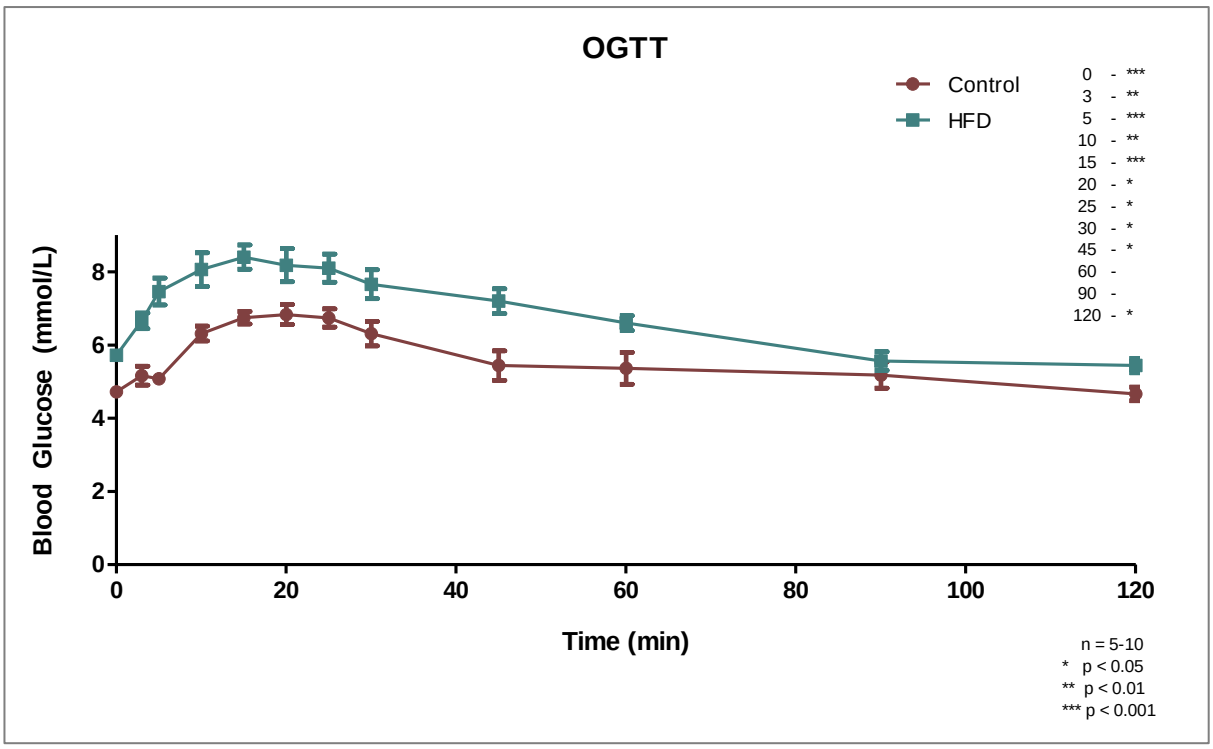

Figure 3.3: *OGTT (mmol/L plasma glucose) of control and HFD animals measured in week 15 at 3 min, 5 min, 10 min, 15 min, 20 min, 25 min, 30 min, 45 min, 60 min and 120 min respectively, after the administration 1g/kg sucrose*

1.5. Basal blood glucose levels

After 16 weeks on the respective diets, the basal blood glucose levels of the HFD group (5.4 ± 0.15 mmol/L; n =10) was significantly increased when compared to the control group (4.71 ± 0.05 mmol/L; n = 10); p = 0.0004 (HFD vs. control) *(Table 3.1; Figure 3.4).*

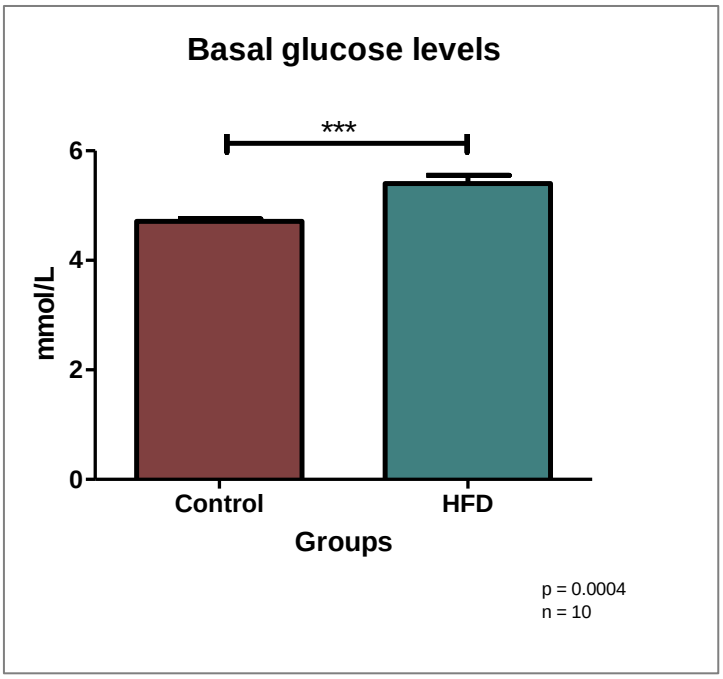

Figure 3.4: *Basal glucose levels (mmol/L) of fasting control vs. HFD animals measured after 16 weeks*

1.6. Insulin levels

The fasting insulin levels of the HFD group was significantly elevated when compared to the control group; p= 0.03 (HFD vs. control). The HFD animals (n = 5) displayed insulin levels of 14.58 ± 2.03 mIU/ml, whereas the control group (n = 6) presented with lower insulin levels of 6.68 ± 2.21 mIU/ml *(Table 3.1; Figure 3.5).*

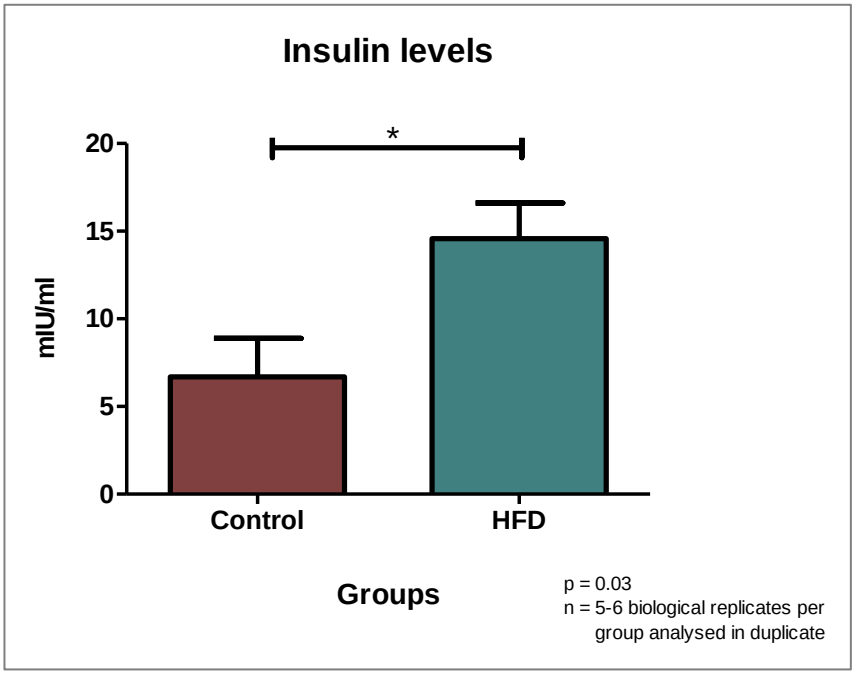

Figure 3.5: *Insulin levels (*mIU/ml*) of the control vs. the HFD animals measured after 16 weeks*

1.7. HOMA IR index

The HOMA IR index of the HFD group (4.68 ± 0.87; n = 5) was significantly higher when compared to the control group (1.55 ± 0.70, n = 6); p = 0.0188 (HFD vs. control) *(Table 3.1; Figure 3.6).*

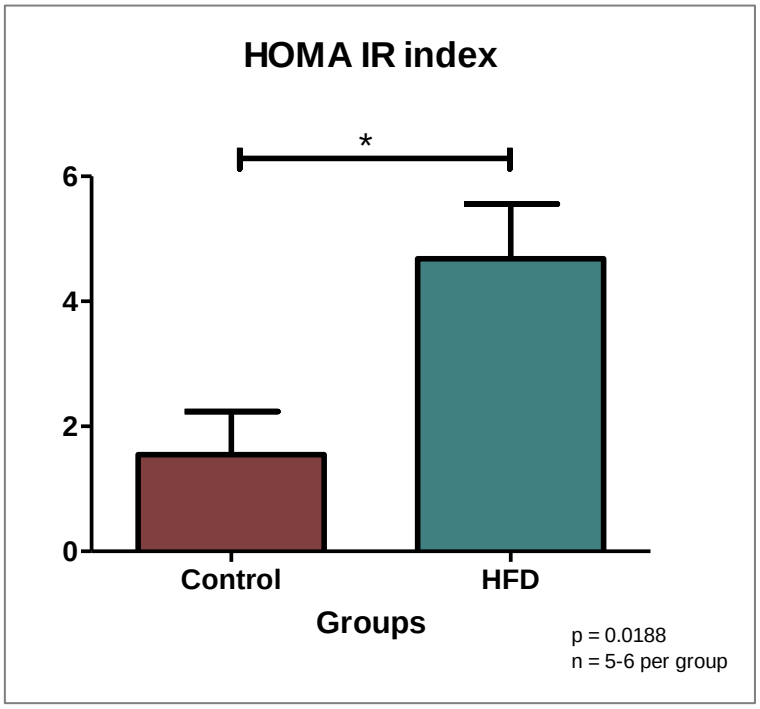

Figure 3.6: *HOMA IR index values of the control vs. the HFD animals after 16 weeks*

2. 2DG uptake

2.1. 2DG uptake levels (pmol 2DG/mg protein/30min) in cardiomyocytes from young control animals in response to Chloroquine stimulation

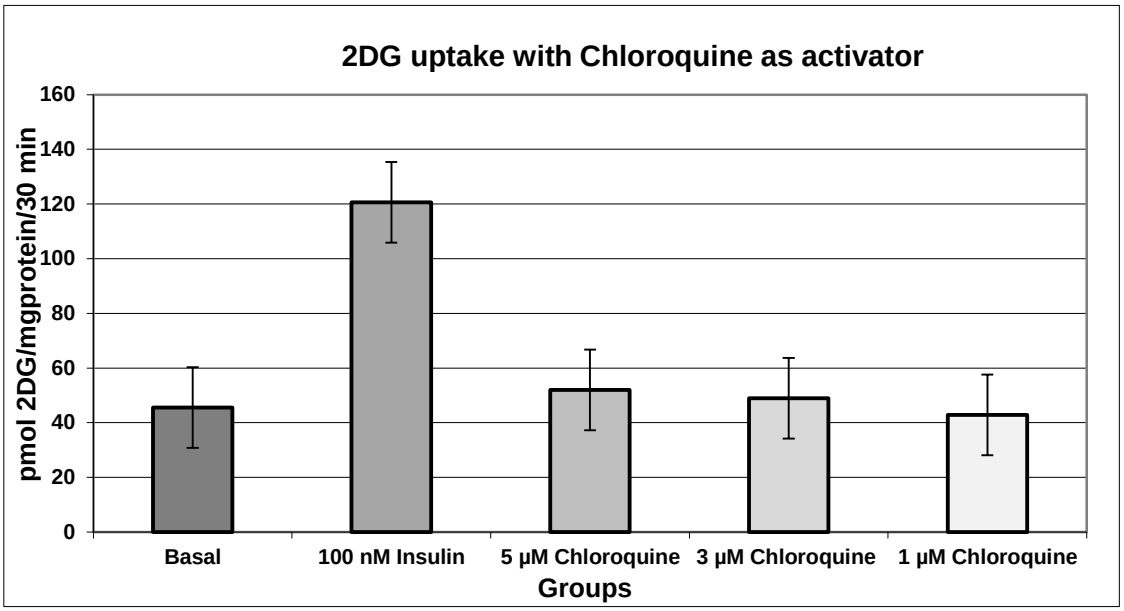

Figure 3.7(a): *2DG uptake levels (pmol 2DG/mg protein/30min) in response to treatment with 5 µM, 3 µM and 1 µM Cholorquine*

As Choloroquine did not initiate 2DG uptake, it was not further used in the study as an activator.

2.2. 2DG uptake levels (pmol 2DG/mg protein/30min) in the cardiomyocytes from control, age-matched control and HFD animals in response to insulin stimulation (1 nM, 10 nM, 100 nM)

Cardiomyocytes from the age-matched control animals presented with significantly lower basal 2DG uptake levels and also in response to INS 10 and INS 100 stimulation when compared to cardiomyocytes from the young control animals (n = 3-11 biological replicates per group analysed in duplicate; #, ##, ###, $p < 0.01$ to the respective column with similar sign) *(Figure 3.7(b)).* Stimulation with INS 10 and INS 100 respectively increased 2DG uptake in cardiomyocytes from young control animals when compared to cardiomyocytes from baseline young control values, n = 3-11 biological replicates per group analysed in duplicate; $p < 0.01$. Furthermore, in cardiomyocytes from the age-matched controls INS 10 and INS 100 also significantly increased 2DG uptake when compared to baseline cardiomyocyte age-matched values, n = 5 biological replicates per group analysed in duplicate; $p < 0.05$ and $p < 0.01$ respectively. In the HFD animals INS 10 and INS 100 significantly increased 2DG uptake in the cardiomyocytes when compared to baseline HFD values; n = 3-5 biological replicates per group analysed in duplicate; $p < 0.05$. No differences were observed between the cardiomyocytes from age-matched control and HFD animals.

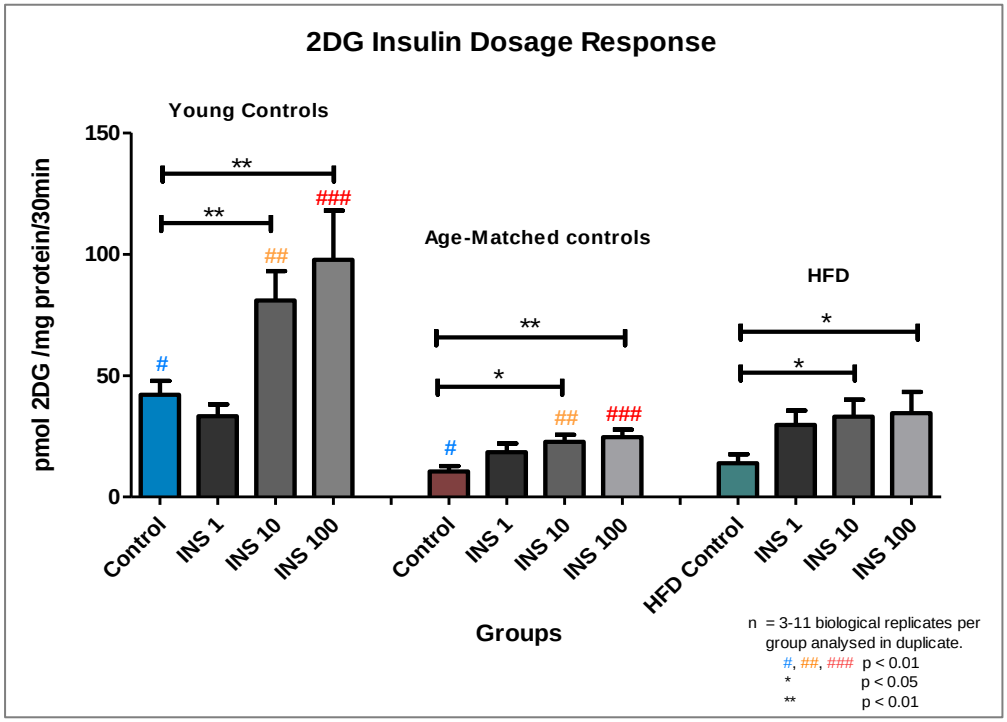

Figure 3.7(b): *2DG uptake levels (pmol 2DG/mg protein/30min) in response to the respective stimulation with 1 nM, 10 nM and 100 nM insulin in young control, age-matched control and HFD cardiomyocytes*

2.3. 2DG uptake levels (pmol 2DG/mg protein/30min) measured in the cardiomyocytes from control and HFD animals in response to treatment with activator (INS 10) and inhibitors (WM & KU 60019).

The 2DG uptake in the cardiomyocytes from control animals were significantly elevated in response to INS 10 stimulation when compared to baseline control values (n = 3-7 biological replicates per group analysed in duplicate; $p < 0.05$). When the control cardiomyocytes were further treated with both WM and KU 60019 in combination with INS 10, the 2DG uptake levels significantly decreased for both conditions ($p < 0.05$ and $p < 0.01$ respectively) when compared to INS 10 *(Figure 3.8).*

HFD cardiomyocytes stimulated with INS 10, presented with significantly higher 2DG uptake levels when compared to the baseline HFD values (n= 3-5 biological replicates per group analysed in duplicate; $p < 0.001$). Furthermore, after treatment with WM in combination with INS 10, 2DG uptake was significantly decreased when compared to HFD INS 10; $p < 0.001$. Treatment with the ATM inhibitor, KU 60019 in combination with INS 10 also significantly lowered 2DG uptake when compared to HFD INS 10; $p < 0.05$) *(Figure 3.8).* No differences were observed between cardiomyocytes from the control and HFD animals.

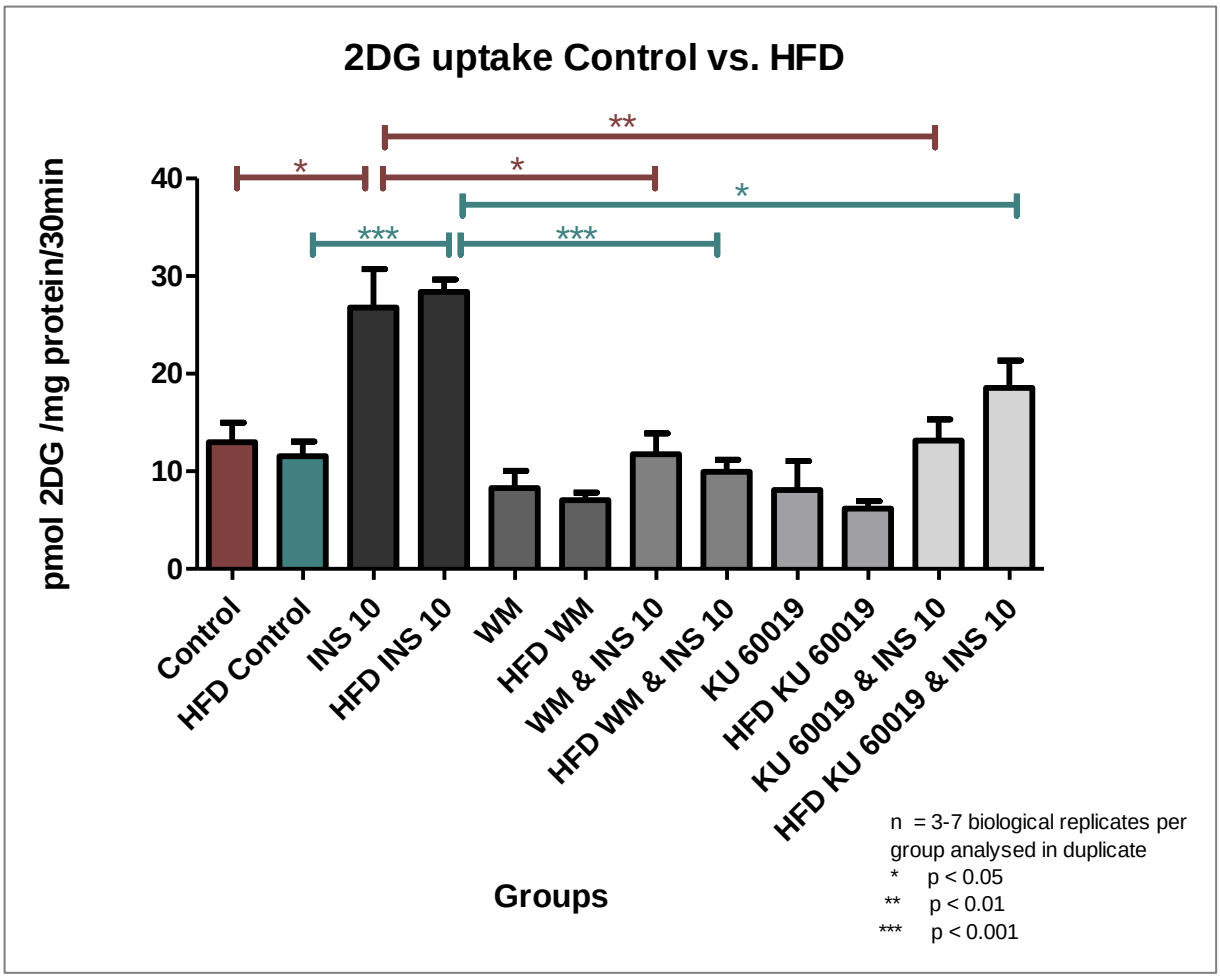

Figure 3.8: *2DG uptake values for cardiomyocytes from control and HFD animals treated respectively with the specific activator (INS 10 nM) and inhibitors (WM and KU 60019)*

3. Western Blot data

Western Blotting was performed on cardiomyocytes from both the age-matched control and HFD animas manipulated with the activator, INS 10; the PI3K inhibitor, WM; and the ATM inhibitor, KU 60019, to measure the expression and activation of important insulin signalling intermediates such as IRS1, PI3K, PTEN, PKB, AS160, GSK-3β, AMPK and GLUT4. The expression and phosphorylation of ATM was also determined in cardiomyocytes from both animal models treated under the same conditions, to identify the postulated relationship between ATM and insulin signalling.

In the following Sections, the total expression (a & b), phosphorylation (c & d) and the P:T Ratio (e & f) will be presented as graphs for cardiomyocytes from both the age-matched control and HFD animals.

The total- and phospho-protein graphs of the HFD animals are presented as a ratio to the age-matched control loaded on that same gel. Consequently the HFD animals could be compared to the control animals.

The positive control (+C), a 7-8 week untreated control, was loaded in to the first well of each blot for normalization purposes only.

3.1. IRS1

a) Total (T) expression control

No significant differences were observed in the T-IRS1 expression in the cardiomyocytes from control animals; n = 2 biological replicates per group analysed in duplicate *(Figure 3.9).*

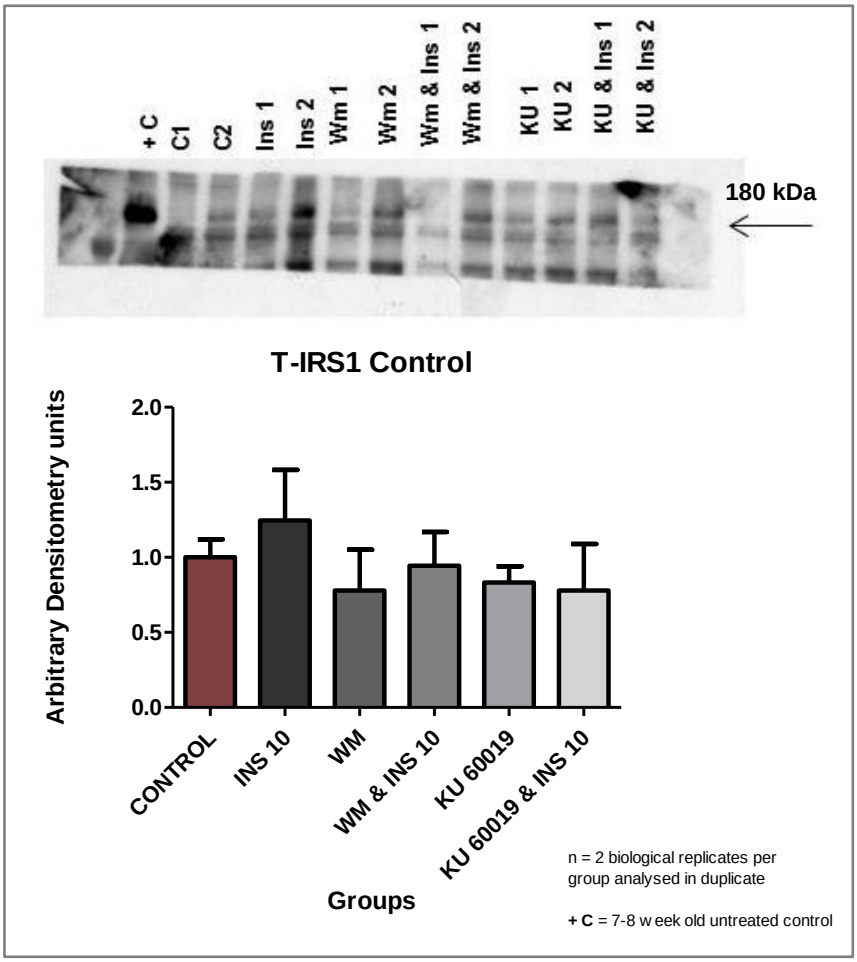

Figure 3.9*: T-IRS1 expression (Arbitrary Densitometry units) in the cardiomyocytes from control animals*

b) Total (T) expression HFD

In response to the inhibition with WM, T-IRS1 expression in the cardiomyocytes from HFD animals were downregulated when compared to the baseline HFD animals; n = 1 biological replicate per group analysed in duplicate; $p < 0.05$ (WM vs. HFD control) *(Figure 3.10).*

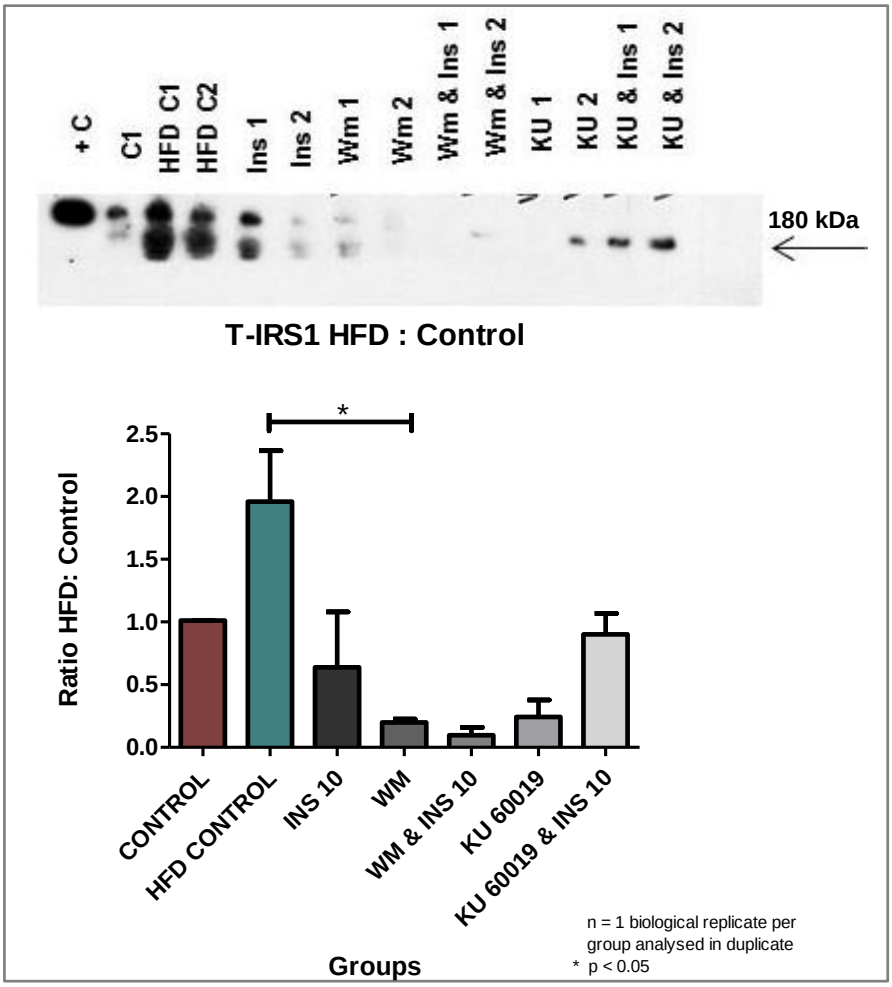

***Figure 3.10**: T-IRS1 expressed as a HFD: Control Ratio*

c) *Phosphorylated (P) levels control*

In the cardiomyocytes from control animals, no significant differences were observed in the phosphorylation of IRS1; n = 2 biological replicates per group analysed in duplicate *(Figure 3.11).*

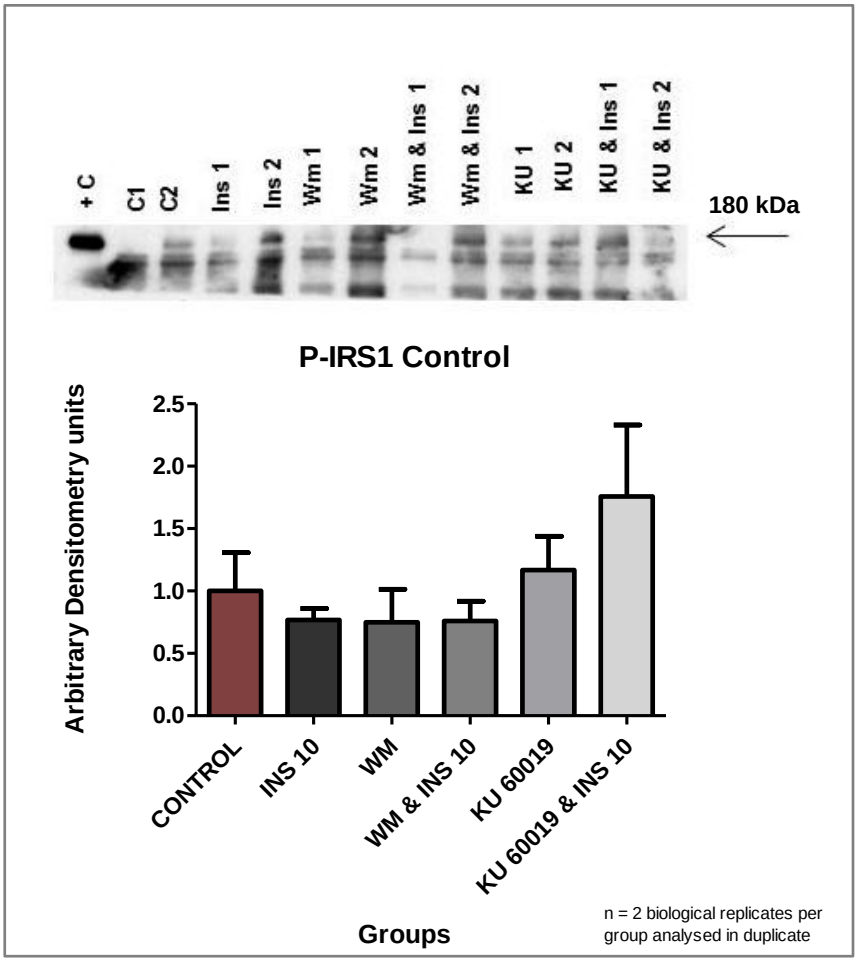

Figure 3.11*: P-IRS1 levels (Arbitrary Densitometry units) in the cardiomyocytes from control animals*

d) Phosphorylated (P) levels HFD

The cardiomyocytes from HFD animals showed significantly increased basal phosphorylation of IRS1 at Ser307 when compared to the cardiomyocytes from control animals; n = 1 biological replicate per group analysed in duplicate; $p < 0.05$ (HFD control vs. control). Furthermore, the cardiomyocytes from HFD animals treated with WM and KU 60019 respectively, and in combination with INS 10, presented with significantly decreased phosphorylation of IRS1 when compared to the baseline HFD group and the INS 10 group respectively; $p < 0.05$ (KU 60019 or WM vs. HFD control; KU 60019 & INS 10 or WM & INS 10 vs. INS 10) *(Figure 3.12).*

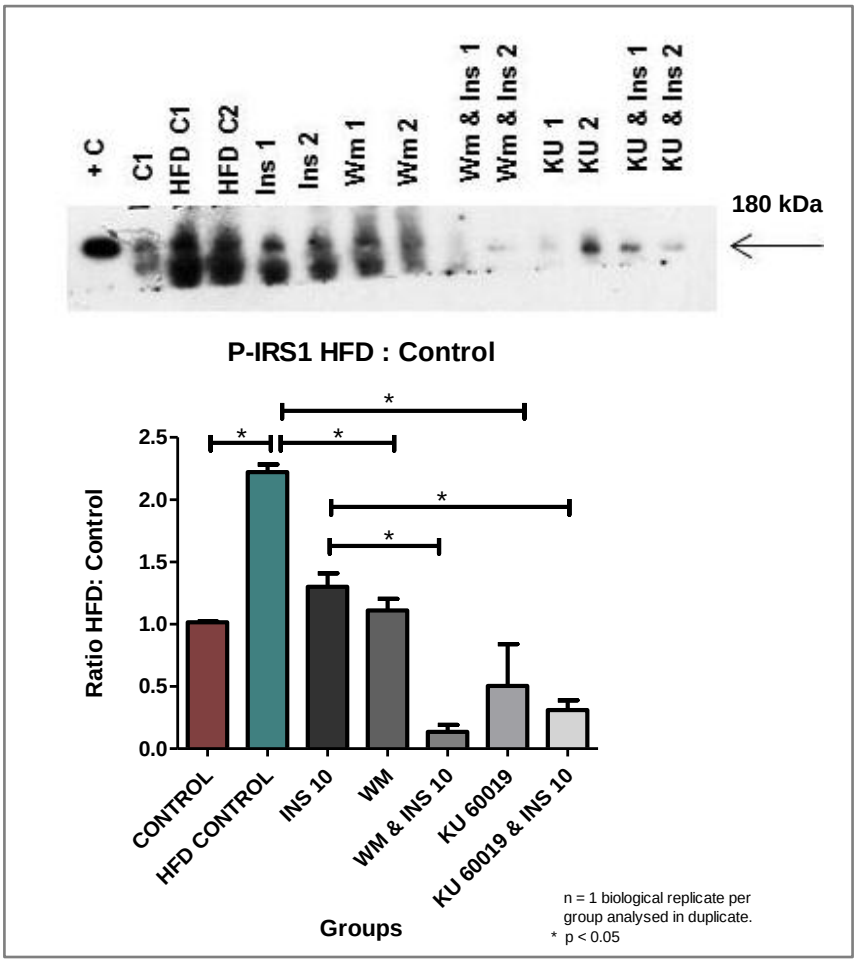

***Figure 3.12**: P-IRS1 levels expressed as a HFD: Control Ratio*

e) P:T Ratio control

The Ratio of phosphorylated vs. total IRS1 showed no significant differences in the cardiomyocytes from the control untreated and treated animals; n = 2 biological replicates per group analysed in duplicate *(Figure 3.13).*

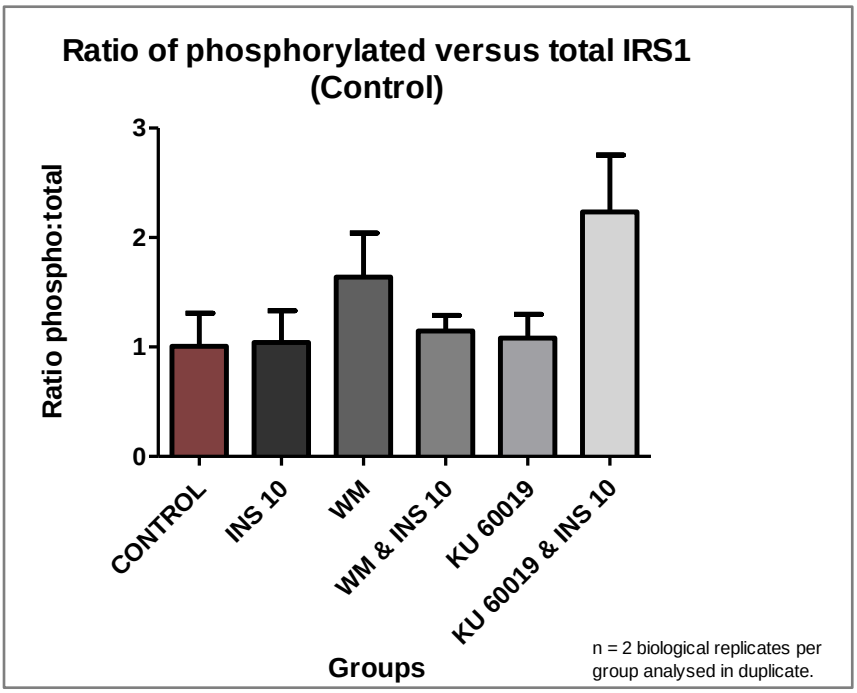

Figure 3.13*: Ratio of phosphorylated vs. total levels of IRS1 in the cardiomyocytes from control animals*

f) P:T Ratio HFD

The Ratio of phosphorylated vs. total IRS1 in cardiomyocytes from the baseline HFD animals significantly increase when treated with WM; n = 1 biological replicate per group analysed in duplicate; $p < 0.05$ (WM vs. HFD control) *(Figure 3.14).*

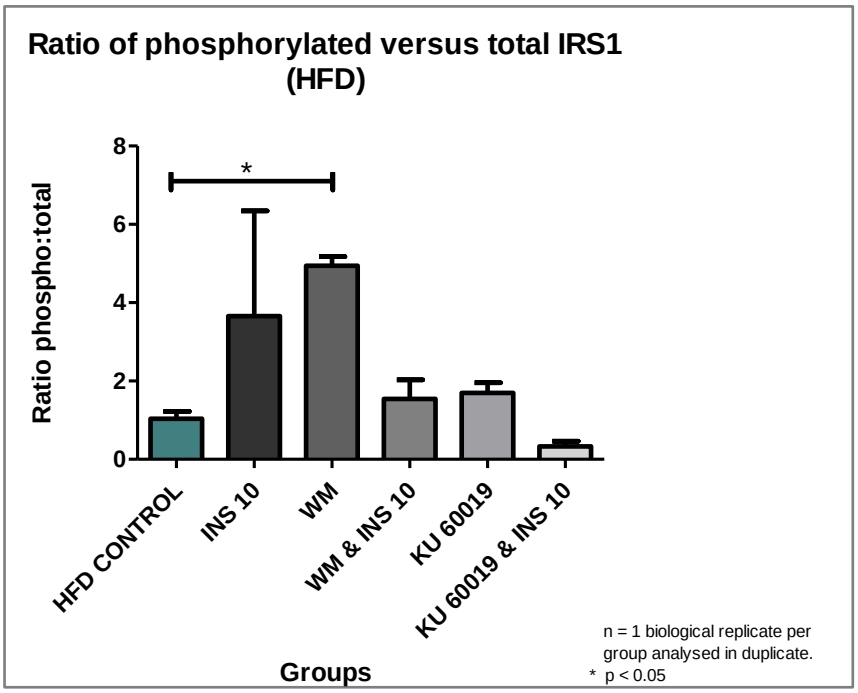

Figure 3.14*: Ratio of phosphorylated vs. total levels of IRS1 in the cardiomyocytes from HFD animals*

3.2. PI3K

a) Total (T) expression control

No significant differences were observed in the total expression of PI3K in the cardiomyocytes from control animals; n = 4-6 biological replicates per group analysed in duplicate *(Figure 3.15).*

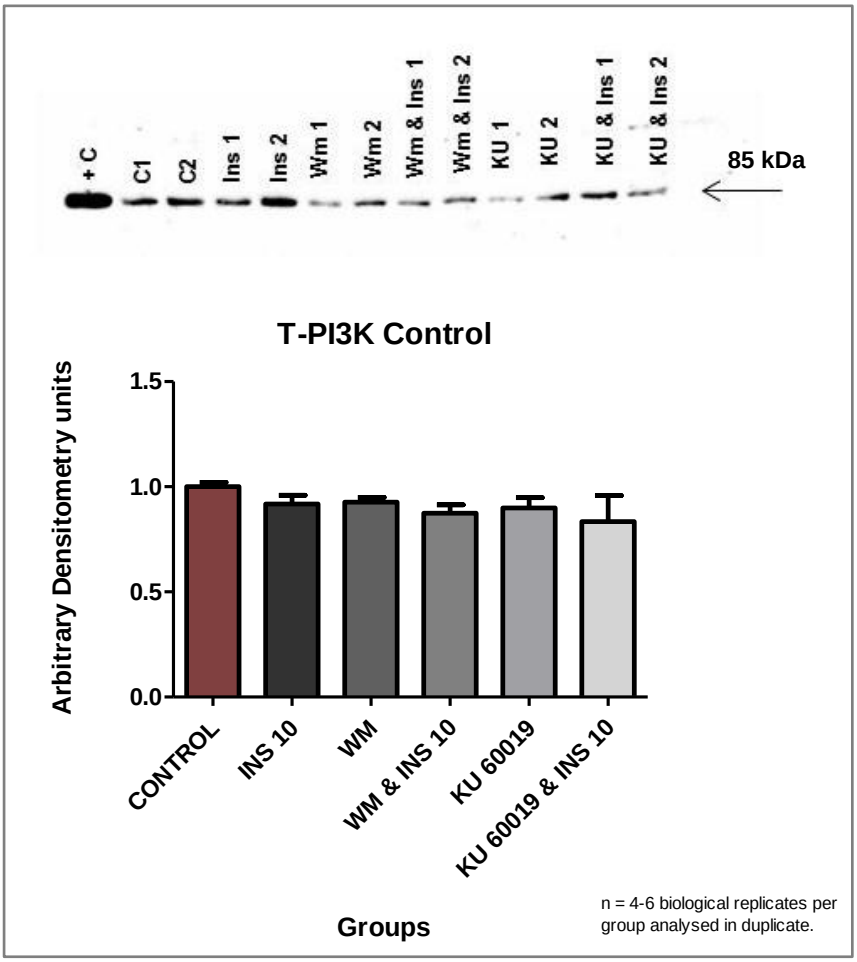

Figure 3.15*: T-PI3K expression (Arbitrary Densitometry units) in the cardiomyocytes from control animals*

b) Total (T) expression HFD

T-PI3K expression in the cardiomyocytes from HFD animals were significantly downregulated at baseline when compared to the cardiomyocytes from control animals; n = 3-5 biological replicates per group analysed in duplicate; $p < 0.01$ (HFD control vs. control) *(Figure 3.16).*

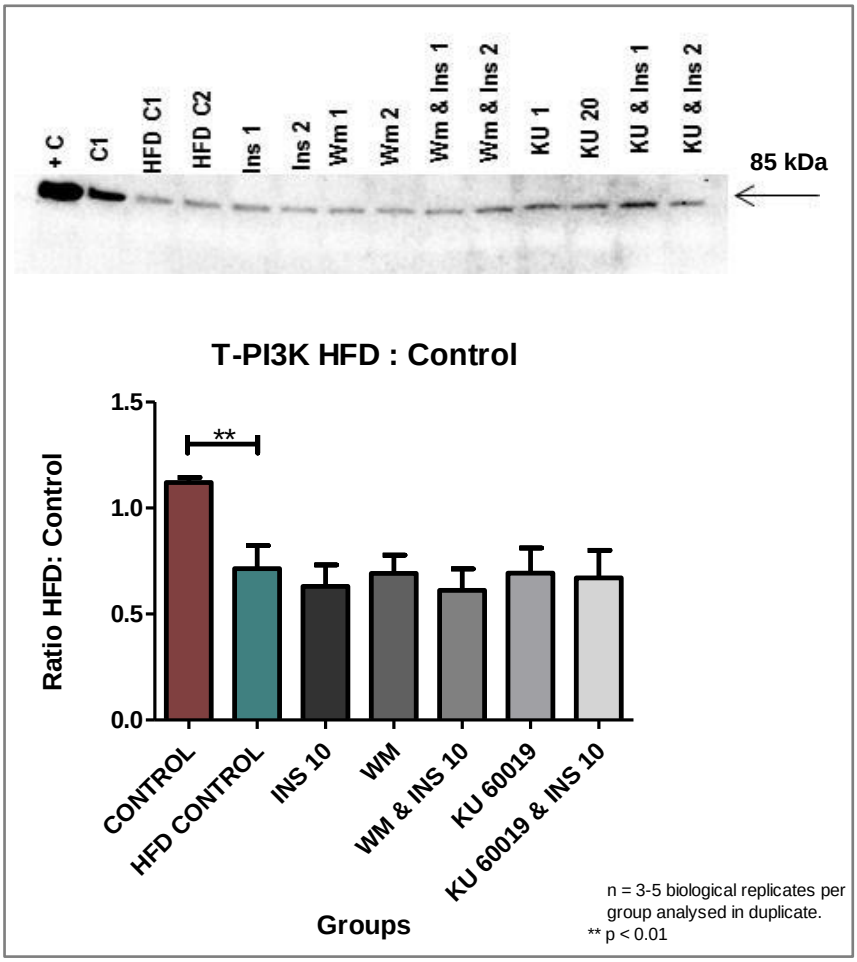

***Figure 3.16**: T-PI3K expressed as a HFD: Control Ratio*

c) Phosphorylated (P) levels control

The phosphorylation of PI3K significantly decreased in the cardiomyocytes from control animals when treated with KU 60019; n = 4-6 biological replicates per group analysed in duplicate; $p < 0.01$ (KU 60019 vs. control) *(Figure 3.17).*

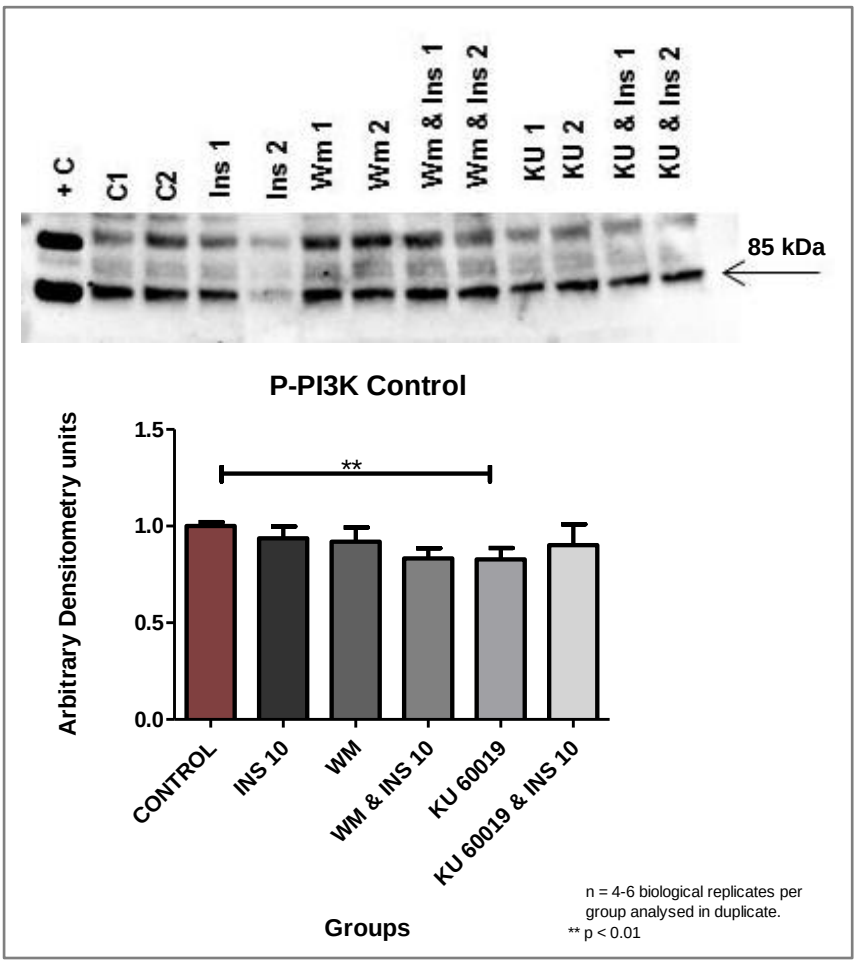

***Figure 3.17**: P-PI3K levels (Arbitrary Densitometry units) in the cardiomyocytes from control animals*

d) Phosphorylated (P) levels HFD

No significant differences were observed between the phosphorylation of PI3K in the cardiomyocytes from control and HFD animals at baseline. Furthermore, there were also no differences in phosphorylation of PI3K in the cardiomyocytes from different HFD treated groups; n = 3-5 biological replicates per group analysed in duplicate *(Figure 3.18).*

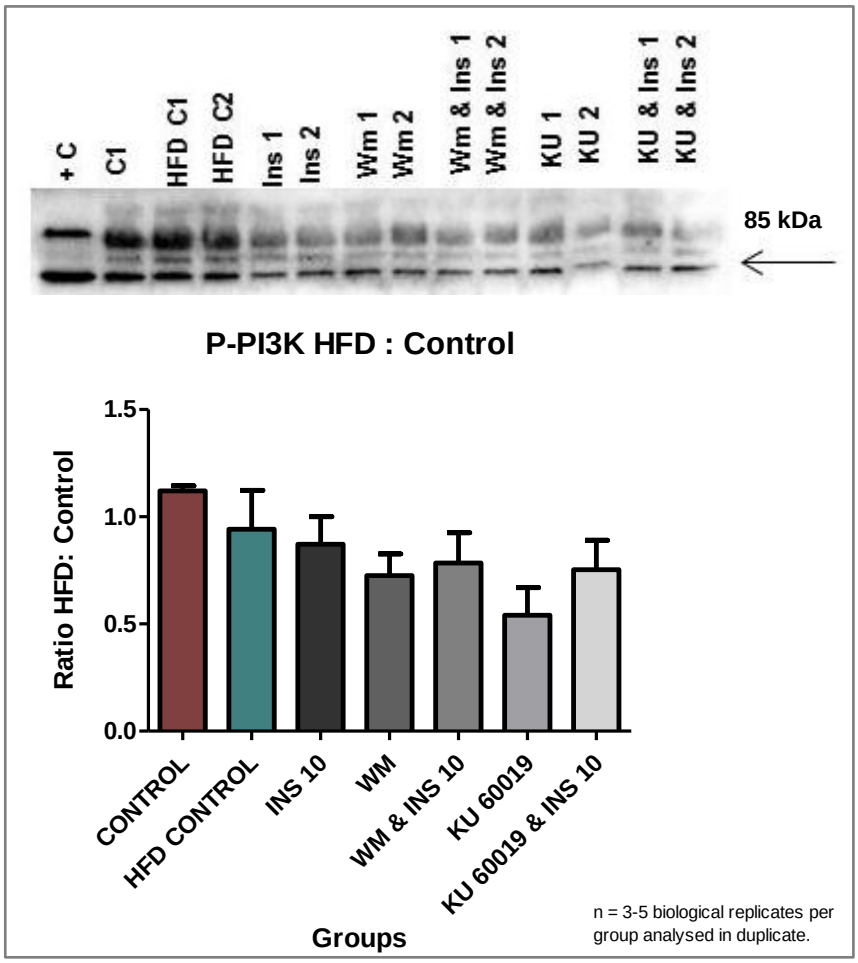

***Figure 3.18**: P-PI3K levels expressed as a HFD: Control Ratio*

Two-way ANOVA to illustrate the effect of KU 60019 on P-PI3K in cardiomyocytes from both the control and HFD animals

The effect of KU 60019 on P-PI3K was significant in cardiomyocytes from both animal groups, n = 3-6 biological replicates per group analysed in duplicate; p < 0.05 (KU 60019 vs. control; KU 60019 vs. HFD control) (Figure 3.19).

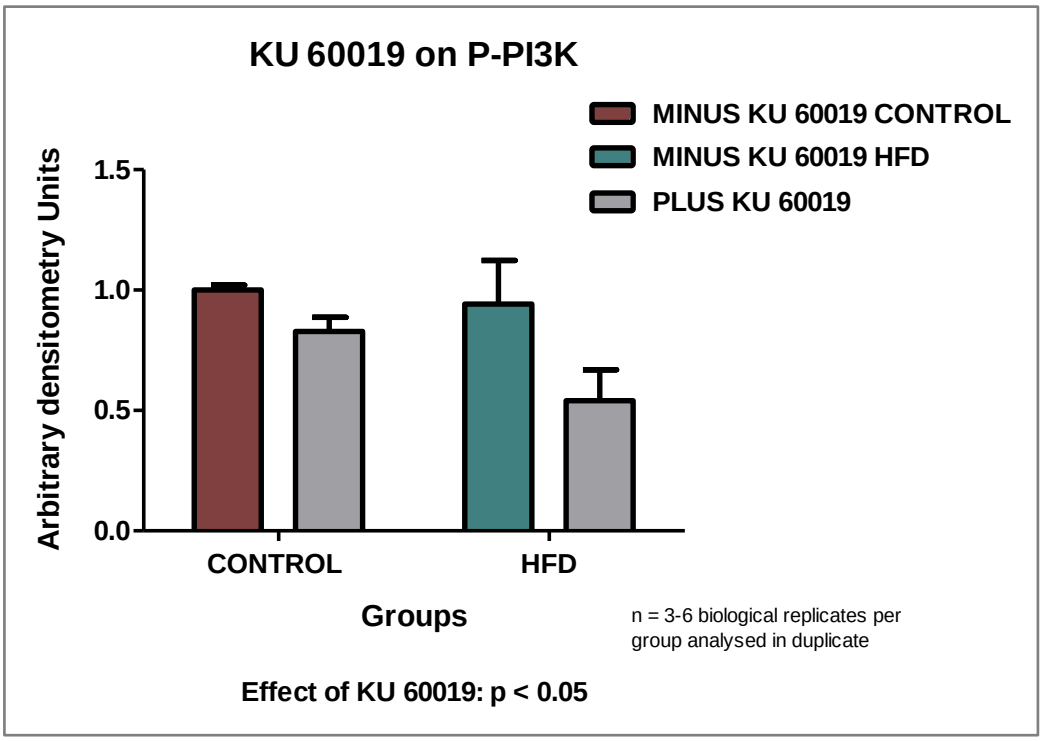

***Figure 3.19**: The effect of KU 60019 on P-PI3K*

e) P:T Ratio control

No significant differences in the PI3K P:T Ratio were observed; n = 4-6 biological replicates per group analysed in duplicate *(Figure 3.20).*

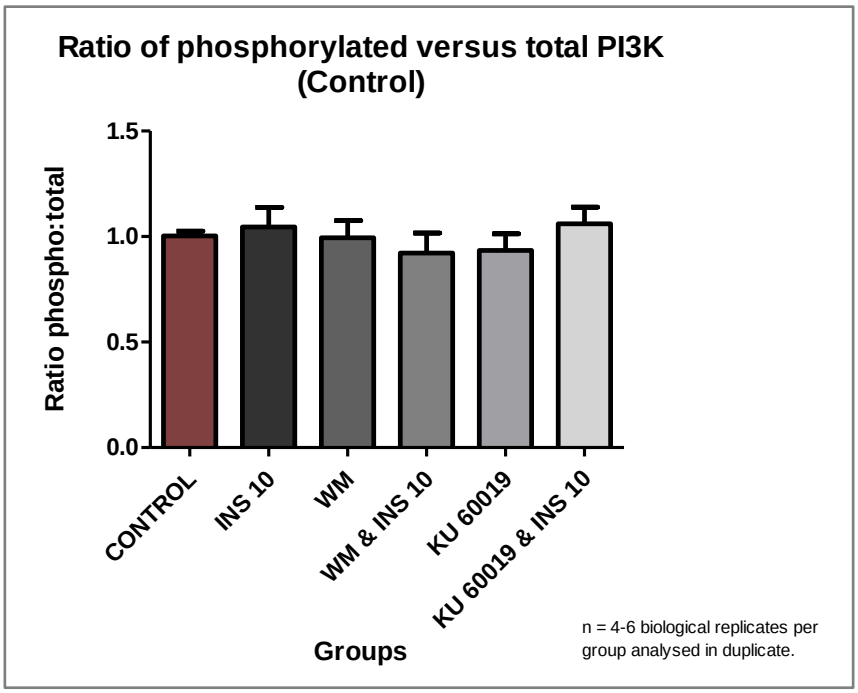

Figure 3.20*: Ratio of phosphorylated vs. total levels of PI3K in the cardiomyocytes from control animals*

f) P:T Ratio HFD

No significant differences in the PI3K P:T Ratio were observed in the cardiomyocytes from HFD animals; n = 3-5 biological replicates per group analysed in duplicate *(Figure 3.21).*

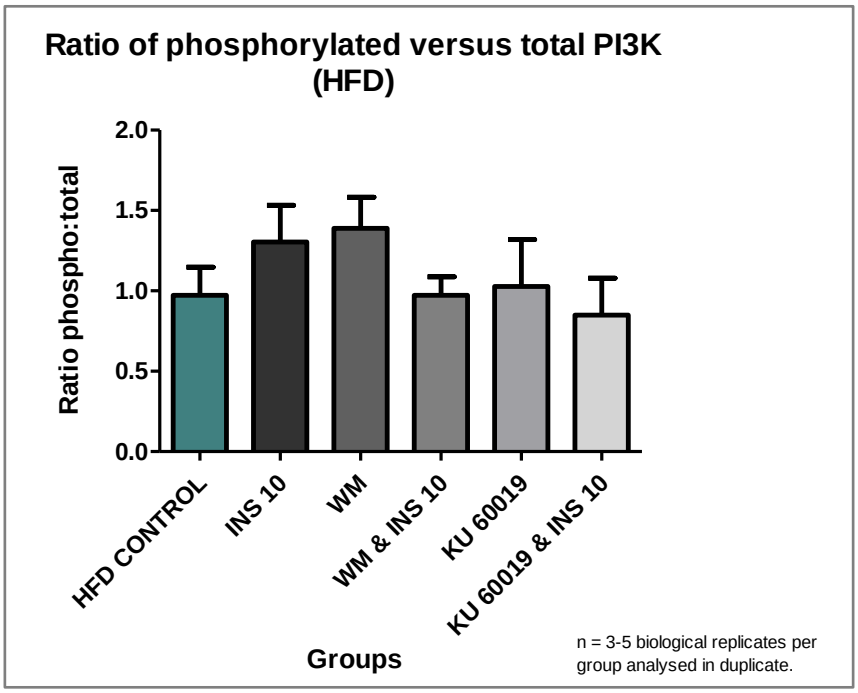

Figure 3.21*: Ratio of phosphorylated vs. total levels of PI3K in the cardiomyocytes from HFD animals*

3.3. PTEN

a) Total (T) expression control

No significant differences in the total expression of PTEN was observed between the cardiomyocytes from different control treated animals; n = 4 biological replicates per group analysed in duplicate *(Figure 3.22).*

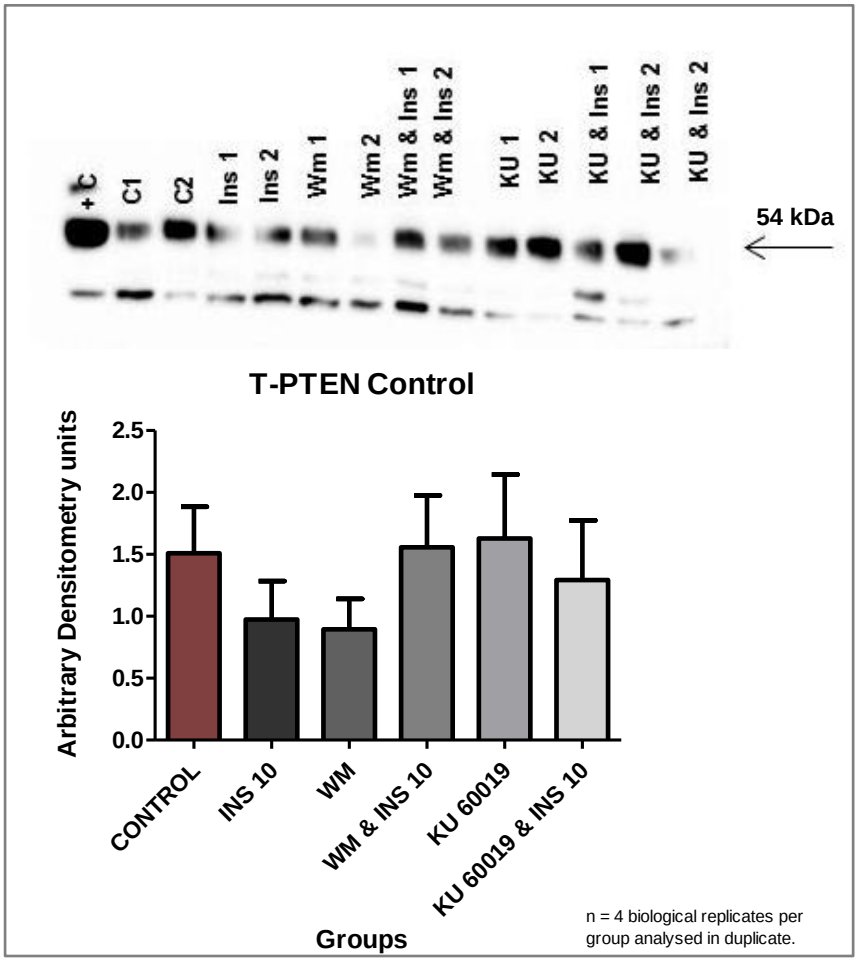

Figure 3.22*: T-PTEN expression (Arbitrary Densitometry units) in the cardiomyocytes from control animals*

b) Total (T) expression HFD

The total expression of PTEN in the cardiomyocytes from HFD animals did not differ from the cardiomyocytes from control animals at baseline. Furthermore, when the cardiomyocytes from different HFD treatment groups were analysed, no significant differences were observed in the total expression of PTEN; n = 3 biological replicates per group analysed in duplicate *(Figure 3.23).*

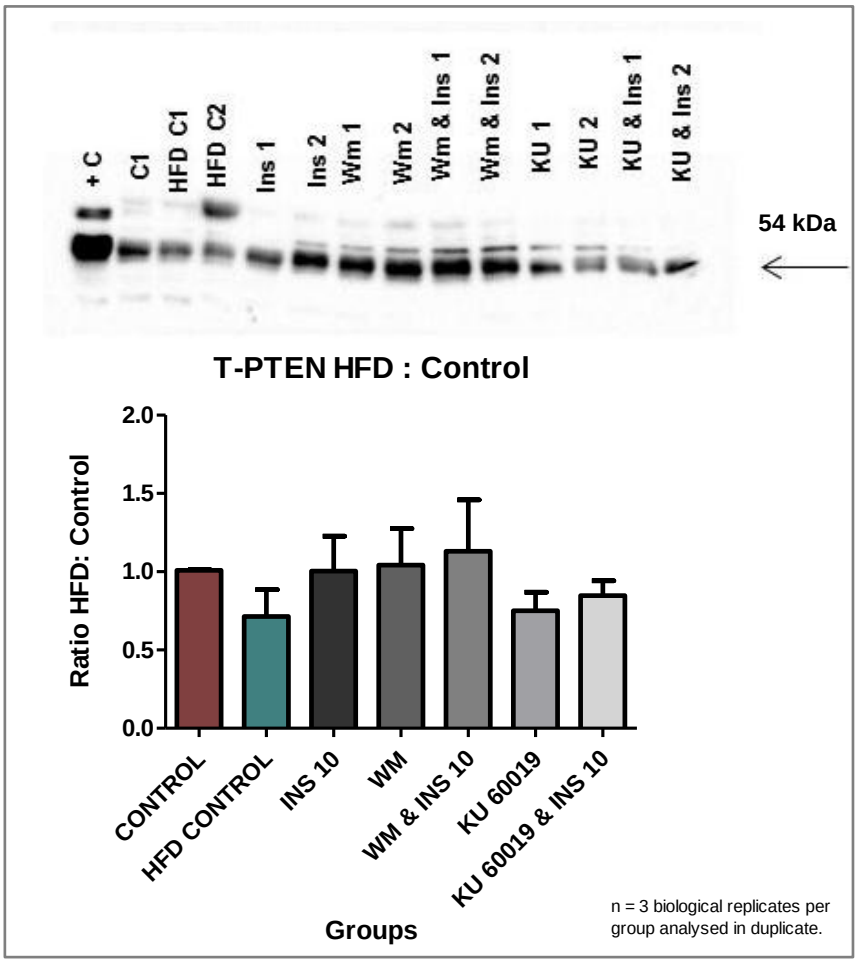

***Figure 3.23**: T-PTEN expressed as a HFD: Control Ratio*

c) *Phosphorylated (P) levels control*

Cardiomyocytes from the control animals showed no significant differences in the phosphorylation of PTEN; n = 4 biological replicates per group analysed in duplicate *(Figure 3.24).*

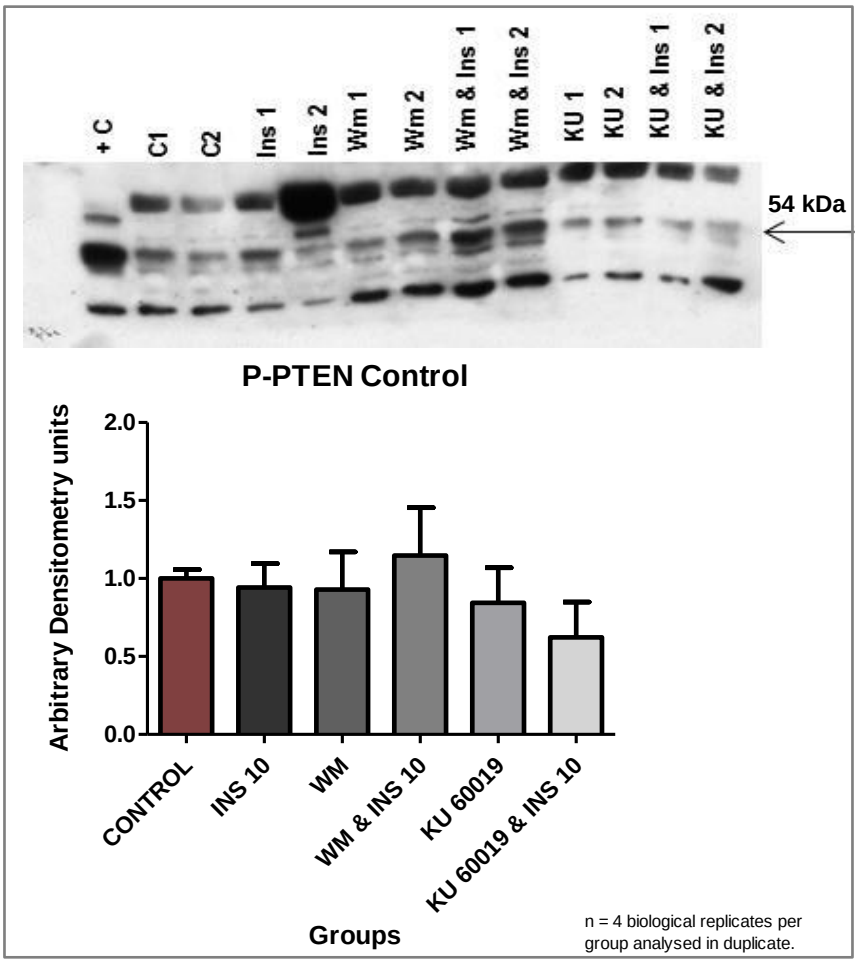

Figure 3.24*: P-PTEN levels (Arbitrary Densitometry units) in the cardiomyocytes from control animals*

d) Phosphorylated (P) levels HFD

No significant differences were observed between the phosphorylation of PTEN in the cardiomyocytes from HFD and control animals at baseline. Also, no significant differences in PTEN phosphorylation were observed among the cardiomyocytes from different HFD treated animals; n = 2-3 biological replicates per group analysed in duplicate *(Figure 3.25).*

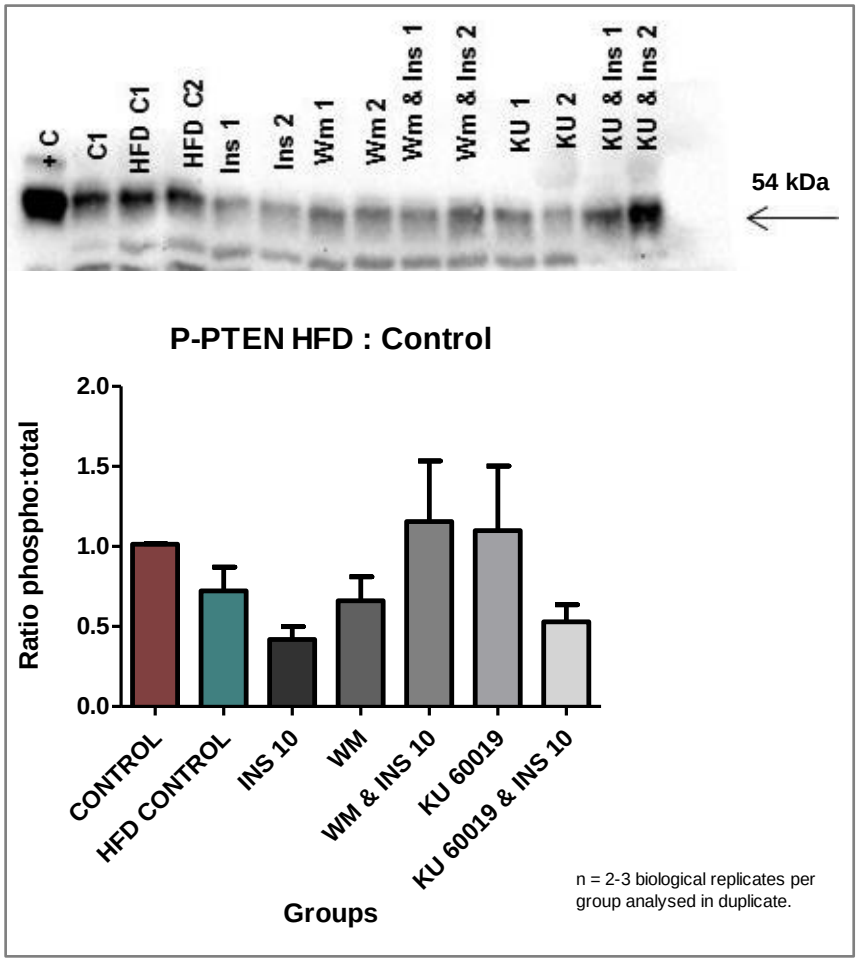

***Figure 3.25**: P-PTEN levels expressed as a HFD: Control Ratio*

e) P:T Ratio control

No significant differences in the PTEN P:T Ratio were observed; n = 4 biological replicates per group analysed in duplicate *(Figure 3.26).*

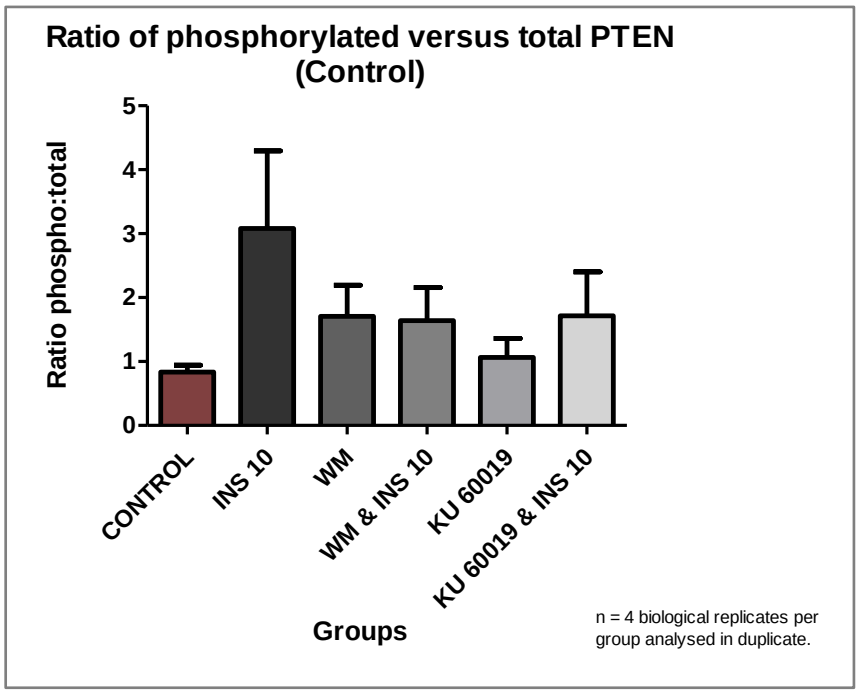

Figure 3.26*: Ratio of phosphorylated vs. total levels of PTEN in the cardiomyocytes from control animals*

f) P:T Ratio HFD

No significance was observed in the PTEN P:T Ratio in the cardiomyocytes from HFD animals *(Figure 3.27).*

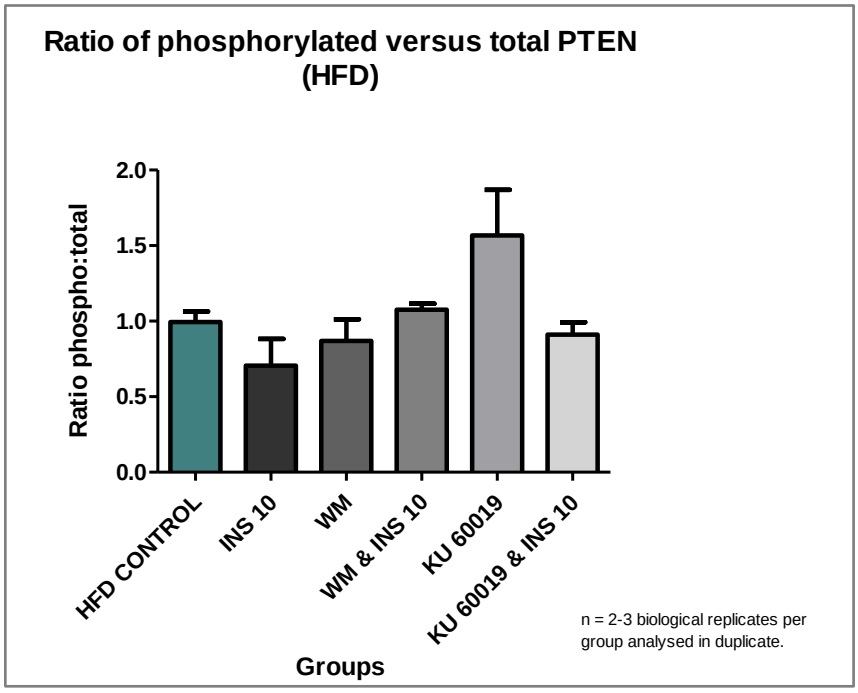

Figure 3.27*: Ratio of phosphorylated vs. total levels of PTEN in the cardiomyocytes from HFD animals*

3.4. ATM

a) Total (T) expression control

In the cardiomyocytes from control animals, the expression of T-ATM was significantly downregulated when the INS 10 group and the INS 10 in combination with KU 60019 group were compared; n = 4-8 biological replicates per group analysed in duplicate; $p < 0.001$ (KU 60019 & INS 10 vs. INS 10) *(Figure 3.28).*

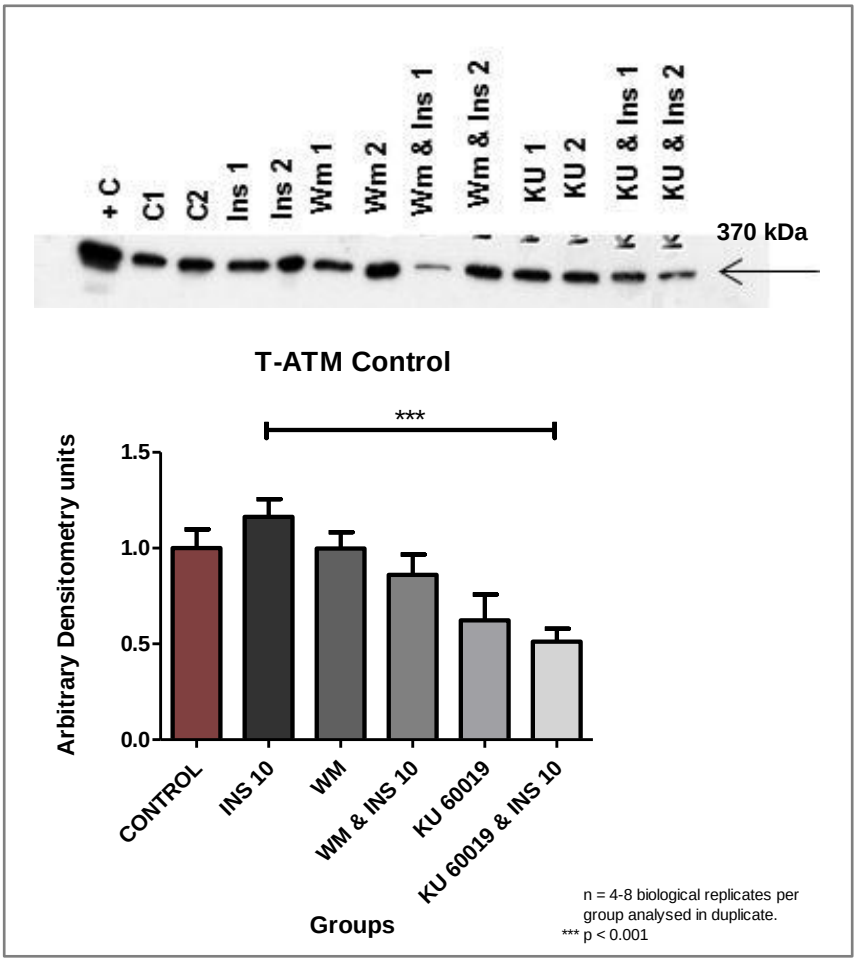

Figure 3.28: *T-ATM expression (Arbitrary Densitometry units) in the cardiomyocytes from control animals*

b) Total (T) expression HFD

The total expression of ATM was significantly downregulated in the cardiomyocytes from HFD animals when compared to the control animals at baseline; n = 4-9 biological replicates per group analysed in duplicate; $p < 0.001$ (HFD control vs. control) *(Figure 3.29).* Furthermore, the KU 60019 in combination with INS 10 group, significantly lowered the total expression of ATM when compared to the INS 10 group; $p < 0.05$ (KU 60019 & INS 10 vs. INS 10).

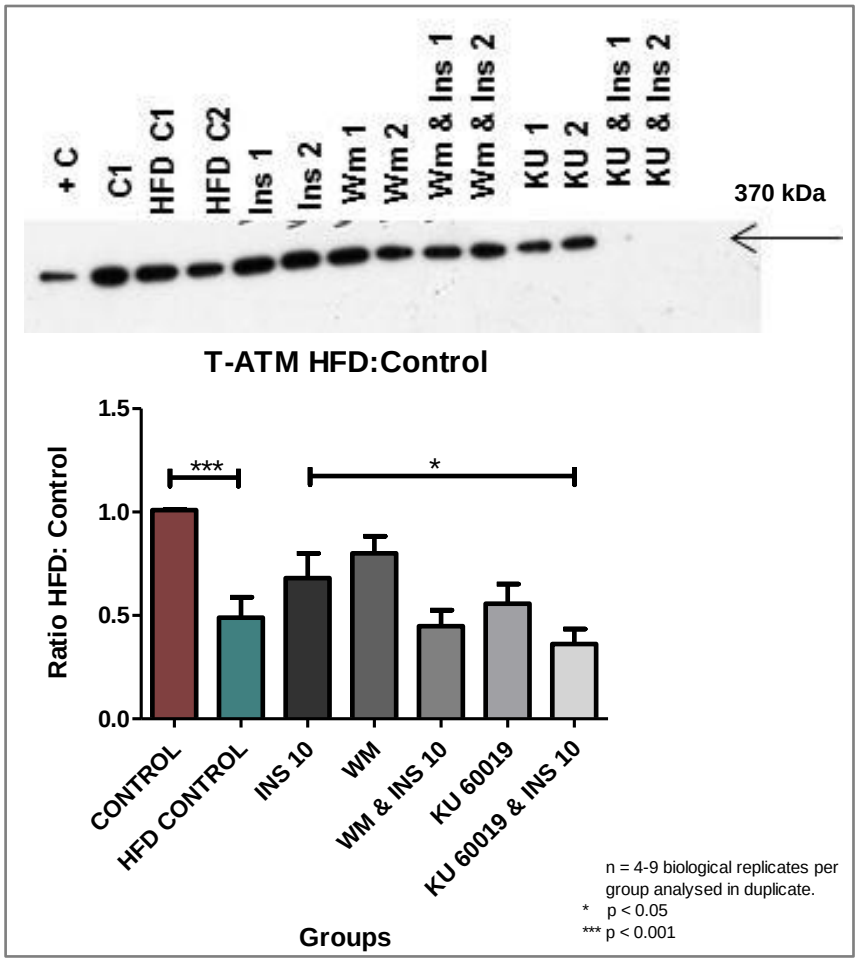

Figure 3.29: *T-ATM expressed as a HFD: Control Ratio*

c) *Phosphorylated (P) levels control*

The cardiomyocytes from control animals showed no significant differences in the phosphorylation of ATM after the different manipulations; n = 4-6 biological replicates per group analysed in duplicate *(Figure 3.30).*

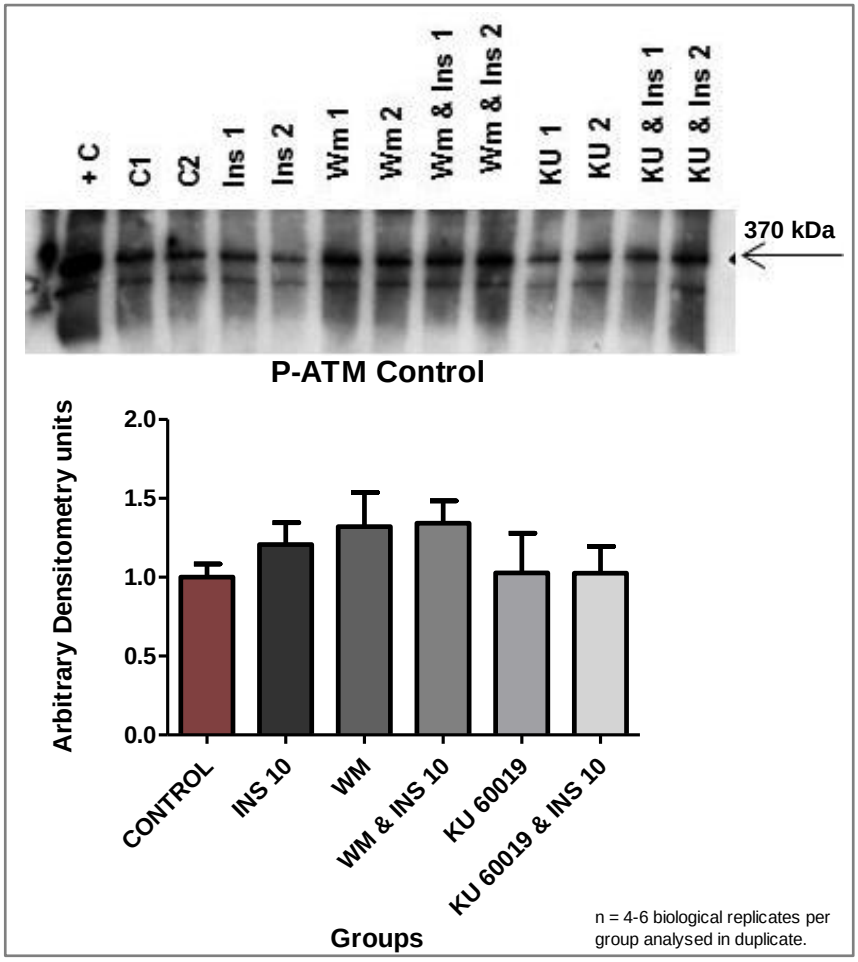

Figure 3.30: *P-ATM levels (Arbitrary Densitometry units) in the cardiomyocytes from control animals*

d) Phosphorylated (P) levels HFD

The phosphorylation of ATM was significantly decreased in the cardiomyocytes from HFD animals when compared to the cardiomyocytes from control animals at baseline; n = 4-6 biological replicates per group analysed in duplicate; $p < 0.05$ (HFD control vs. control) *(Figure 3.31).* The KU 60019 & INS 10 group significantly decreased the phosphorylation of ATM when compared to the INS 10 treated group; $p < 0.05$ (KU 60019 & INS 10 vs. INS 10).

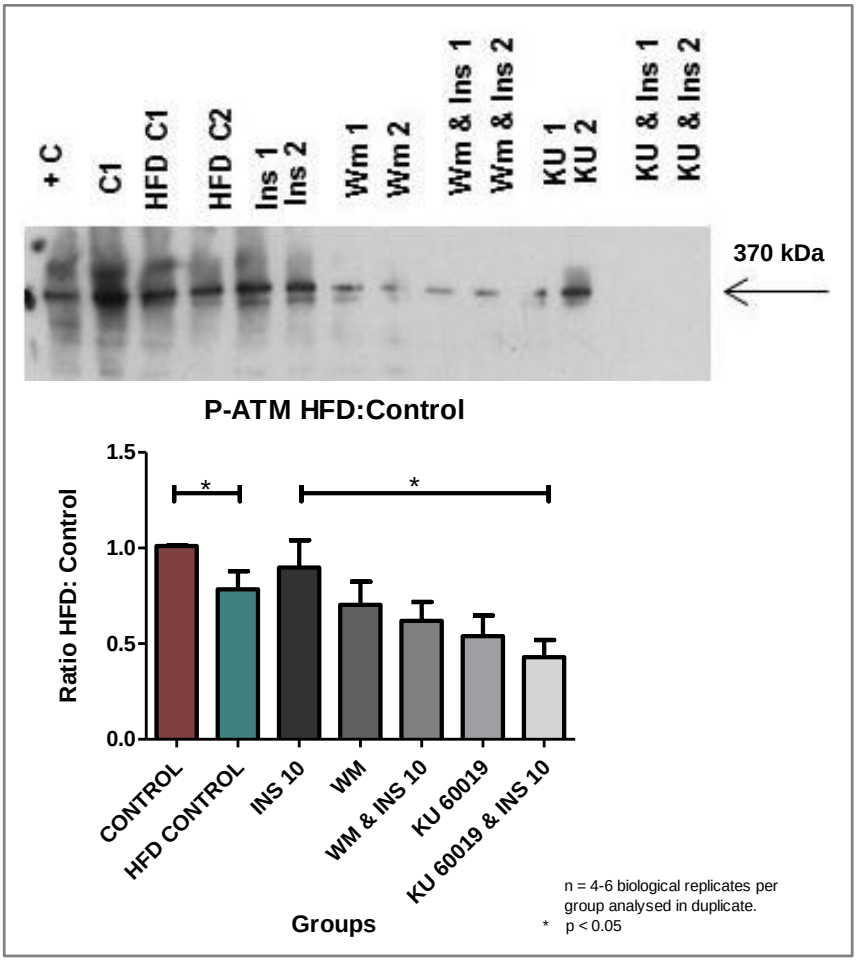

Figure 3.31: *P-ATM levels expressed as a HFD: Control Ratio*

Two-way ANOVA to illustrate the effect of KU 60019 on insulin-stimulated P-ATM in cardiomyocytes from both the control and HFD animals

The effect of KU 60019 on P-ATM was significant in cardiomyocytes from both animal models, n = 5-6 biological replicates per group analysed in duplicate; p=0.02 (KU 60019 & INS 10 vs. control & INS 10; KU 60019 & INS 10 vs. HFD & INS 10) (Figure 3.32).

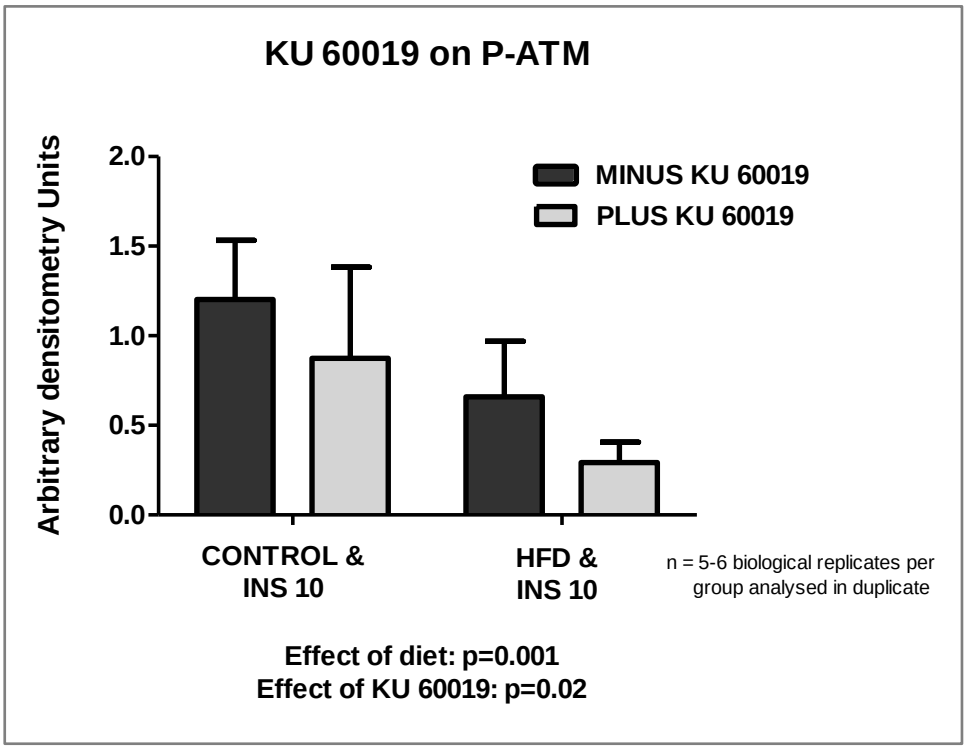

Figure 3.32: *Effect of KU 60019 on insulin-stimulated P-ATM*

e) P:T Ratio control

According to the P:T Ratio of the cardiomyocytes from control animals, the KU 60019 group significantly upregulated the phosphorylation of ATM when compared to the baseline values; n = 3-5 biological replicates per group analysed in duplicate; $p < 0.01$ (KU 60019 vs. control) *(Figure 3.33).*

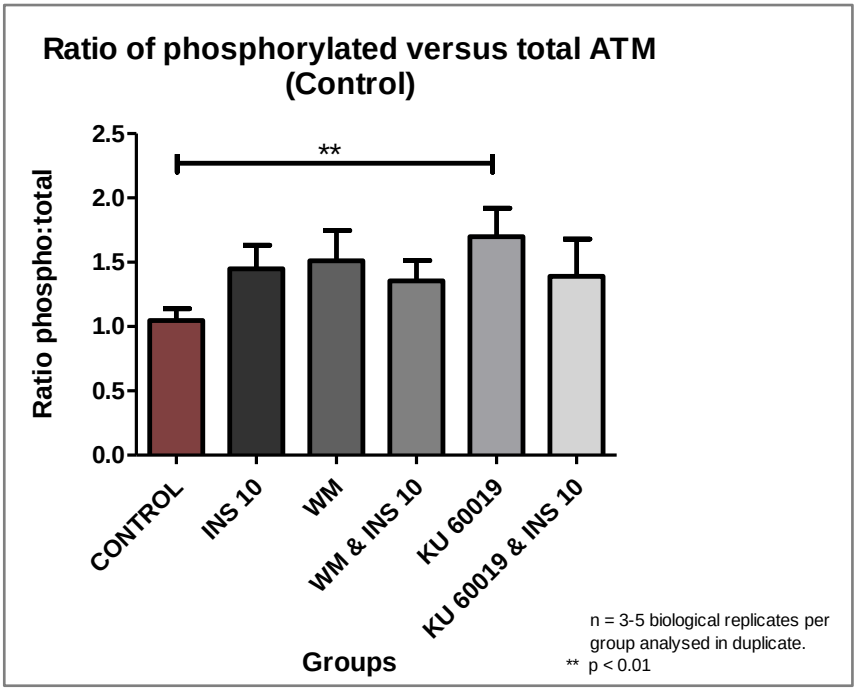

Figure 3.33: *Ratio of phosphorylated vs. total levels of ATM in the cardiomyocytes from control animals*

f) P:T Ratio HFD

The ATM P:T Ratio of the INS 10 group was significantly decreased when compared to the cardiomyocytes from baseline HFD animals; n = 3-6 biological replicates per group analysed in duplicate; $p < 0.05$ (INS 10 vs. HFD control) *(Figure 3.34).* In addition the KU 60019 treated group also significantly decreased the phosphorylation of ATM when compared to the cardiomyocytes from baseline HFD animals; $p < 0.01$ (KU 60019 vs. HFD control).

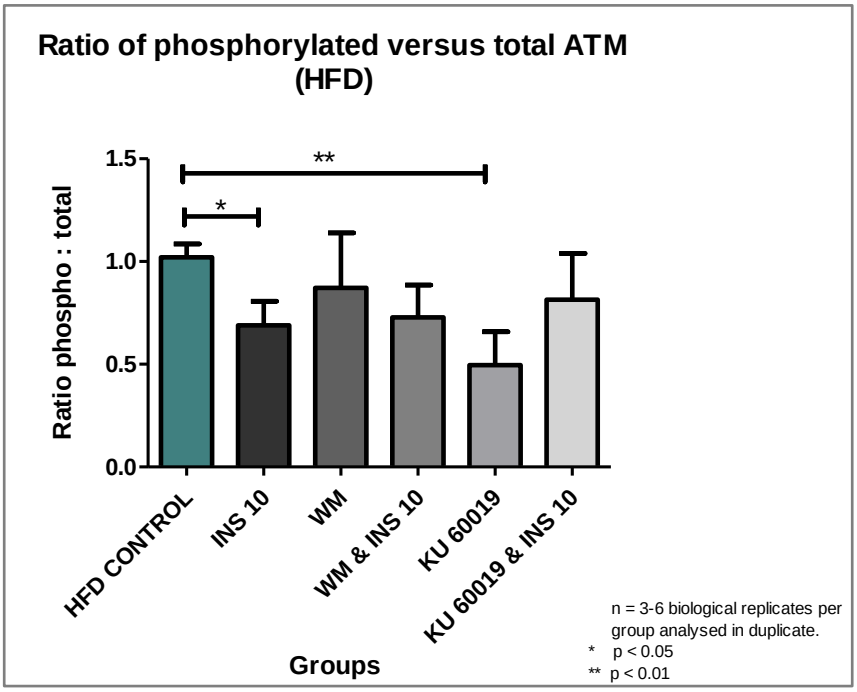

Figure 3.34: *Ratio of phosphorylated vs. total levels of ATM in the* cardiomyocytes from *HFD animals*

3.5. PKB

a) Total (T) expression control

No significant differences were observed in the total expression of PKB in the cardiomyocytes from control animals; n = 4-10 biological replicates per group analysed in duplicate *(Figure 3.35).*

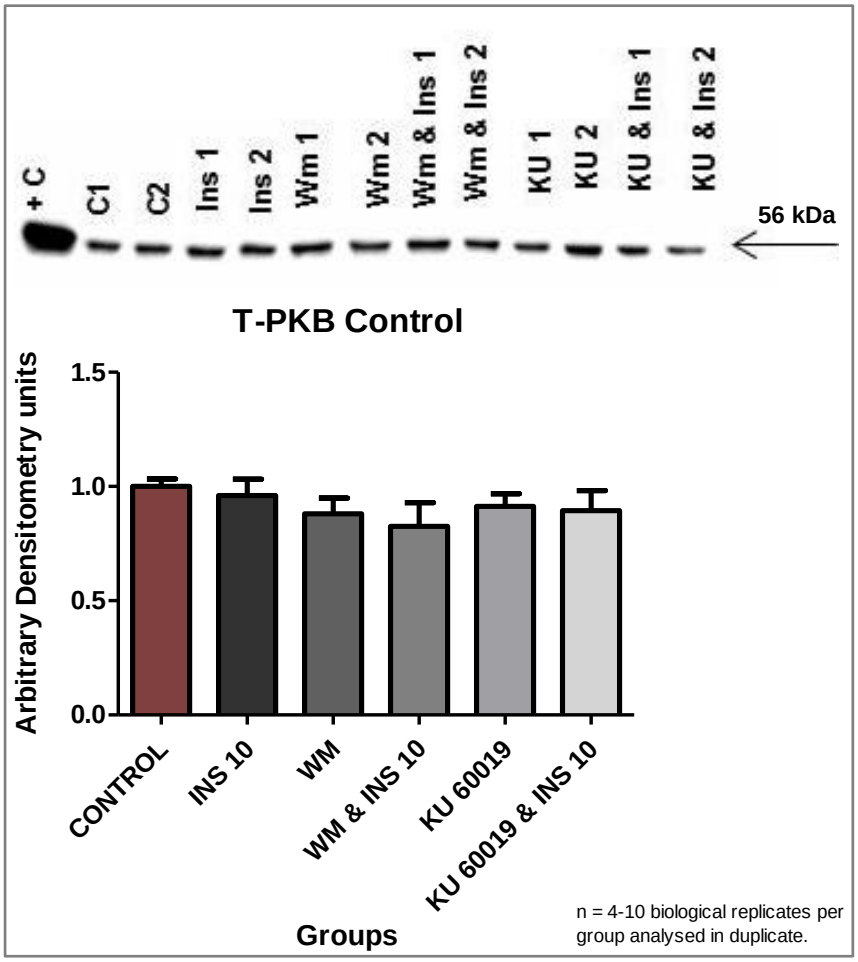

Figure 3.35*: T-PKB expression (Arbitrary Densitometry units) in the cardiomyocytes from control animals*

b) Total (T) expression HFD

The total expression of PKB was downregulated in the cardiomyocytes from HFD animals when compared to the cardiomyocytes from control animals at baseline; n = 4-9 biological replicates per group analysed in duplicate; $p < 0.01$ (HFD control vs. control) *(Figure 3.36).*

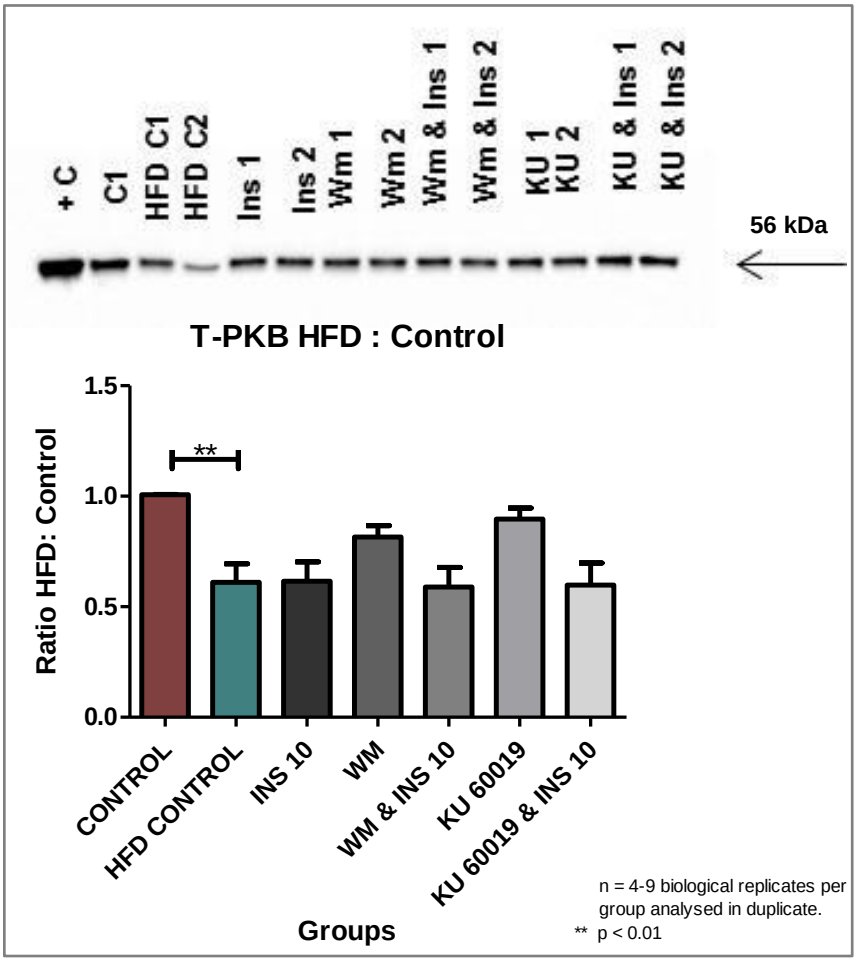

***Figure 3.36**: T-PKB expressed as a HFD: Control Ratio*

c) *Phosphorylated (P) levels control*

No significant differences were observed in the phosphorylation of PKB in the cardiomyocytes from control treated groups; n = 4-7 biological replicates per group analysed in duplicate *(Figure 3.37).*

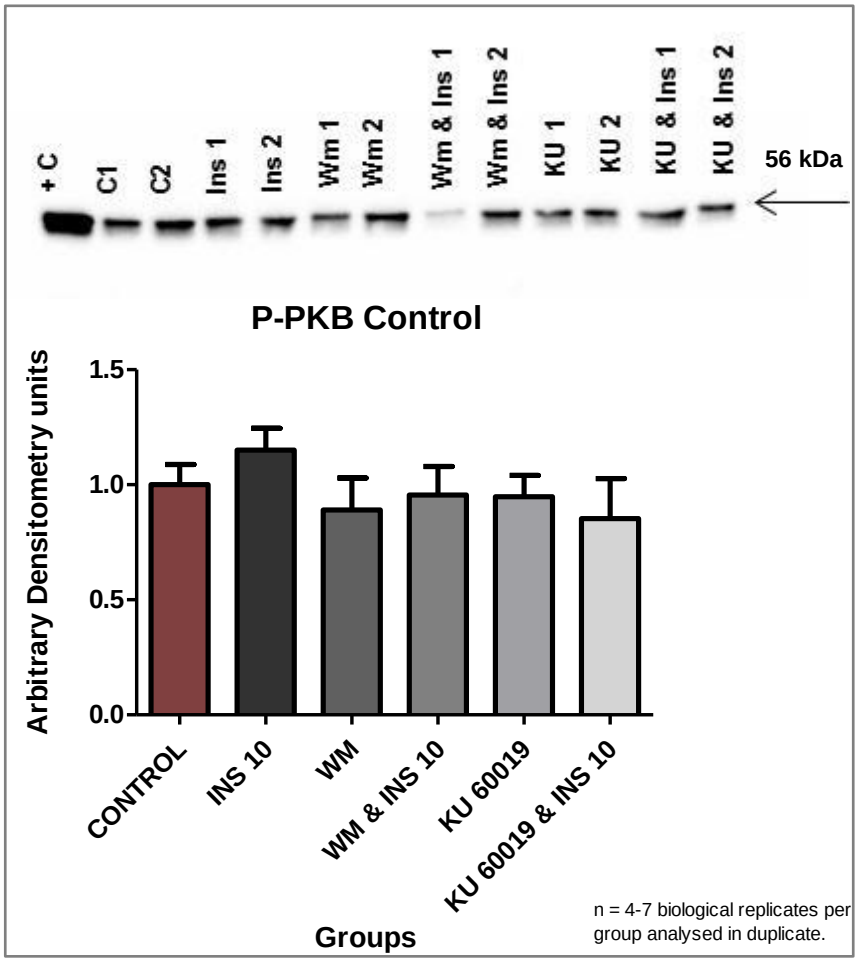

Figure 3.37*: P-PKB levels (Arbitrary Densitometry units) in the cardiomyocytes from control animals*

d) Phosphorylated (P) levels HFD

No significant differences were observed between PKB phosphorylation in the cardiomyocytes from control and HFD animals at baseline; n = 4-7 biological replicates per group analysed in duplicate *(Figure 3.38).* There was also no significant differences in P-PKB among the cardiomyocytes from HFD treated groups.

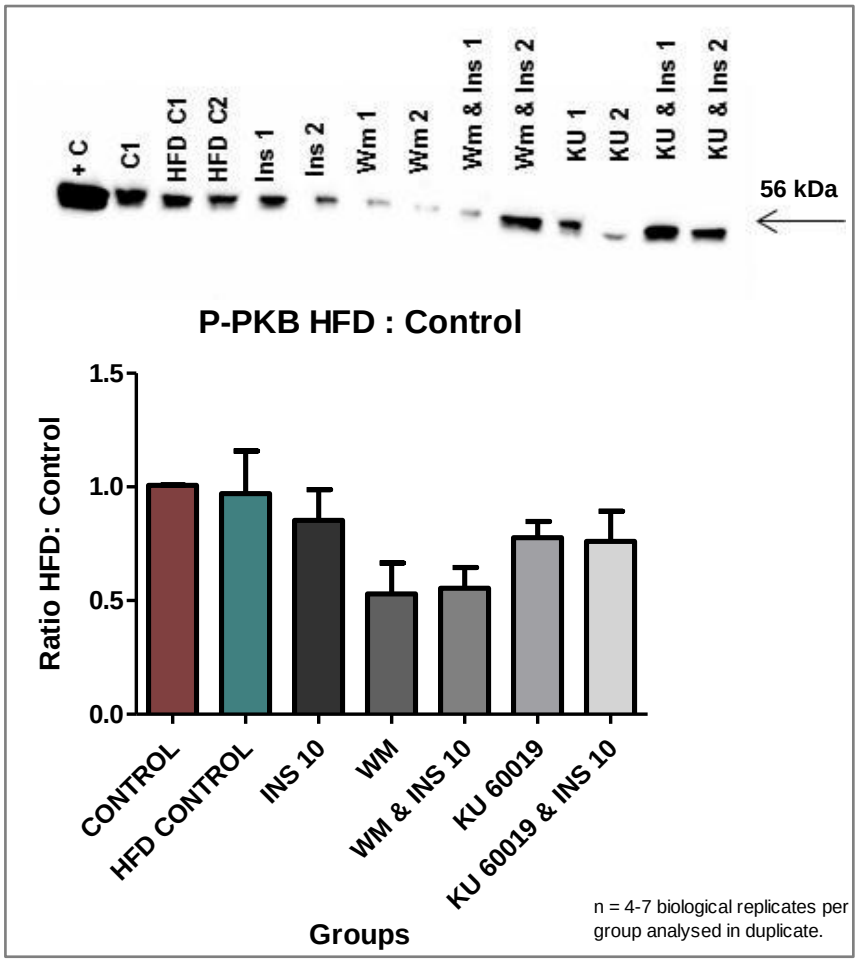

***Figure 3.38**: P-PKB levels expressed as a HFD: Control Ratio*

Two-way ANOVA to illustrate the effect of KU 60019 on insulin-stimulated P-PKB in cardiomyocytes from both the control and HFD animals

Cardiomyocytes from the control animals, treated with KU 60019 significantly downregulated P-PKB when compared to INS 10; n = 3-4 biological replicates per group analysed in duplicate; p < 0.05 (KU 60019 & INS 10 vs. control & INS 10). The overall effect of KU 60019 was significant on cardiomyocytes from both groups; p=0.001 (KU 60019 & INS 10 vs. control & INS 10; KU 60019 & INS 10 vs. HFD & INS 10) (Figure 3.39).

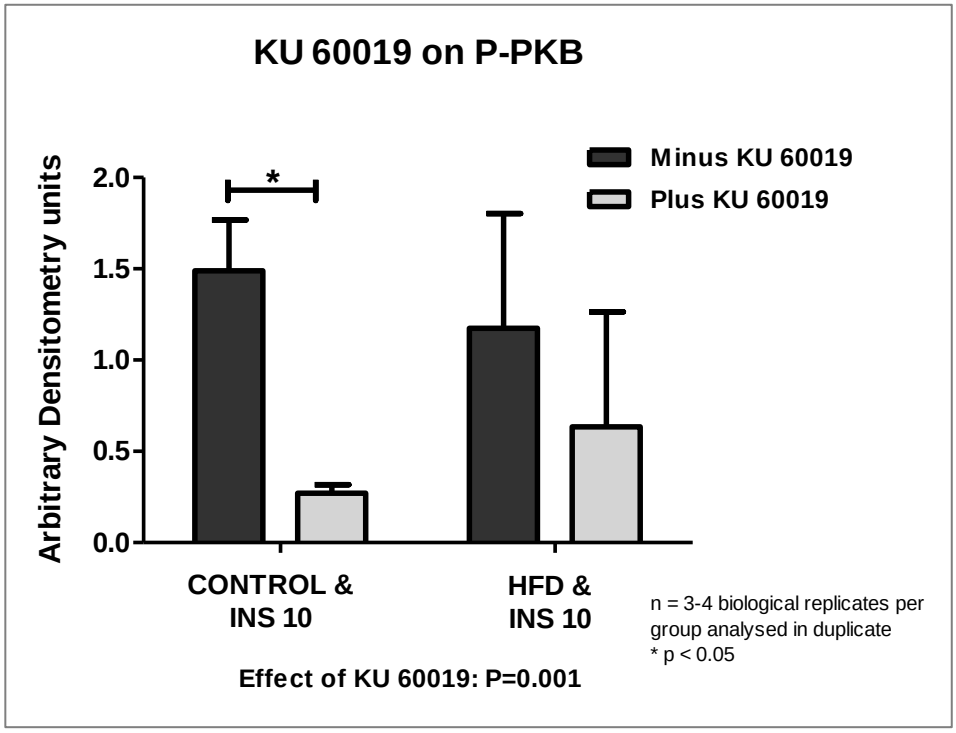

Figure 3.39: *Effect of KU 60019 on insulin-stimulated P-PKB*

e) P:T Ratio control

The cardiomyocytes from control animals presented with no significant differences in the PKB P:T Ratio; n = 4-7 biological replicates per group analysed in duplicate *(Figure 3.40).*

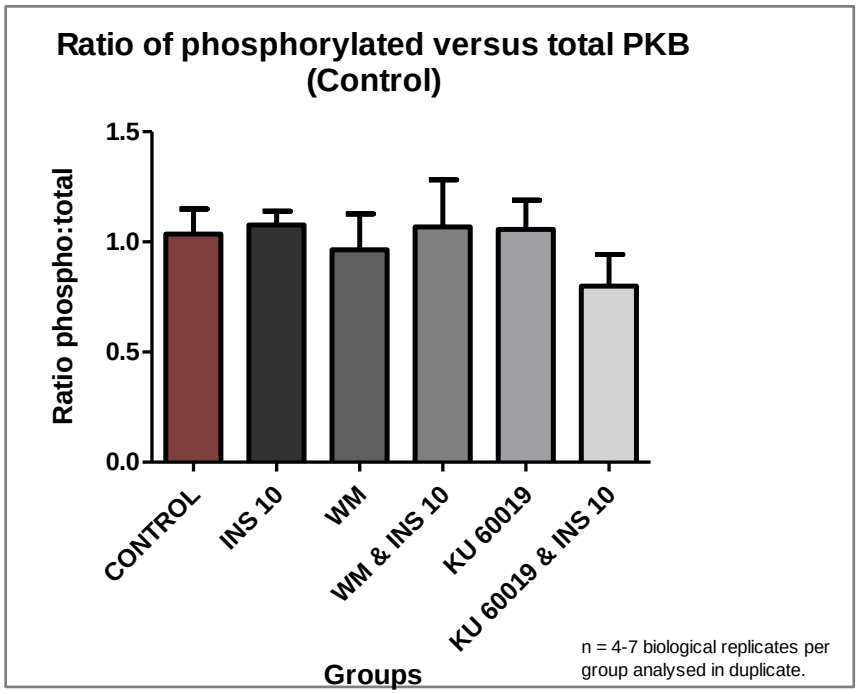

Figure 3.40: *Ratio of phosphorylated vs. total levels of PKB in the cardiomyocytes from control animals*

f) P:T Ratio HFD

No significant differences in the cardiomyocytes from HFD animals were observed in the PKB P:T Ratio; n = 4-7 biological replicates per group analysed in duplicate *(Figure 3.41).*

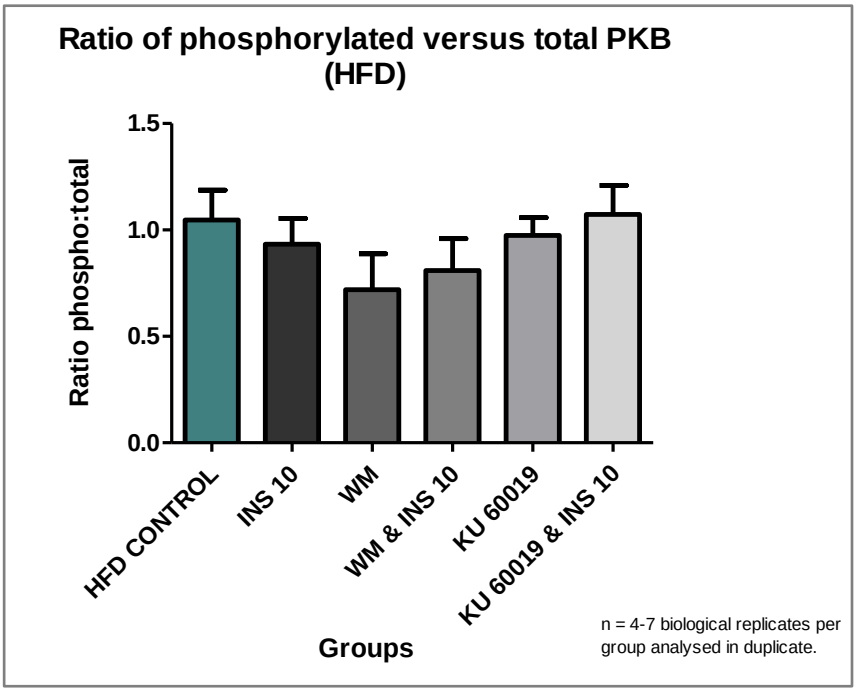

Figure 3.41*: Ratio of phosphorylated vs. total levels of PKB in the cardiomyocytes from HFD animals*

3.6. AS160

a) Total (T) expression control

No significant differences were observed in the total expression of AS160 in the cardiomyocytes from control animals; n = 3 biological replicates per group analysed in duplicate *(Figure 3.42).*

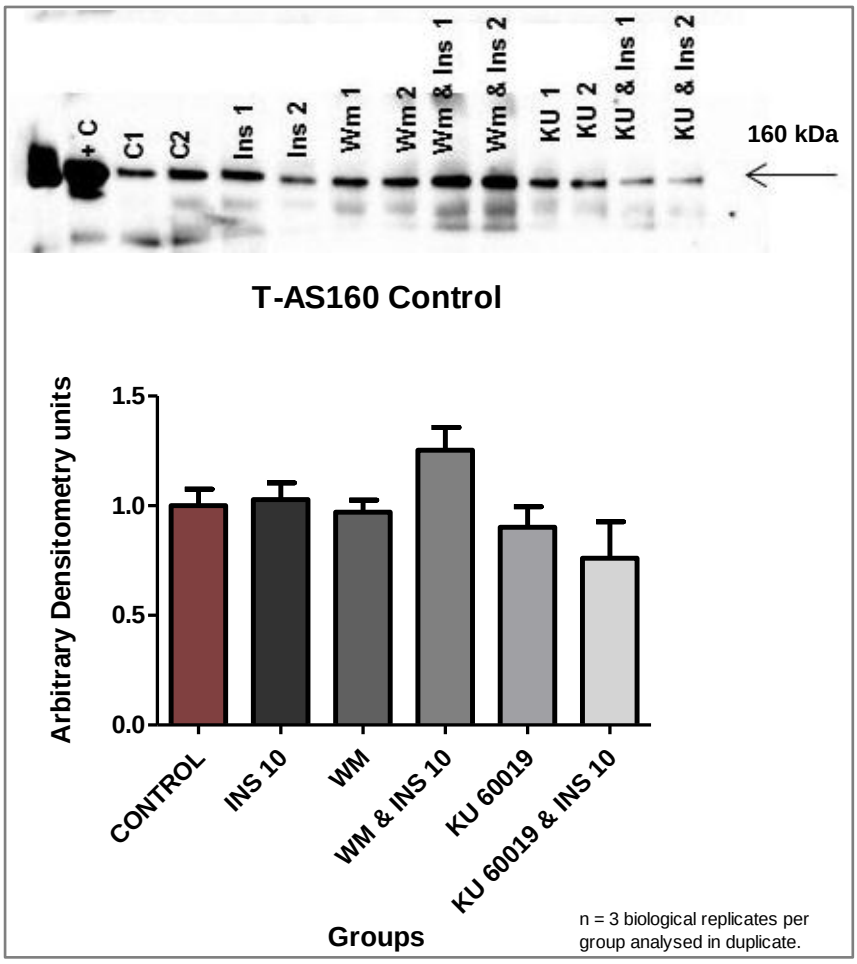

Figure 3.42*: T-AS160 expression (Arbitrary Densitometry units) in the cardiomyocytes from control animals*

b) Total (T) expression HFD

No significant differences were observed in the total expression of AS160 in the cardiomyocytes from HFD vs. the control animals; n = 3 biological replicates per group analysed in duplicate *(Figure 3.43).* There were also no significant differences in T-AS160 expression among the cardiomyocytes from HFD treated animals.

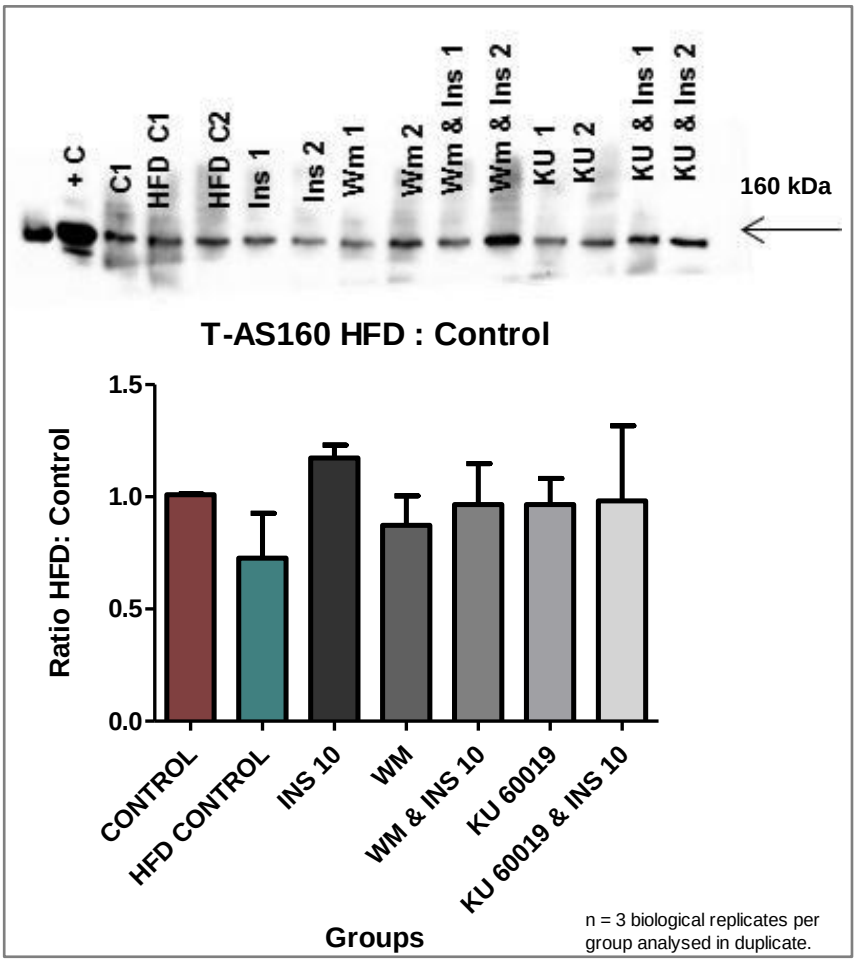

***Figure 3.43**: T-AS160 expressed as a HFD: Control Ratio*

c) Phosphorylated (P) levels control

In the cardiomyocytes from control animals, treatment with WM decreased the basal phosphorylation levels of AS160; n = 3 biological replicates per group analysed in duplicate; p < 0.001 (WM vs. control) *(Figure 3.44).*

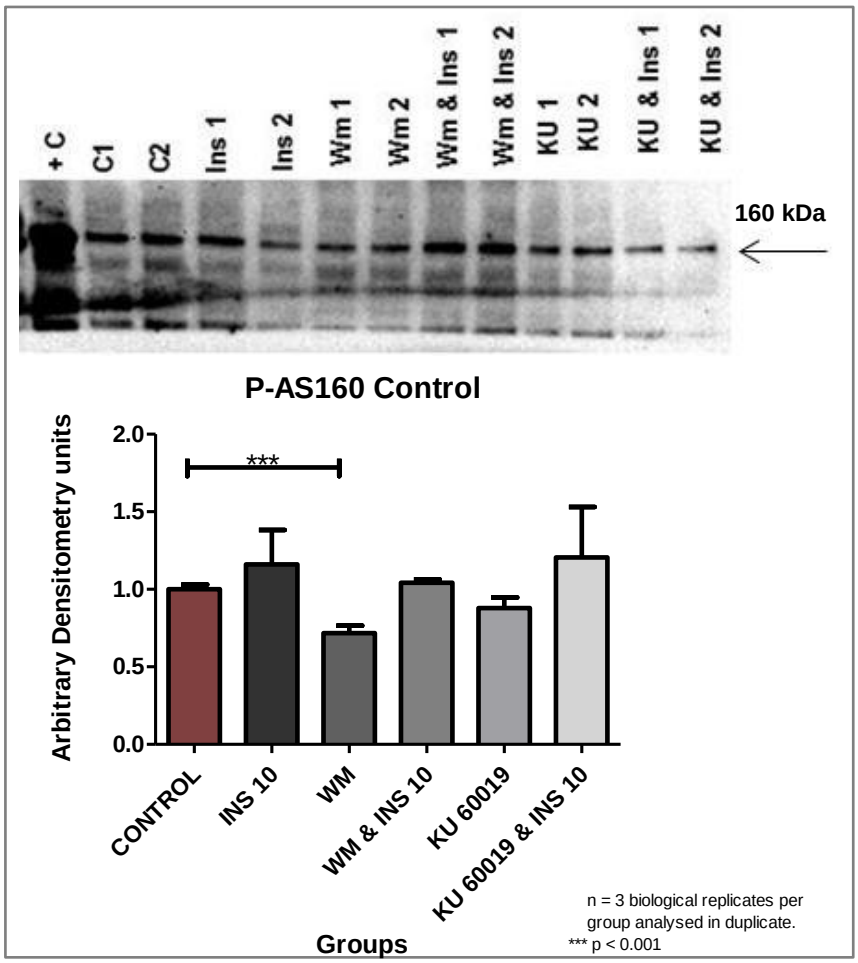

Figure 3.44*: P-AS160 levels (Arbitrary Densitometry units) in the cardiomyocytes from control animals*

d) Phosphorylated (P) levels HFD

Phosphorylation of AS160 in the cardiomyocytes from HFD animals were significantly lower at baseline when compared to the cardiomyocytes from control animals; n = 3 biological replicates per group analysed in duplicate; $p < 0.001$ (HFD control vs. control) *(Figure 3.45).* In contrast to the cardiomyocytes from control animals, cells from HFD animals stimulated with INS 10 resulted in significantly upregulated phosphorylation of AS160; $p < 0.01$ (INS 10 vs. HFD control). Furthermore, WM but not KU 60019, inhibited this stimulation; $p < 0.05$ (WM & INS 10 vs. INS 10).

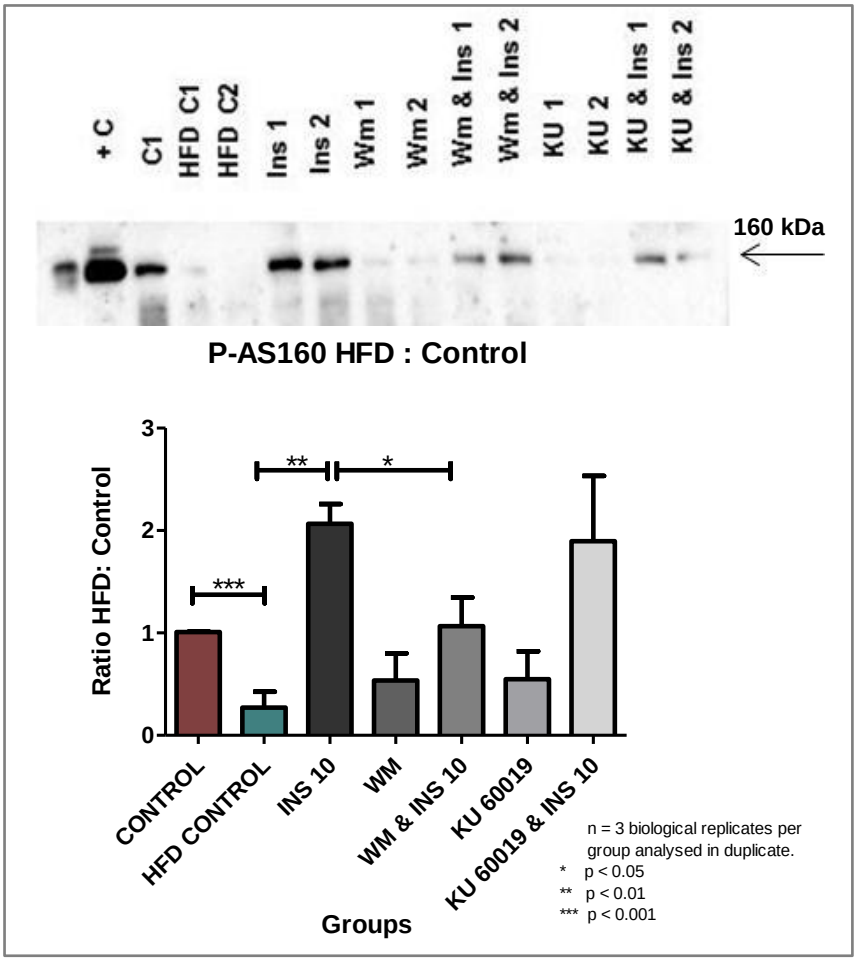

***Figure 3.45**: P-AS160 levels expressed as a HFD: Control Ratio*

e) P:T Ratio control

The AS160 P:T Ratio significantly decreased in the cardiomyocytes from control animals treated with WM when compared to the baseline values; n = 3 biological replicates per group analysed in duplicate; p < 0.01 (WM vs. control) *(Figure 3.46).*

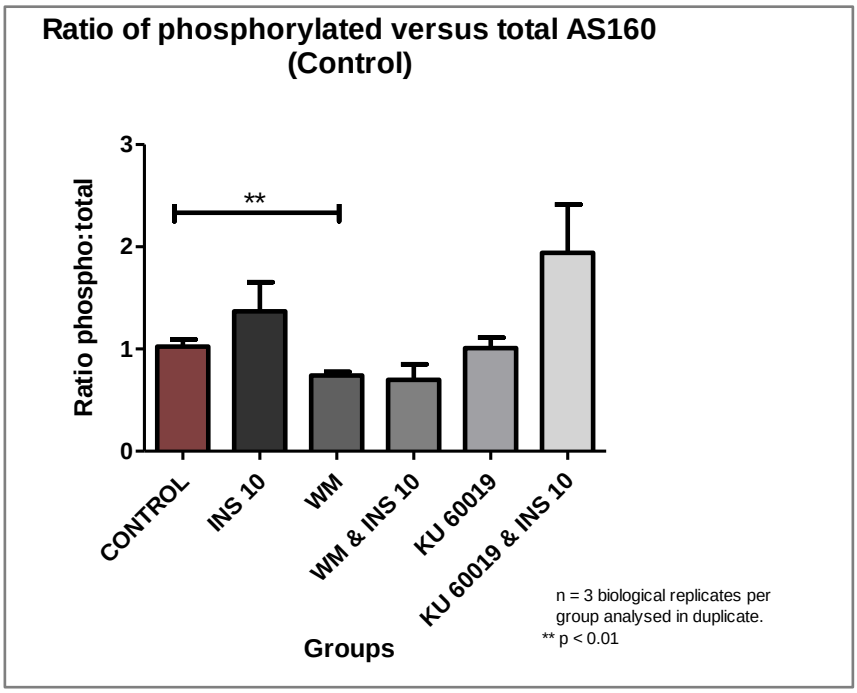

***Figure 3.46**: Ratio of phosphorylated vs. total levels of AS160 in the cardiomyocytes from control animals*

f) P:T Ratio HFD

The AS160 P:T Ratio significantly increased in the cardiomyocytes from HFD animals in response to INS 10 stimulation when compared to the cardiomyocytes from baseline HFD animals; n = 3 biological replicates per group analysed in duplicate; $p < 0.01$ (INS 10 vs. HFD control) *(Figure 3.47).*

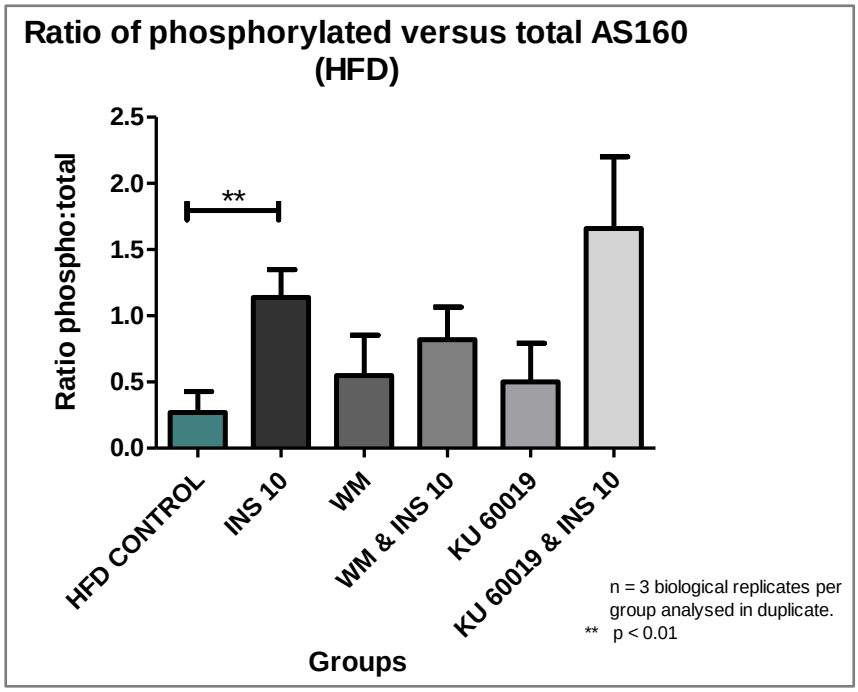

***Figure 3.47**: Ratio of phosphorylated vs. total levels of AS160 in the cardiomyocytes from HFD animals*

3.7. GSK-3β

a) Total (T) expression control

Cardiomyocytes from control animals treated with KU 60019 & INS 10 showed a significant increase in the total expression of GSK-3β when compared to the cardiomyocytes from control animals treated with only INS 10; n = 4-5 biological replicates per group analysed in duplicate; $p < 0.05$ (KU 60019 & INS 10 vs. INS 10) *(Figure 3.48).*

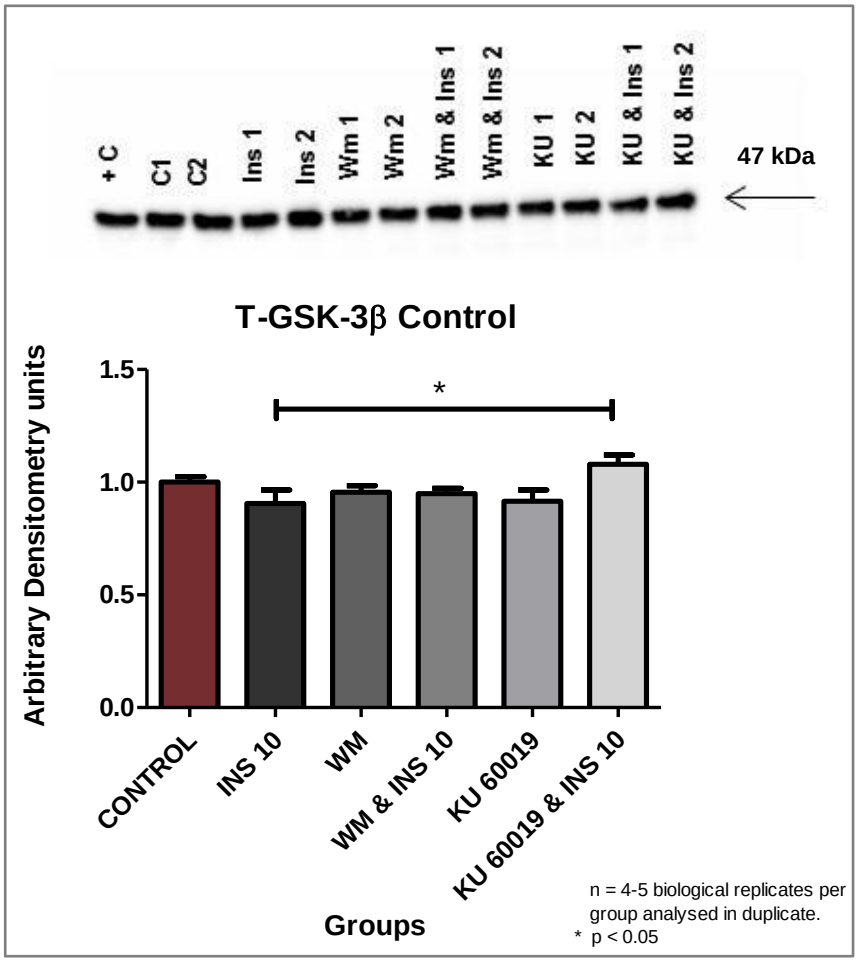

***Figure 3.48**: T-GSK-3β expression (Arbitrary Densitometry units) in the cardiomyocytes from control animals*

b) Total (T) expression HFD

The total expression of GSK-3β was significantly downregulated in the cardiomyocytes from HFD animals when compared to the cardiomyocytes from control animals at baseline; n = 3-4 biological replicates per group analysed in duplicate; $p < 0.01$ (HFD control vs. control) *(Figure 3.49).*

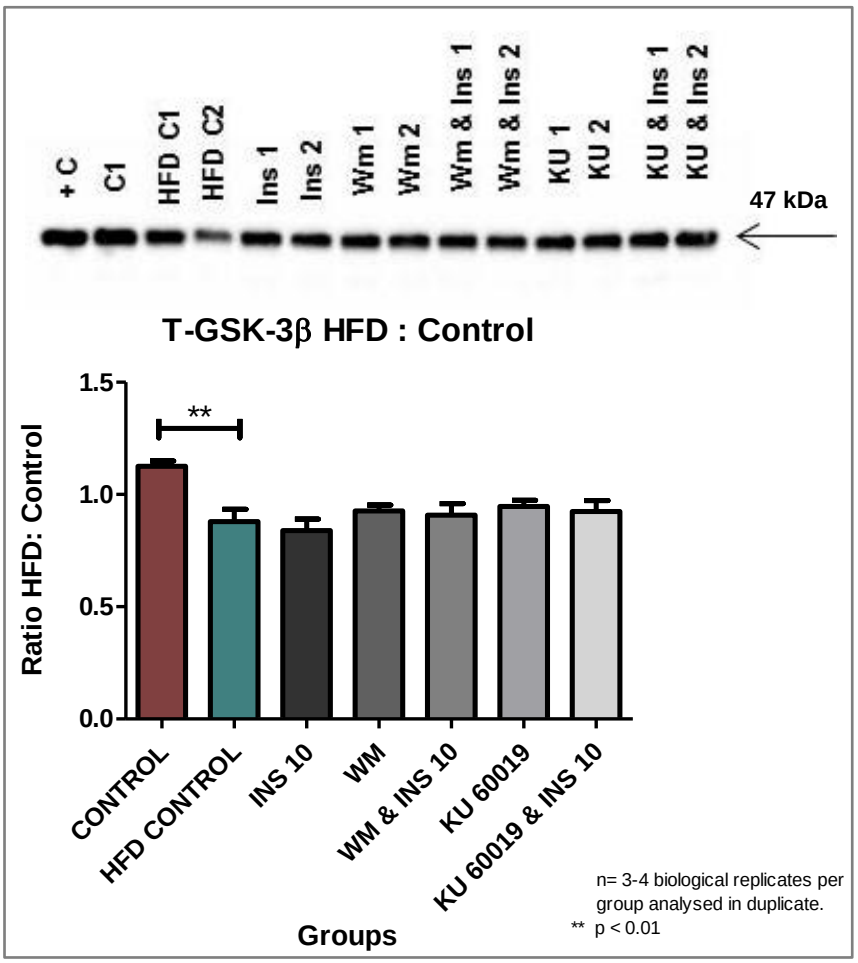

***Figure 3.49**: T-GSK-3β expressed as a HFD: Control Ratio*

c) *Phosphorylated (P) levels control*

No significant differences were observed in the phosphorylation of GSK-3β in the cardiomyocytes from control animals, n = 4-5 biological replicates per group analysed in duplicate *(Figure 3.50).*

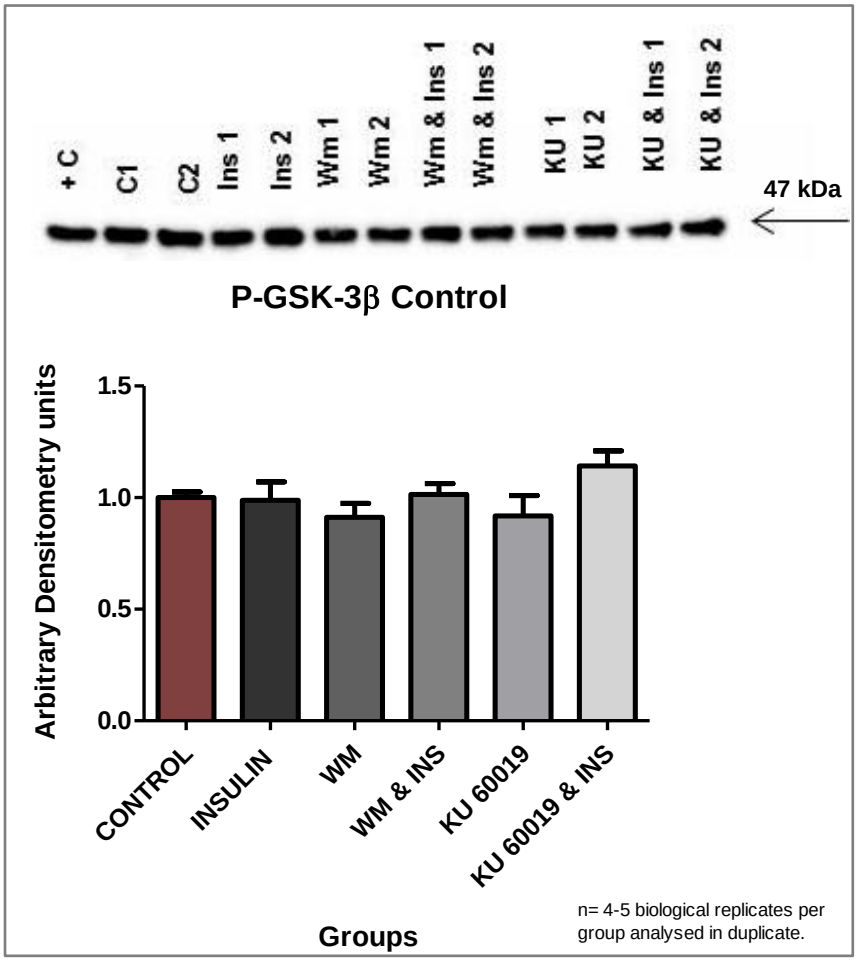

Figure 3.50*: P-GSK-3β levels (Arbitrary Densitometry units) in the cardiomyocytes from control animals*

d) Phosphorylated (P) levels HFD

The cardiomyocytes from HFD control animals presented with a significantly lower GSK-3β phosphorylation than the cardiomyocytes from control animals at baseline; n = 3-4 biological replicates per group analysed in duplicate; $p < 0.05$ (HFD control vs. control) *(Figure 3.51).*

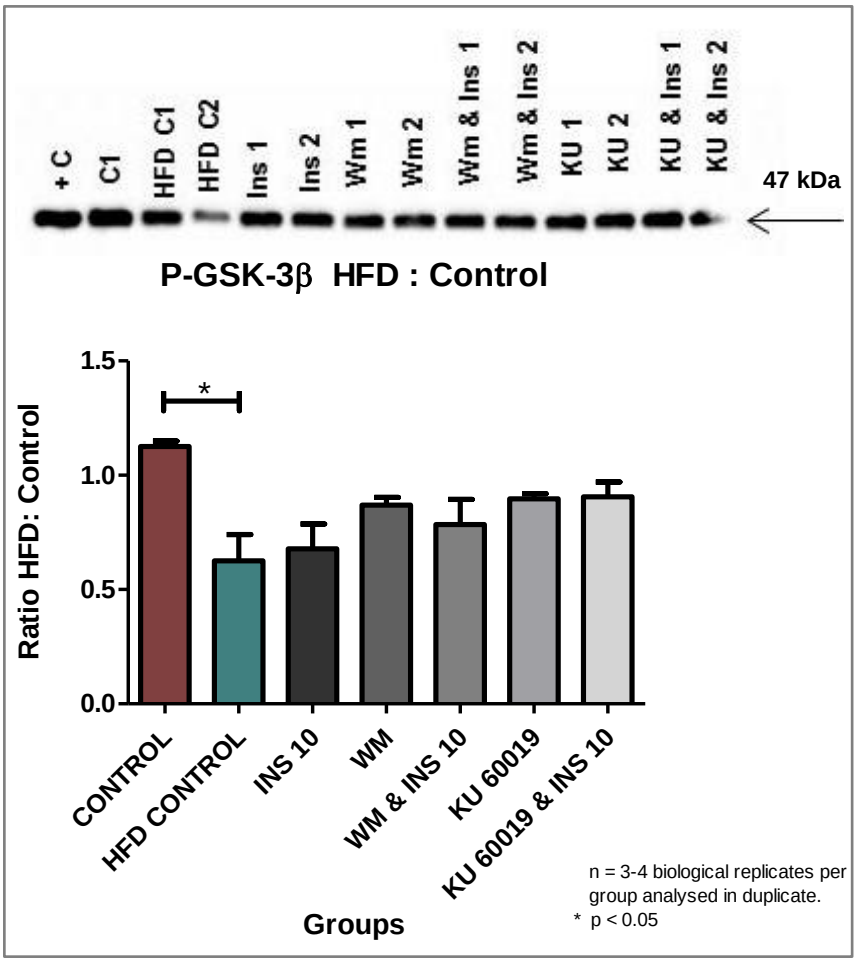

***Figure 3.51**: P-GSK-3β levels expressed as a HFD: Control Ratio*

e) P:T Ratio control

No significant differences were observed in the GSK-3β P:T Ratio in the cardiomyocytes from control animals; n = 4-5 biological replicates per group analysed in duplicate *(Figure 3.52).*

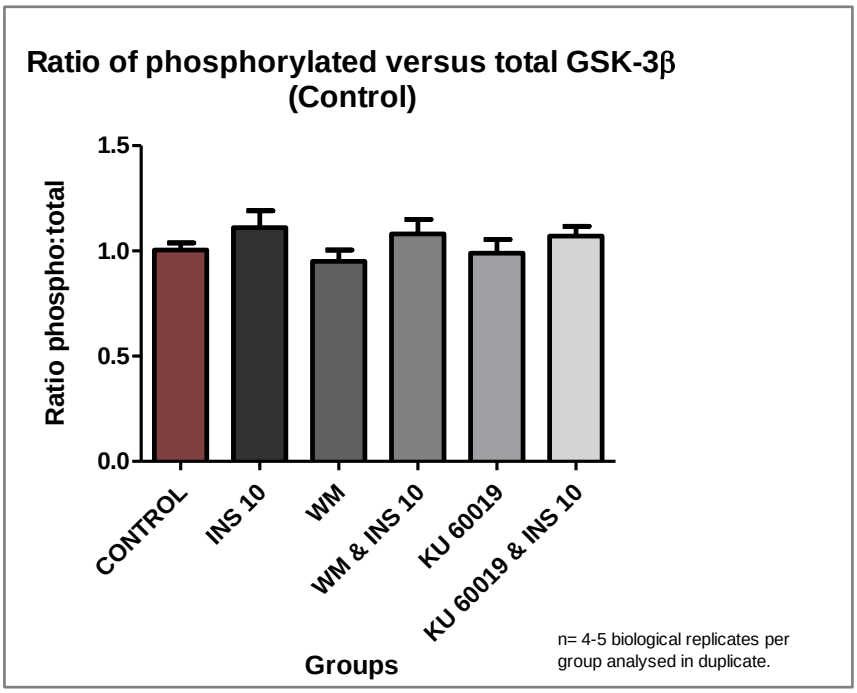

Figure 3.52*: Ratio of phosphorylated vs. total levels of GSK-3β in the cardiomyocytes from control animals*

f) P:T Ratio HFD

Stimulation with INS 10 in the cardiomyocytes from HFD animals significantly increased the P:T Ratio of GSK-3β when compared to cardiomyocytes from baseline HFD values; n = 3-4 biological replicates per group analysed in duplicate; $p < 0.05$ (INS 10 vs. HFD control) *(Figure 3.53).*

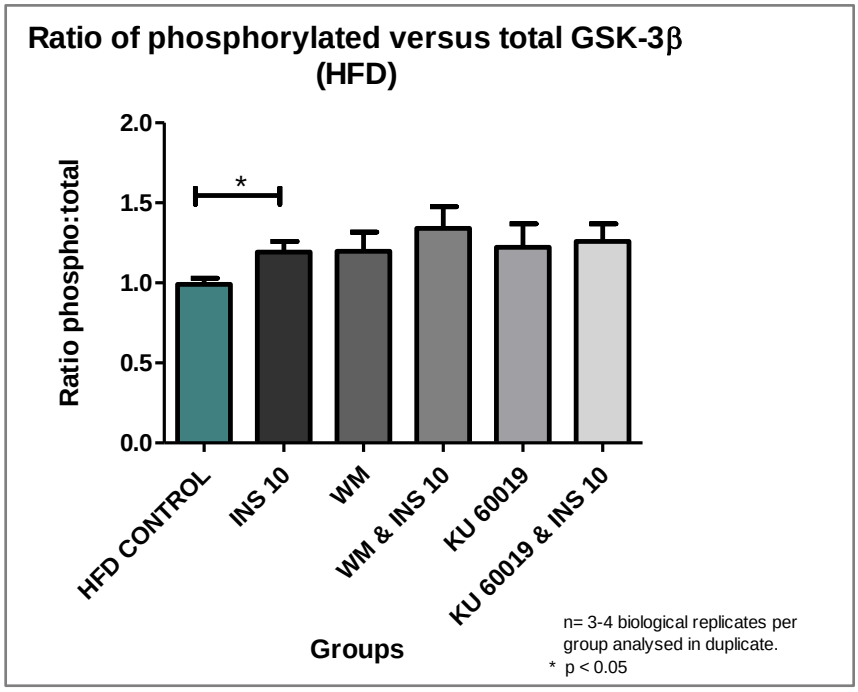

Figure 3.53*: Ratio of phosphorylated vs. total levels of GSK-3β in the cardiomyocytes from HFD animals*

3.8. AMPK

a) Total (T) expression control

Cardiomyocytes from control animals treated with WM showed a significant increase in the total expression of AMPK when compared to the cardiomyocytes from baseline values; n = 4-6 biological replicates per group analysed in duplicate; $p < 0.05$ (WM vs. control) *(Figure 3.54).*

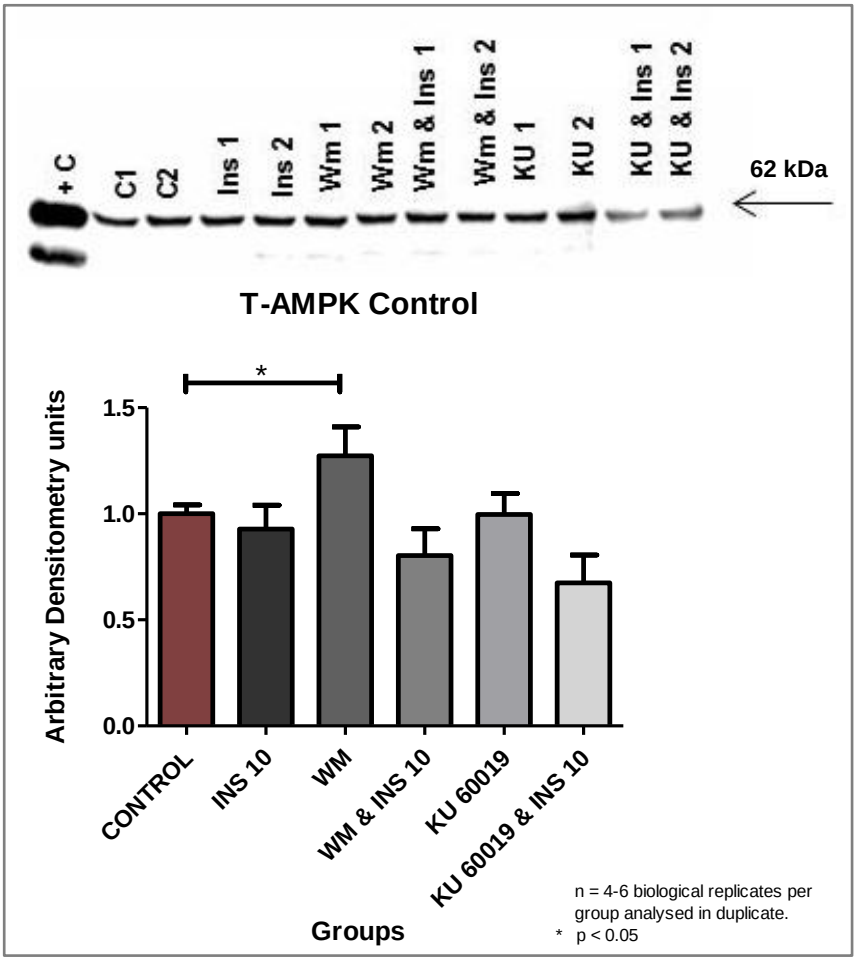

***Figure 3.54**: T-AMPK expression (Arbitrary Densitometry units) in the cardiomyocytes from control animals*

b) Total (T) expression HFD

The cardiomyocytes from HFD animals at baseline presented with significantly lower T-AMPK expression when compared to the cardiomyocytes from control animals; n = 3-5 biological replicates per group analysed in duplicate; $p < 0.05$ (HFD control vs. control) *(Figure 3.55).*

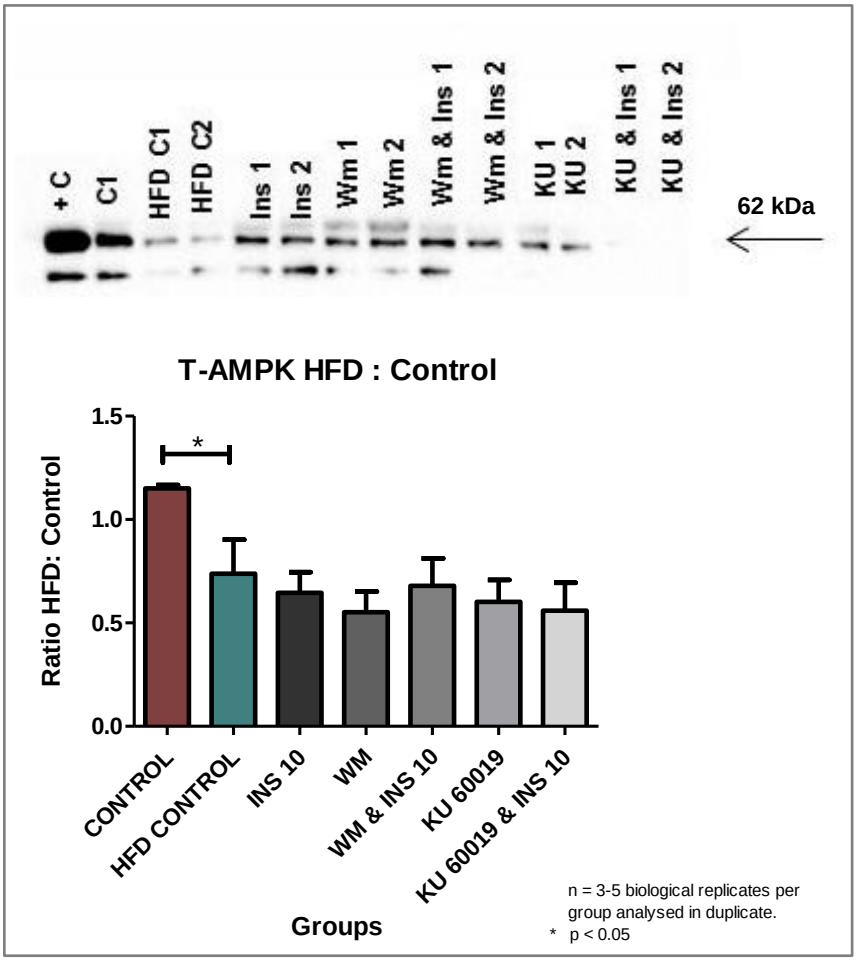

***Figure 3.55**: T-AMPK expressed as a HFD: Control Ratio*

c) *Phosphorylated (P) levels control*

No significant differences were observed in the phosphorylation of AMPK in the cardiomyocytes from control animals with any of the interventions; n = 4-6 biological replicates per group analysed in duplicate *(Figure 3.56).*

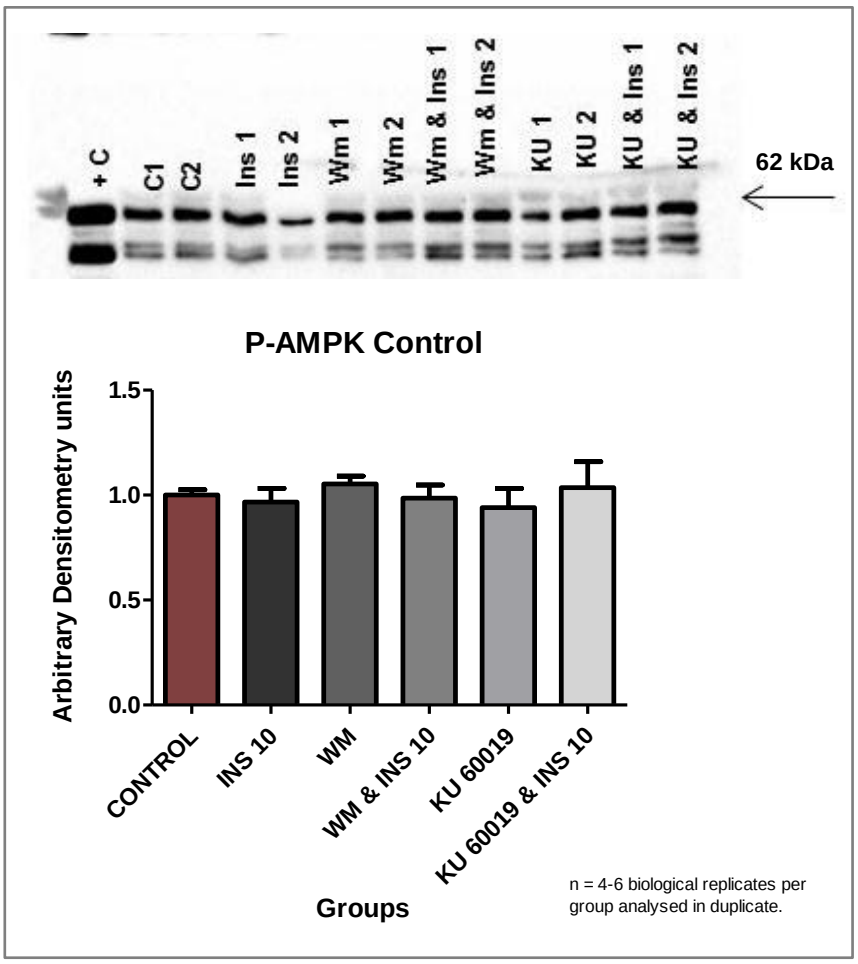

Figure 3.56*: P-AMPK levels (Arbitrary Densitometry units) in the cardiomyocytes from control animals*

d) Phosphorylated (P) levels HFD

The phosphorylation of AMPK was significantly downregulated in the cardiomyocytes from HFD animals at baseline when compared to the cardiomyocytes from control animals; n = 3-5 biological replicates per group analysed in duplicate; $p < 0.001$ (HFD control vs. control) *(Figure 3.57).*

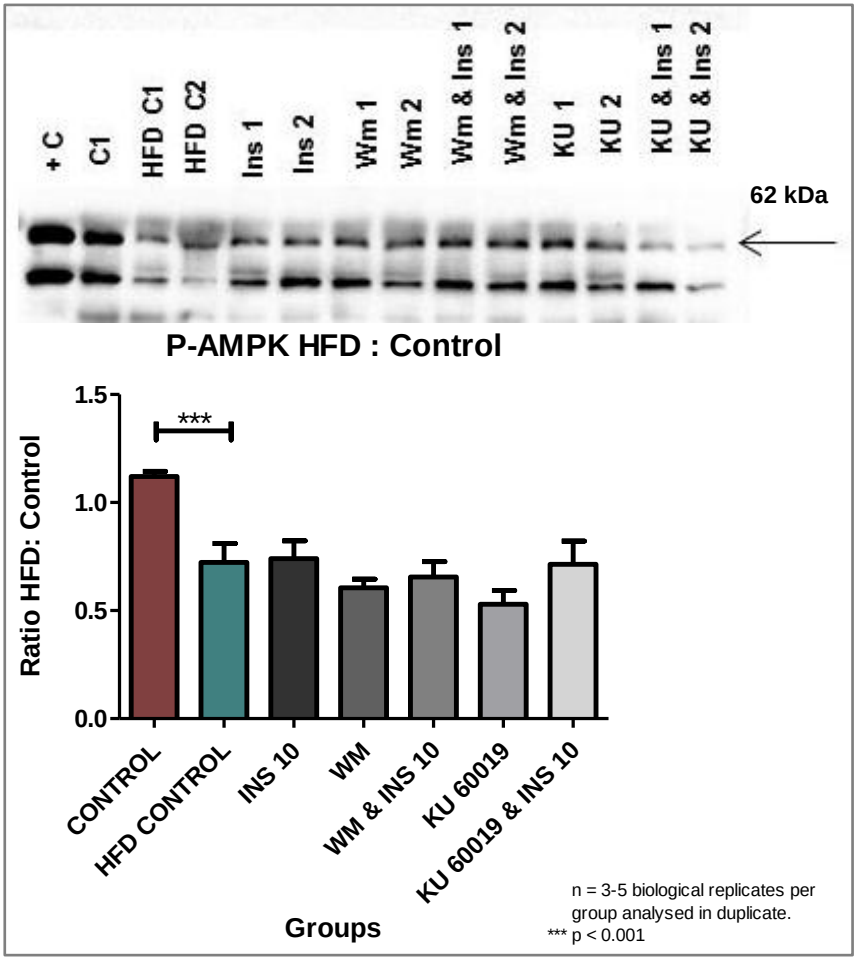

Figure 3.57*: P-AMPK levels expressed as a HFD: Control Ratio*

e) P:T Ratio control

No significant differences were observed in the AMPK P:T Ratio in the cardiomyocytes from control animals; n = 4-6 biological replicates per group analysed in duplicate *(Figure 3.58).*

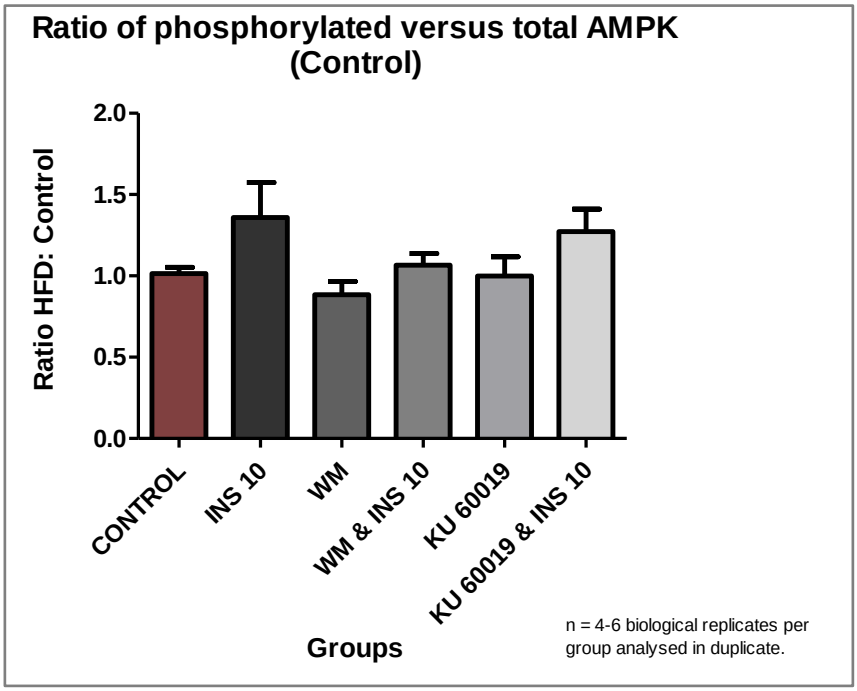

Figure 3.58*: Ratio of phosphorylated vs. total levels of AMPK in the cardiomyocytes from control animals*

f) P:T Ratio HFD

No significant differences were observed in the AMPK P:T Ratio in the cardiomyocytes from HFD animals; n = 3-5 biological replicates per group analysed in duplicate *(Figure 3.59).*

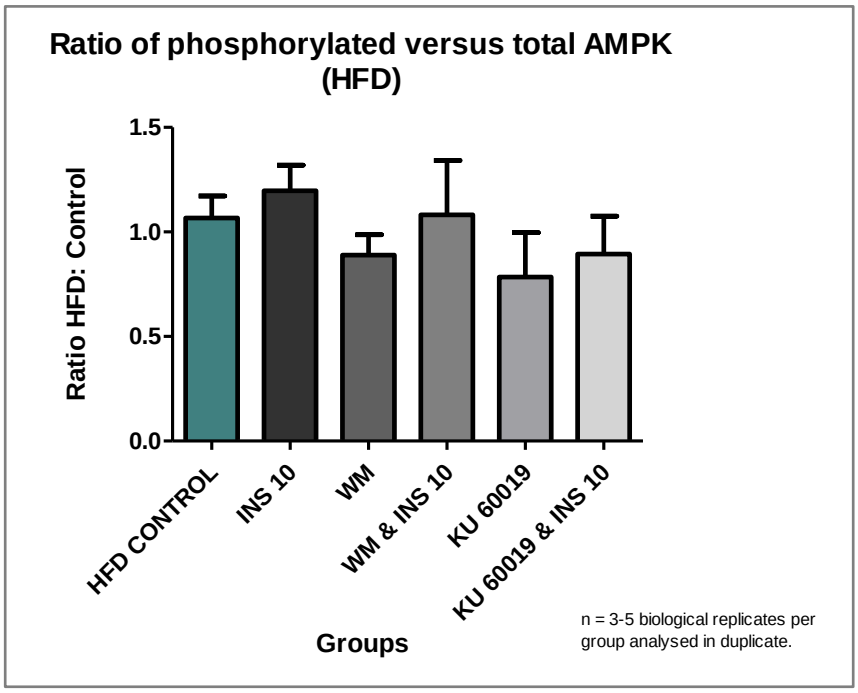

Figure 3.59: *Ratio of phosphorylated vs. total levels of AMPK in the cardiomyocytes from HFD animals*

.

3.9. GLUT4

a) Total (T) expression control

The expression of GLUT4 in cardiomyocytes from the control animals respectively increased significantly in response to INS 10 and WM stimulation when compared to the cardiomyocytes from baseline values; n = 3 biological replicates per group analysed in duplicate, $p < 0.05$ (INS 10 vs. control; WM vs. control) *(Figure 3.60)*

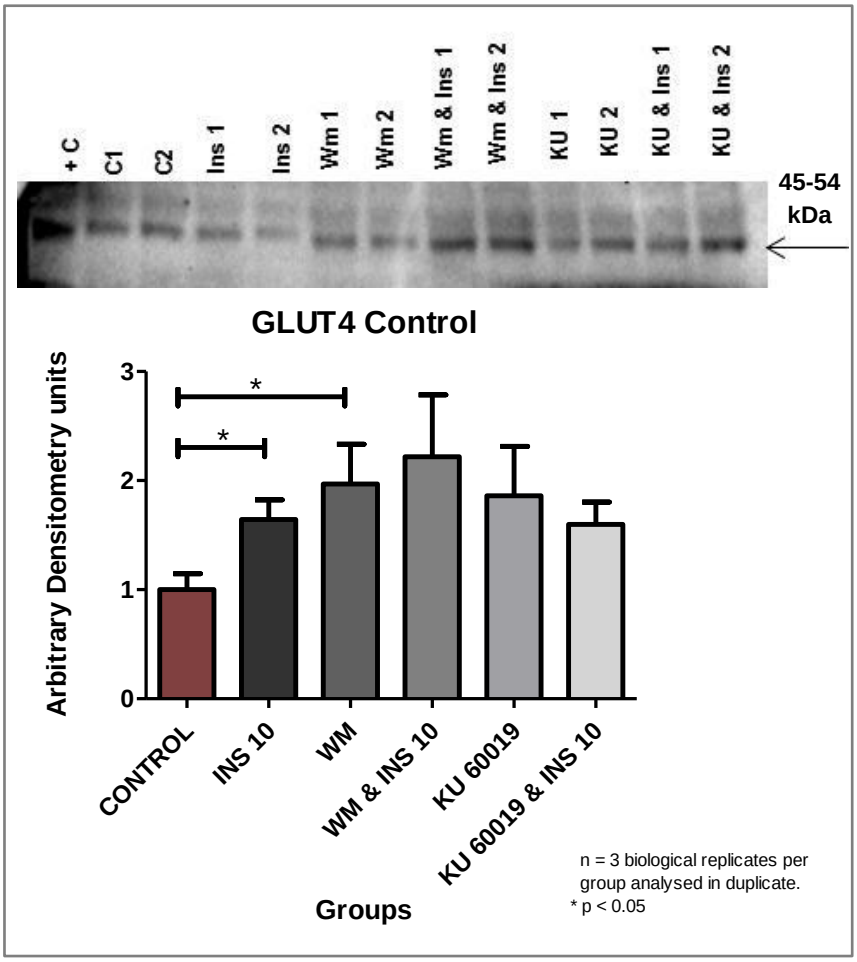

***Figure 3.60**: GLUT4 expression (Arbitrary Densitometry units) in the cardiomyocytes from control animals*

b) Total (T) expression HFD

No significant differences were observed between the GLUT4 expression in the cardiomyocytes from control and HFD animals at baseline; n = 2 biological replicates per group analysed in duplicate *(Figure 3.61).* Furthermore, GLUT4 expression in the cardiomyocytes from HFD animals was not influenced in response to the different treatments.

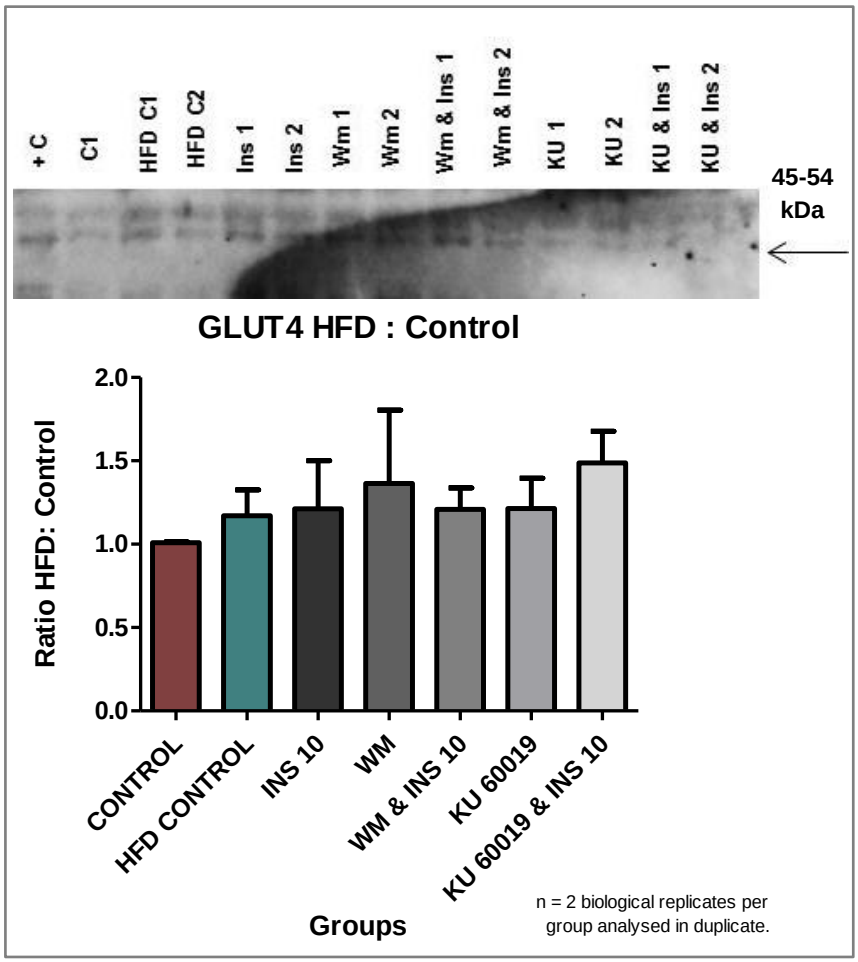

Figure 3.61*: GLUT4 expressed as a HFD: Control Ratio*

CHAPTER 4: DISCUSSION

4. Summary of main findings:

- The HFD was coupled to the development of insulin resistance, as these animals presented with higher:
    - IP fat weight
    - basal glucose
    - insulin levels
    - HOMA IR values
    - downregulated metabolic insulin signalling proteins in the heart.

- The older age-matched control animals were also more resistant to the action of insulin when compared to the young control animals.

- KU 60019 inhibited insulin stimulated 2DG uptake in cardiomyocytes from the control and HFD animals, placing ATM in the pathway whereby insulin stimulates glucose uptake in the heart.

- KU 60019 also significantly attenuated baseline PI3K activation and insulin-stimulated activation of ATM and PKB but did not affect AMPK or GLUT4 levels.

4.1. Body weight & IP fat weight

An increase in the consumption of food containing high fat, cholesterol, sugar and carbohydrate levels are generally associated with an increase in body weight due to the imbalance between the amount of energy intake and energy expenditure. Due to such an imbalance, insulin resistance can develop when the lipolytic activity of the visceral fat cells increases, consequently releasing FFAs in to circulation.

Before commencing experimentation, we characterized the biometric parameters of the model of diet-induced obesity that we aimed to use to ascertain that the animals indeed developed obesity and insulin resistance by feeding them a HFD containing high levels of fat, cholesterol, sugar and carbohydrates compared to the chow-fed control animals.

Results indicated that there was no significant difference between the body weight of the control and HFD animals; however the HFD animals presented with significantly higher IP fat weight gain *(Table 3.1; Figure 3.1-3.2).* According to Defronzo (2004), obesity and

insulin resistance is associated with a larger upper body fat volume (including visceral fat and subcutaneous fat) than with a lower body fat volume.

Visceral fat refers to the fat formation around the organs in the abdomen, whereas subcutaneous fat is located directly under the skin (Hirani, 2013).

Obesity is furthermore also associated with excessive fat storage causing hyperplasia and hypertrophy of adipocytes (Goedecke et al, 2006). Hypertrophied adipocytes cause activation of several macrophage-attracting chemokines followed by macrophage recruitment. The macrophages secrete cytokines (TNF-α and IL-6), causing an inflammatory cascade consequently inducing insulin resistance in the mature adipocytes (Virtue, 2010). With diet management the number of adipocytes cannot be altered, although adipocyte size can decrease (Virtue, 2010).

If Defronzo's (2004) observation is taken into consideration, it might be that the HFD animals stored most of their fat as abdominal body fat, while the control animals stored theirs subcutaneously. As only abdominal fat was evaluated in this study, it might serve as a potential reason for the same body weights but different IP fat weights observed in the control and HFD animals. Alternatively, the fact that the HFD contained less protein than the control diet, may have resulted in a measure of muscle wasting which was not assessed in this study. Muscle wasting refers to an imbalance between protein degradation and protein synthesis (Livestrong, 2013 – www.livestrong.com).

4.2. Basal glucose levels, Insulin levels & HOMA IR index

Basal glucose levels, measured after a stable overnight fast, serves as an important marker to indicate whether blood glucose levels are regulated normally. Basal blood glucose levels in humans according to the American Diabetes Association (ADA) ranges between 3.9 mmol/L to 5.5 mmol/L. Glucose, the end product of dietary carbohydrate digestion, glycogenolysis (glycogen breakdown in the liver) and gluconeogenesis (glucose formation from non-carbohydrate substances) serves as one of the main sources of energy for mammalian cells.

Obesity is associated with an imbalance between energy demand and energy expenditure. Consequently, the energy is stored as fat in the adipose tissue, enhancing the lipolytic activity of the adipocytes and thereby subsequently causing insulin resistance in the liver and muscle tissues (Defronzo, 2004).

From the results of this study, the HFD animals had significantly higher basal glucose levels *(Table 3.1-3.2; Figure 3.3-3.4)* when compared to the control animals. The control group presented with a basal fasting glucose concentration within the normal range; however blood glucose levels of HFD group was only 0.2 mmol/l lower than the insulin resistant/prediabetic mark in humans according to Diabetes.co.uk. Thus it appears that the HFD animals were in the process of developing, or were already, insulin resistant. Furthermore, after administration of 1g/kg sucrose *(Table 3.2; Figure 3.3)* the HFD animals exhibited lower glucose clearance rates than the control animals within the first 45 min and at 120 min respectively, indicating that the HFD animals were glucose intolerant.

Due to the high circulating glucose levels associated with obesity, insulin secretion from the pancreas increases to compensate for and lower the high glucose levels. From the results obtained, the HFD animals had higher insulin levels when compared to the control animals, *(Table 3.1; Figure 3.5),* compensating partly to lower their glucose levels. According to the The New Health Advisor (2015), fasting insulin levels in humans greater than 25 mIU/ml are considered as insulin resistant. However, the HFD animals presented with 118% elevated insulin levels in comparison to the control animals, indicating a pre-diabetic state.

The HOMA IR index was calculated to quantify insulin resistance in the different groups *(Table 3.1; Figure 3.6)*. From the results, the HFD animals had a significantly higher HOMA IR index value than the control animals, indicating that they were insulin resistant.

In summary, the HFD did increase the IP fat weight gain but not the total body weight measured; indicating that the different animal models may have diverse fat storage distributions. The glucose and insulin levels were elevated as expected in obesity, but not to such an extent that they match the criteria for diabetes. However, the HOMA IR index values and OGTT indicated insulin resistance in the HFD animals.

4.3. Insulin dose response in cardiomyocytes from young control, age-matched control and HFD animals

To determine the efficiency and potency of three different insulin concentrations (1 nM, 10 nM and 100 nM) we used cardiomyocytes from young control, age-matched control and HFD animals *(Figure 3.7(b)).* They were 7-8 weeks and 22 weeks of age respectively. Stimulation with INS 10 and INS 100 both enhanced the glucose uptake

levels in the cardiomyocytes from control, age-matched control and HFD animals; however the response of the age-matched animals were much lower than the younger animals, indicating that the age-matched control, older animals, could not respond as efficiently to insulin than the younger animals. For the following experiments, we decided to use the physiological concentration 10 nM insulin as it will allow any additive effects to be detected, whereas the pharmacological concentration of 100 nM insulin would have elicited a maximal response that would mask any inhibitory effect such as treatment with WM and KU 60019.

4.4. 2DG uptake and insulin signalling in the control and HFD animals

Insulin secretion and its action on peripheral, insulin sensitive cells like cardiomyocytes are associated with the activation of the PI3K- dependent or the PI3K-independent signalling pathways, which consequently results in GLUT4 vesicle translocation for increased glucose uptake. From the 2DG uptake results *(Figure 3.8)* INS 10 stimulation increased the 2DG uptake levels in cardiomyocytes from both the control and HFD animals, indicating that either the PI3K-dependent or -independent pathway (investigated via Western blotting) were activated in both these animal models to increase the amount of 2DG uptake by the cells. As expected, treatment with WM and KU 60019 decreased the insulin-stimulated 2DG uptake in cardiomyocytes from both the control and HFD animals.

WM acts via the covalent attachment of PI3K at the electrophilic C-21 site of WM (Norman et al, 1996). Consequently, the activation of all the downstream proteins was downregulated, resulting in decreased 2DG uptake. Furthermore, KU 60019 inhibited the phosphorylation of the ATM protein (Ying et al, 2014) in cardiomyocytes from both the control and HFD animals, resulting in decreased insulin-stimulated 2DG uptake levels via an unknown mechanism. From these findings, it was concluded that ATM, in cardiomyocytes from both animal models, had an effect on 2DG uptake, and would therefore be important in insulin signalling. To gain more insight into ATM's mode of action, Western blotting was performed on cardiomyocytes from control and HFD animals as described in the following section (Chapter 4, Section 4.5).

4.5. Proteins in the insulin signalling pathway

IRS1: Ser307 phopshorylation of IRS1 was determined in the present study. Ser307 phosphorylation results in the inhibition of IRS1's PTB domain function, which is known

to disrupt its association with the catalytic domain of the IR (Aguirre et al, 2002). In the cardiomyocytes from HFD animals, T-IRS1 expression was significantly upregulated while this was in turn downregulated when treated with WM, indicating that the levels of IRS1 are regulated in a PI3K-dependent manner *(Figure 3.10)*. A study by Ruiz-Alcaraz et al (2005) using muscle biopsies from patients, demonstrated that high insulin levels result in a biphasic response on IRS levels, elevating them before the well-known downregulation of IRS levels in diabetes. This effect could be inhibited by the PI3K inhibitor, LY294002. Furthermore, there was a twofold increase in the cardiomyocytes from HFD animals in IRS1 phosphorylation at Ser307 when compared to the cardiomyocytes from control animals at baseline, suggesting that these HFD animals were insulin resistant and insulin signalling through the PI3K-dependent pathway was therefore most likely disrupted *(Figure 3.12).* ATM deficient mice have been found to have increased JNK levels, which lead to the serine phosphorylation of IRS1 and ultimately contributes to the development of insulin resistance (Schneider et al, 2006).

Furthermore, treatment with WM and KU respectively decreased the phosphorylation of IRS1 at Ser307 in cardiomyocytes from the HFD animals. In addition, treatment with WM & INS 10 and KU 60019 & INS 10 respectively in the cardiomyocytes from HFD animals also resulted in decreased Ser307 phosphorylation when compared to INS 10. Thus the inhibition of IRS1 through phosphorylation at Ser307 was no longer restricted in response to the two inhibitors. It has previously been shown that the mTOR-p70^{s6K} pathway controls serine phosphorylation of IRS1 (Ruiz-Alcaraz et al, 2005). Results from the IRS1 P:T Ratio in the cardiomyocytes from HFD animals *(Figure 3.14),* indicated that WM significantly increased the phosphorylation of IRS1 at Ser307, however this result may be misleading, as the T-IRS1 expression after WM treatment was very low. It can however, be assumed all of the IRS1 proteins, although low in expression, were phosphorylated.

The IRS1 results might not be completely accurate, as the n-values were very small, due to the inability to get any good results with the available antibodies (total and phospho) after numerous repetitions. It might be that the specific IRS1 antibodies were not working optimally; the IRS1 protein was too big and did not separate or transfer completely on to the blot; or that the protein concentration in the cardiomyocytes was too low which makes it impossible to visualize on the blot.

IRS1 and ATM: Role of ATM was evaluated by the use of the specific ATM inhibitor, KU 60019, as this KU analogue was tested on 229 kinases and had no or little effect on these kinases (Golding et al, 2009).

As indicated by the use of KU 60019, ATM had no effect on the total expression or phosphorylation of IRS1 in cardiomyocytes from the control animals (Figure 3.9; 3.11) indicating that ATM is most probably involved in the regulation of downstream insulin signalling. In cardiomyocytes from the HFD animals however, further inhibition of the low levels of ATM in the presence or absence of INS 10 was able to lower the Ser307 phosphorylation of IRS1, indicating that ATM activity plays a formerly unrecognized role in the inhibition of insulin signalling at the level of IRS1, probably via activation of the mTOR-p70^{s6k} signalling pathway (Figure 3.12).

PI3K: Cardiomyocytes from the HFD animals presented with lower total P85 catalytic subunit of PI3K expression when compared to the cardiomyocytes from control animals at baseline *(Figure 3.16)*. According to Nadler et al (2001) the downregulation of PI3K is associated with insulin resistance, underscoring the results indicating insulin resistance in cardiomyocytes from the HFD animals. In cardiomyocytes from the control and HFD animals, PI3K phosphorylation was not upregulated in response to INS 10 *(Figure 3.17-3.18).* This observation indicates that the PI3K-dependent pathway was not activated in cardiomyocytes from both groups to increase the 2DG uptake levels as indicated in *Figure 3.8.* It may be that cardiomyocytes from the age-matched control animals already have a measure of insulin resistance at this level as it was also noted that the 2DG uptake was significantly lower in cardiomyocytes from these animals than in younger control animals *(Figure 3.7(b)).*

It may also be that in cardiomyocytes from both animal models, INS 10 stimulation resulted in the activation of the PI3K-independent pathway, however no signalling proteins in the independent pathway were investigated, so no true assumption can be made. Although not significant, we expected cardiomyocytes from the HFD animals to have lower PI3K activation levels *(Figure 3.18)*, due to the upregulated Ser307 phosphorylation which inhibited IRS1 activation *(Figure 3.12)* and consequently the association of PI3K with the pTyr residues of IRS1.

PI3K and ATM: According to the literature, ATM up to date displayed no direct effects on PI3K. Treatment with KU 60019 alone in cardiomyocytes from both the control and HFD animals decreased the phosphorylation of PI3K when compared to the respective control baseline values (Figure 3.19). In addition, KU 60019 also reduced 2DG uptake in

cardiomyocytes from both the control and HFD animals (Figure 3.8). This indicates that KU 60019 may have effects on PI3K activity although it is stated in literature that it is specific for ATM (Golding et al, 2009).

PTEN: PTEN is known for its ability to terminate insulin signalling via the hydrolization of PIP3 to PIP2, or via the direct de-phosphorylation of IRS1. From the results, no differences were observed in the expression or phosphorylation of PTEN in response to the different treatments in cardiomyocytes from both the control and HFD animals *(Figure 3.22-3.27),* therefore PTEN activity were not changed.

PTEN and ATM: The inhibition of ATM did not alter PTEN expression or phosphorylation (Figure 3.22-27, therefore any changes in the insulin signalling pathway in response to ATM cannot be attributed to changes in PTEN activity.

ATM: As described in Chapter1, Section 6.5, ATM according to several studies plays an important role in the regulation of insulin signalling. From what is known, ATM in response to insulin stimulation, can activate 4EBP1 (Yang & Kastan, 2000), PKB via PP1 or PP4-6 (Viniegra et al, 2005; Halaby et. al, 2008) or AMPK via LKB phosphorylation (Shackelford & Shaw, 2009).

From the results of the current study, cardiomyocytes from the HFD animals, as expected, presented with lower T-ATM expression levels when compared to cardiomyocytes from the control animals at baseline, which therefore correlate with the observation of Schneider et al (2006) that downregulated ATM is associated with insulin resistance *(Figure 3.29).* Interestingly, cardiomyocytes from both groups treated with KU 60019 & INS 10 had decreased T-ATM expression levels when compared to the respective INS 10 groups *(Figure 3.28-3.29)*, which suggests that ATM expression is regulated through the insulin signalling pathway. This may be because ATM regulates the activation of both eIF-4E and $p70^{s6k}$ activity, thereby regulating protein synthesis (Bevan, 2009). Consequently these effects are inhibited by KU 60019, resulting in lower expression of the protein.

KU 60019 treatment in cardiomyocytes from the control and HFD animals significantly decreased the insulin-stimulated phosphorylation of ATM in the cytosol when compared to INS 10 *(Figure 3.31-3.32).* It is possible that the effect of KU 60019 under basal conditions was more outspoken in cardiomyocytes from the HFD animals with their lower baseline expression and phosphorylation levels of ATM.

The ATM P:T Ratio of cardiomyocytes from the control animals indicated that KU 60019 increased the phosphorylation levels of ATM when compared to baseline values *(Figure 3.33)*. However, KU 60019 also downregulated the expression levels of ATM. It is therefore not possible to extrapolate the active kinase from this result *(Figure 3.28).*

The ATM P:T Ratio of cardiomyocytes from the HFD animals showed that INS 10 treatment decreased the phosphorylation of ATM when compared to baseline values *(Figure 3.34)*, thus exacerbating the effects of the lower T-ATM expressed in these HFD animals *(Figure 3.29).* It must also be kept in mind that these animals are insulin resistant, therefore present with low insulin-stimulated activity. Furthermore, the P:T Ratio confirmed that treatment with KU 60019 in cardiomyocytes from the HFD animals significantly inhibited the phosphorylation of ATM when compared to the HFD baseline group *(Figure 3.34).*

From the above it is evident that ATM in cardiomyocytes of the HFD animals was not activated in response to INS 10 stimulation as expected. This may again be attributed to cardiomyocytes from the age-matched, older animals who already display aspects of insulin resistance, as observed in the 2DG uptake results *(Figure 3.7(b))*.

PKB: In cardiomyocytes from the HFD animals, T-PKB expression was 40% lower when compared to the control animals at baseline *(Figure 3.36).* As shown in *Figure 3.49 and Figure 3.51*, we also found that GSK3β expression and activity was lower in cardiomyocytes from the HFD animals. It has been demonstrated previously that inhibition of GSK-3β leads to downregulation of PKB expression through the beta-catenin pathway. This pathway, which is normally inhibited by GSK-3β, regulates PKB expression (Wade, 2009).

Stimulation with INS 10 in cardiomyocytes from the control and HFD animals resulted in no detectable activation of PKB *(Figure 3.37-3.38)*. We would have expected this observation in cardiomyocytes from the HFD animals, as they were insulin resistant and signalling through IRS1 was disrupted. This again, is a clear indication that cardiomyocytes from the age-matched, older animals were also becoming insulin resistant.

PKB and ATM: According to Viniegra et al (2005) and Halaby et al (2008) ATM phosphorylates PKB which results in increased glucose uptake by the cell. In these experiments, the effect of KU 60019 on insulin-stimulated cardiomyocytes from both the

control and HFD animals was significant (Figure 3.39). Thus our results correlated with literature that ATM might be a potential activator of PKB in the context of glucose uptake.

AS160: AS160 is activated in response to the insulin mediated activation of PKB (Klip et al, 2014) or, according to new evidence via the ATM/LKB/AMPK pathway (Shackelford & Shaw, 2009). When AS160 is activated, it initiates GLUT4 vesicle translocation via the conversion of Rab-GDP to Rab-GTP, consequently increasing glucose uptake by the cell.

From the results *(Figure 3.42-3.43)*, the T-AS160 expression levels of cardiomyocytes from the control and HFD animals showed no significant differences in response to the different treatments. In cardiomyocytes from the control animals, treatment with WM significantly decreased the phosphorylation of AS160 when compared to the baseline control animals *(Figure 3.43; 3.46).* One would expect WM to decrease the activation of AS160 as it inhibits the PI3K pathway; however no direct inhibition of phosphorylation in response to WM was seen in the PI3K results.

As observed in a previous study conducted by Middelbeek et al (2013), cardiomyocytes from the HFD animals presented with impaired AS160 phosphorylation at Thr642 when compared to cardiomyocytes from the control animals at baseline *(Figure 3.45).* Stimulation with INS 10 however still increased the phosphorylation of AS160 in cardiomyocytes from the HFD animals when compared to baseline values *(Figure 3.45; 3.47)*, although it could not have been via the PKB pathway, as PKB was not activated in cardiomyocytes from both the control and HFD animals. Therefore, the activation of AS160 in cardiomyocytes from the HFD animals in response to INS 10 was either via ATM/LKB/AMPK or directly from the IR through an unknown mechanism.

AS160 and ATM: Inhibition of ATM had no significant effect on the phosphorylation of AS160 in cardiomyocytes from both animal groups either in the presence or absence of INS 10 stimulation. This therefore still leaves the inhibition of 2DG uptake by KU 60019 unresolved.

GSK-3β: The phosphorylation of GSK-3β at Ser9 via PKB results in the inactivation of this protein, consequently activating GS for glycogen synthesis.

From the results, once again, cardiomyocytes from the HFD animals presented with significantly less T-GSK-3β and P-GSK-3β levels when compared to cardiomyocytes from the control animals, indicating the HFD induced insulin resistance in these animals

(Figure 3.49; 3.51). As argued above, GSK-3β probably regulated the expression of PKB as observed in cardiomyocytes from the HFD animals. According to the GSK-3β P:T Ratio in cardiomyocytes from the HFD animals, INS 10 was able to significantly upregulate the phosphorylation of GSK-3β, indicating that INS 10 was still able to phosphorylate the low T-GSK-3β levels expressed in these HFD animals *(Figure 3.53).*

GSK-3β and ATM: In cardiomyocytes from the control animals, the inhibition of ATM resulted in a significantly higher T-GSK-3β expression level, indicating that active ATM supresses the T-GSK-3β levels and less glycogen synthesis can occur via this pathway (Figure 3.48). ATM had no effect on the activation of GSK-3β in cardiomyocytes from both the control or HFD animals (Figure 3.50-3.53).

AMPK: According to Shackelford & Shaw (2009) AMPK is activated in response to insulin via ATM; however the exact mechanism is not yet fully understood. From the results, WM stimulated T-AMPK expression in cardiomyocytes from the control animals, but not in cardiomyocytes from the HFD animals when compared to the respective baseline values *(Figure 3.54),* which indicates that AMPK expression is regulated negatively by the insulin-PI3K pathway. The drivers that regulate AMPK expression have not been defined (Zaha & Young, 2012) but both the actions of MiRNA's as well degradation through the proteasomal pathway, are mentioned as possible regulatory mechanisms.

AMPK in cardiomyocytes from both the control and HFD animals were not activated at all via INS 10 stimulation when compared to the respective baseline values *(Figure 3.56-3.57)* which correlates with the ATM Western blot results where ATM also wasn't activated in response to INS 10 stimulation *(Figure 3.30-3.31)*.

Cardiomyocytes from the HFD once again resulted in downregulation of T-AMPK and P-AMPK levels *(Figure 3.55; 3.57)* when these cardiomyocytes were compared to the cardiomyocytes from the control animals at baseline. This downregulation may have an effect on the PI3K-independent pathway for glucose uptake via GLUT4 as AMPK is believed to regulate GLUT4 expression (Ojuka et al, 2000).

AMPK and ATM: ATM did not have any effect of the regulation of AMPK levels in cardiomyocytes from the control or the HFD animals (Figure 3.54-3.59).

GLUT4: The initiation of GLUT4 vesicle translocation to the plasma membrane is important for glucose uptake by the cell. GLUT4 is translocated via the PI3K-dependent

pathway or via the ATM/LKB/AMPK pathway. From the results, stimulation with INS 10 significantly increased the total expression of GLUT4 in cardiomyocytes from the control animals when compared to baseline values, indicating that GLUT4 protein levels may be controlled by insulin levels in the cell *(Figure 3.60)*. WM surprisingly also increased the expression of GLUT4 in cardiomyocytes from the control animals when compared to baseline values, which correlates with the increase in T-AMPK in response to WM *(Figure 3.54)*, indicating that a different pathway than the PI3K-dependent pathway may be responsible for the increase in GLUT4 expression. This underscores the observation by Ojuka et al (2000) that 5-Aminoimidazole-4-carboxamide ribonucleotide (AICAR), an activator of AMPK, which is converted to the adenosine monophosphate (AMP) analog, AICAR monophosphate (ZMP) once it enters the cell, can result in the upregulation of GLUT4 expression in skeletal muscle.

In cardiomyocytes from the HFD animals, we expected the GLUT4 expression to be downregulated when compared to the control animals, as the HFD animals presented with lower AMPK expression *(Figure 3.55)* and a 30% downregulated phosphorylation of AS160 *(Figure 3.45).* From the results, there were no differences observed in GLUT4 expression in cardiomyocytes from these HFD animals *(Figure 3.61).* These results might not be completely accurate, as the n-value was very small, due to the inability to get any results after numerous repetitions of the Western blots, but it has been demonstrated in skeletal muscle, that GLUT4 expression is mostly downregulated in conditions of severe insulin deficiency but not consistently in diabetes (Zaha & Young, 2012). In addition, it is argued in literature that the low insulin-responsive glucose uptake in skeletal muscle is not because of low GLUT4 expression but because of defective translocation of the protein, an aspect that has not been measured in the current study.

GLUT4 and ATM: Inhibition of ATM had no direct effect on GLUT4 expression in cardiomyocytes from both the control and HFD animals, correlating with the lack of effect seen on AMPK.

4.6. General discussion and conclusion

The HFD was coupled to whole-body insulin resistance as the HFD animals were less responsive to insulin within the first 60 min, and on 120 min *(Figure 3.3)* of the OGTT when compared to the control animals. In addition they also presented with significantly higher basal glucose *(Figure 3.4),* insulin *(Figure 3.5)* and HOMA IR *(Figure 3.6)* levels when compared to the control animals. From the Western blot results, cardiomyocytes

from the HFD animals had downregulated T-PI3K, T-ATM, T-PKB, T-GSK3β and T-AMPK expression as well as downregulated phosphorylation of ATM, AS160, GSK3β, AMPK and increased phosphorylation of IRS1 at Ser307. These observations also, therefore demonstrate that the cardiomyocytes from the HFD animals presented with a profile of insulin resistance.

The 2DG uptake results *(Figure 3.8)* showed that stimulation with INS 10 in both the control and HFD animals increased the amount of glucose uptake in the cardiomyocytes to the same extent. Importantly, especially for the current study was to determine whether ATM plays a direct role in the regulation of glucose uptake by the cells and the development of insulin resistance.

2DG uptake results in both animal models indicated that the inhibition of ATM via KU 60019 decreased the amount of 2DG uptake in insulin-stimulated cardiomyocytes. We can therefore conclude that the activity of ATM is necessary for insulin-stimulated glucose uptake. Due to this observation, we investigated signalling events controlling 2DG uptake, using Western blotting techniques to determine how ATM is involved in the regulation of glucose uptake. Inhibition of ATM also lowered the Ser307 phosphorylation of IRS1 in cardiomyocytes from the HFD animals *(Figure 3.12)*, indicating a possible improvement in insulin signalling.

Western blot data demonstrated that stimulation with INS 10 in cardiomyocytes from both animal models did not activate ATM as measured by phosphorylation of Ser1981 *(Figure 3.30-3.31)*. ATM therefore must have been activated via a different mechanism to initiate glucose uptake as seen in the 2DG uptake results. According to studies done by Guo et al (2010) and Pellegrini et al (2006), ATM is not only active once phosphorylated at Ser1981. As ATM is believed to have three additional autophosphorylation sites including: Ser367, Ser1893, and Ser2996 (Kozlov et al, 2011) and we only investigated phosphorylation of ATM at the Ser1981 site, it might be that ATM was phosphorylated at a different phosphorylation site resulting in activation. This however needs to be investigated in future studies.

Furthermore, inhibition of ATM, regulated the phosphorylation of the P85 subunit of PI3K in cardiomyocytes from both animal models *(Figure 3.19)*, indicating that the inhibitor may not be as specific as reported in literature (Golding et al, 2009). This observation makes it very difficult to distinguish between ATM effects and PI3K-mediated effects. As activation of PI3K is a prerequisite for insulin-stimulated glucose uptake, this sheds some doubt on the above conclusion that ATM activity is necessary for insulin-stimulated

glucose uptake. It will only be possible to determine this association accurately by either silencing ATM in cardiomyocytes or using a commercially available ATM-KO cell line as surrogate.

According to a study done by Andrisse et al (2013), ATM can directly phosphorylate GLUT1 in the skeletal muscle at a specific Ser490 site. GLUT1, located predominately in the plasma membrane of the skeletal muscle, has a COOH-terminus containing a PDZ binding motif on which the specific ATM Ser490 phosphorylation site is located. Once phosphorylated, it interacts with the Gα-interacting protein C terminus 1 (GIPC1) (Matsuoka et al, 2007). This interaction between GLUT1 and GIPC1 is believed to increase GLUT1's externalization to the plasma membrane for GLUT1-mediated glucose transport (Andrisse et al, 2013). Whether this mechanism was active in our study is not known, as we did not investigate the relationship between ATM and GLUT1 in the current study. Therefore more studies are needed to elucidate the specific relationship between ATM and GLUT1 in cardiomyocytes.

More-over, ATM is associated with vesicular structures and can bind to the membrane proteins Vesicle-associated membrane protein 2 (VAMP2) and synapsin, two major components of synaptic vesicles (Li et al, 2009). Both these proteins are also components of the glucose transporter GLUT4-containing vesicles in muscle cells and therefore are involved in insulin-mediated GLUT4 translocation to the plasma membrane (Dugani & Klip, 2005). In L6 myoblasts, inhibition of ATM abolished the insulin-regulated GLUT4 translocation process (Halaby et al, 2008).

It is therefore possible that the primary effect of KU 60019 to inhibit glucose uptake, does not lie in any of the signalling intermediates that was determined in this study, but that it inhibits the insertion of the GLUT4 protein into the plasma membrane.

4.7. Summarized effect of HFD (indicated in red) and ATM (KU 60019) (indicated in green) on the insulin signalling proteins

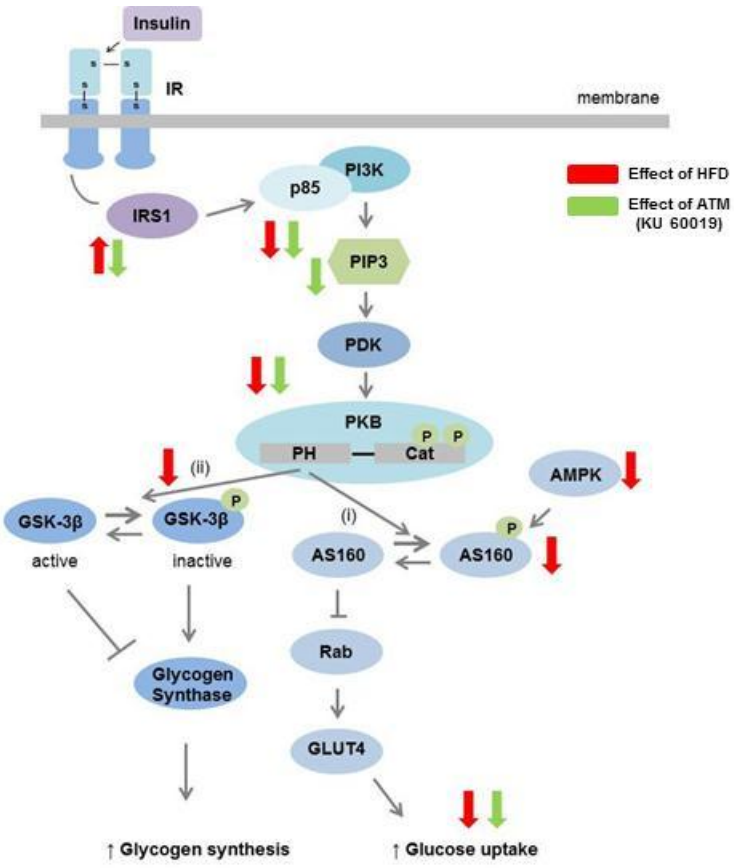

Figure 4.1: *Summarized effect of HFD and ATM (KU 60019) on the insulin signalling proteins*

Conclusion: The HFD was coupled to the development of insulin resistance, as these animals presented with higher IP fat weight, basal glucose and insulin levels as well as downregulation of multiple metabolic insulin signalling proteins and insulin sensitivity in the heart. The older age-matched control animals were also more resistant to the action of insulin when compared to the young control animals. KU 60019 inhibited insulin stimulated 2DG uptake in cardiomyocytes from the control and HFD animals, placing ATM in the pathway whereby insulin stimulates glucose uptake in the heart. KU 60019 also significantly attenuated baseline PI3K activation and insulin-stimulated activation of ATM and PKB but did not affect AMPK or GLUT4 levels. We conclude that the downregulation of expression of ATM in insulin resistant states may be central to the development of myocardial insulin resistance.

CHAPTER 5: LIMITATIONS AND FUTURE RESEARCH

- The age-matched control animals were less responsive to insulin when compared to young control animals, indicating possible insulin resistance in this model.
- The effect of Metformin on ATM activation should be investigated.
- The n-value of IRS1 in both the age-matched control and HFD animals should be enlarged for consistency in the results.
- GLUT4 expression as well as the translocation of GLUT4 vesicles should be investigated in the age-matched control and HFD animals.
- The effect of ATM on GLUT1 should be investigated to determine the possible relationship of ATM and GLUT1 for glucose uptake.
- The phosphorylation of ATM at Ser367, Ser1893, and Ser2996 should be studied to determine whether ATM was activated at a different site.
- In view of the possibility that KU 60019 is not specific for ATM, as PI3K was inhibited in response to KU 60019 treatment, silencing of the ATM protein in cardiomyocytes should be attempted or a commercially available KO cell line used to determine specific actions.

REFERENCES

- Abraham, R.T. (2001) Cell cycle checkpoint signaling through the ATM and ATR kinases. Genes Dev. 15: 2177-2196.
- Aguirre, V., Werner, E.D., Giraud, J., Lee, Y.H., Shoelson, S.E., et al (2002) Phosphorylation of Ser307 in insulin receptor substrate-1 blocks interactions with the insulin receptor and inhibits insulin action. J. Biol. Chem. 277(2): 1531-1537.
- Ambrose, M., Goldstine, J.V., Gatti, R.A. (2007) Intrinsic mitochondrial dysfunctions in ATM-deficient lymphoblastoid cells. Hum. Mol. Genet. 16: 2154-2164.
- American Heart Association (2014) - http://www.heart.org, October 2015.
- Anai, M., Ono, H., Funaki, M., Fukushima, Y., Inukai, K., et al (1998) Different subcellular distribution and regulation of expression of insulin receptor substrate (IRS)-3 from those of IRS-1 and IRS-2. J. Biol. Chem. 273: 29686-29692.
- Andrisse, S., Patel, G.D., Chen, J.E., Webber, A.M., Spears, L.D., et al (2013) ATM and GLUT1-S490 Phosphorylation Regulate GLUT1 Mediated Transport in Skeletal Muscle. Journal.pone 10: 1371.
- ApexBio Technology (2013) – www.apexbt.com, November 2015.
- Armata, H.L., Golebiowski, D., Jung, D.Y., Ko, H.J., Kim, J.K., et al (2010) Requirement of the ATM/p53 tumor suppressor pathway for glucose homeostasis. Cell Biol. 30(24): 5787-5794.
- Ashraf, M. *(*1979*)* Correlative studies on sarcolemmal ultrastructure, permeability and loss of intracellular enzymes in the isolated heart perfusion with calcium-free medium*.* Am. J. Pathol. 97*:* 411-432*.*
- Bakkenist, C.J., Kastan, M.B. (2003) DNA damage activates ATM through intermolecular autophosphorylation and dimer dissociation. Nature 421: 499-506.
- Baleta, A., Mitchell, F. (2014) Diabetes and Obesity in South Africa. The Lancet Diabetes Endocrinol. 2(9): 687-688.
- Banin, S. et al (1998) Enhanced phosphorylation of p53 by ATM in response to DNA damage. Science 281: 1674-1677.
- Barlow, C. et al (2000) ATM is a cytoplasmic protein in mouse brain required to prevent lysosomal accumulation. Proc. Natl. Acad. Sci. U.S.A. 97: 871-876.
- Baumgartl, J., Baudler, S., Scherner, M., Babaev, V., Makowski, L., et al (2006) Myeloid lineage cell-restricted insulin resistance protects apolipoproteinE-deficient mice against atherosclerosis. Cell Metab. 3: 247-256.
- Bertrand, L., Alessi, D.R., Deprez, J., Deak, M., Viaene, E., et al (1999) Heart 6-phosphofructo-2-kinase activation by insulin results from Ser-466 and Ser-483

phosphorylation and requires 3-phosphoinositide-dependent kinase-1, but not protein kinase B. J. Biol. Chem. 274: 30927-30933.

- Bevan, P. (2009) Insulin Signalling. Journal of cell science 114(8): 1429-1430.
- Birnbaum, M.J., Shaw, R.J. (2011) Genomics: Drugs, diabetes and cancer. Nature 470(7334): 338-339.
- Boden, G. (2008) Obesity and Free Fatty Acids (FFA). Endocrinol. Metab. Clin. North Am. 37(3): 635-639.
- Boehrs, J.K., et al (2007) Constitutive expression and cytoplasmic compartmentalization of ATM protein in differentiated human neuron-like SHSY5Y cells. J. Neurochem. 100: 337-345.
- Boudina, S., Abel, E.D. (2007) Diabetic Cardiomyopathy Revisited. Circulation 115: 3213-3223.
- Bradford, M.M. (1976) "Rapid and sensitive method for the quantitation of microgram quantities of protein utilizing the principle of protein-dye binding". Anal. Biochem. 72: 248-254.
- Busiguina, S., et al (2000) Neurodegeneration is associated to changes in serum insulin-like growth factors. Neurobiol. Dis. 7: 657-665.
- Canman, C.E., et al (1998) Activation of the ATM kinase by ionizing radiation and phosphorylation of p53. Science 281: 1677-1679.
- Cell signalling - www.cellsignal.com, November 2015.
- Chiang, S.H., Baumann, C.A., Kanzaki, M., Thurmond, D.C., Watson, R.T., et al (2001) Insulin-stimulated GLUT4 translocation requires the CAP-dependent activation of TC10. Nature 410: 944-948.
- Collot-Teixeira, S., Martin, J., McDermott-Roe, C., Poston, R., McGregor, J.L. (2007) CD36 and macrophages in atherosclerosis. International journal of the European Society of Cardiology 75(3): 468-477.
- Coort, S.L., Bonen, A., van der Vusse, G.J., Glatz, J.F., Luiken, J.J. (2007) Cardiac substrate uptake and metabolism in obesity and type-2 diabetes: role of plasma membrane substrate transporters. Mol. Cell Biochem. 299: 5-18.
- Defronzo, R.A. (2004) Dysfunctional fat cells, lipotoxicity and type 2 diabetes. Blackwell Publishing Ltd Int. J. Clin. Pract. 58: 9-21.
- Deprez, J., Bertrand, L., Alessi, D.R., Krause, U., Hue, L., et al (2000) Partial purification and characterization of a wortmannin-sensitive and insulin-stimulated protein kinase that activates heart 6-phosphofructo-2-kinase. Biochem. J347: 305-312.
- Dhand, R., Hara, J., Hiles, I., Bax, B., Gout, I., et al (1994) PI3-kinase: structural and functional analysis of intersubunit interactions. EMBO 13(3): 511-521.

- Diabetes Education online (2007-2016) - www.http://dtc.ucsf.edu, January 2016.
- Dorland's Medical Dictionary (2011), Medical Dictionary.
- Dugani, C.B., Klip, A. (2005) Glucose transporter 4: cycling, compartments and controversies. EMBO 6(12): 1137-1142.
- Dyck, D.J., Steinberg, G., Bonen, A. (2001) Insulin increases FA uptake and esterification but reduces lipid utilization in isolated contracting muscle. Am. J. Physiol. Endocrinol. Metab. 281: E600-E607.
- Elisa analysis - http://www.elisaanalysis.com, June 2015.
- Elliott, P., Andersson, B., Arbustin, E., et al (2008) Classification of the cardiomyopathies: a position statement from the European Society Of Cardiology Working Group on Myocardial and Pericardial Diseases. Eur. Heart J29: 270-276.
- Emami, J., et al (1999) Insulin-sparing effect of hydroxychloroquine in diabetic rats is concentration dependent. Can. J. Physiol. Pharmacol. 77(2): 118-123.
- Enzyme inhibitors - http://www.ucl.ac.uk, May 2015.
- Esposito F., Sinden, R.R. (1987) Supercoiling in prokaryotic and eukaryotic DNA: changes in response to topological perturbation of plasmids in E. coli and SV40 in vitro, in nuclei and in CV-1 cells. Nucleic Acids Res. 15(13): 5105–5124.
- Fantin, V. R., Lavan, B., Wang, Q., Jenkins, N.A., Gilbert, D.J., et al (1999) Cloning, tissue expression, and chromosomal localization of the mouse insulin receptor substrate 4 gene. Endocrinology 140: 1329-1337.
- Fantin, V.R., Keller, S.R., Lienhard, G.E., Wang, Q. (1999) Insulin receptor substrate 4 supports insulin- and interleukin 4-stimulated proliferation of hematopoietic cells. Biochem. Biophys. Res. Commun. 260: 718-723.
- Fatkin, D., McConnell, B.K., Mudd, J.O., et al (2000) An abnormal Ca^{2+} response in mutant sarcomere protein-mediated familial hypertrophic cardiomyopathy. J. Clin. Invest. 106: 1351-1359.
- Ferby, I., Waga, I., Kume, K., Sakanaka, C., Shimizu, T., et al (1996) PAF-induced MAPK activation is inhibited by wortmannin in neutrophils and macrophages. Adv. Exp. Med. Biol. 416: 321-326.
- Fernández-Sánchez, A., Madrigal-Santillán, E., Bautista, M., Esquivel-Soto, J., Morales-González, A., et al (2011) Inflammation, Oxidative Stress, and Obesity. Int. J. Mol. Sci. 12: 3117-3132.
- Fischer, Y., Rose, H., Kammermeier, H. (1991) Highly insulin-responsive isolated rat heart muscle cells yielded by a modified isolation method. Life Science 49: 1679-1688.
- Fonseca-Alaniz, M.H., Takada, J., Alonso-Vale, M.I., Lima, F.B. (2007) Adipose tissue as an endocrine organ: From theory to practice. J. Pediatr. 83 (Suppl. 5): S192–S203.

- Foster, C.R., Singh, M., Subramanian, V., Singh, K. (2011) Ataxia telangiectasia mutated kinase plays a protective role in β-adrenergic receptor-stimulated cardiac myocyte apoptosis and myocardial remodeling. Mol. Cell Biochem. 353: 13-22.
- Frank, J.S., Rich, T.L., Beydler, S., Kreman, M. (1982) Calcium depletion in rabbit myocardium: ultrastructure of the sarcolemma and correlation with the calcium paradox. Circ. Res. 51: 117-130.
- Freemantle, N., Cleland, J., Young, P., Mason, J., Harrison, J. (1999) β Blockade after myocardial infarction: systematic review and meta regression analysis. BMJ 318: 1730-1737.
- Giovannone, B., Scaldaferri, M.L., Federici, M., Porzio, O., Lauro, D., et al (2000) Insulin receptor substrate (IRS) transduction system: distinct and overlapping signalling potential. Diabetes Metab. Res. Rev. 16: 434-441.
- Glatz, J.F., Bonen, A., Ouwens, D.M., Luiken, J.J. (2006) Regulation of plasma membrane transport of substrates in the healthy and diseased heart. Cardiovasc. Drugs Ther. 20: 471-476.
- Goedecke, J.H., Jennings, C.L., Lambert, E.V. (2006) Obesity in South Africa. Chronic Diseases of Lifestyle in South Africa since 1995-2002. Medical Research Council 7: 65-79.
- Golding, S.E., Rosenberg, E., Valerie, N., Hussaini, I., Frigerio, M., et al (2009) Improved ATM kinase inhibitor KU 60019 radiosensitizes glioma cells, compromises insulin, AKT and ERK prosurvival signaling, and inhibits migration and invasion. Mol. Cancer Ther. 8(10): 2894-2902.
- Gorr, M.W., Stevens, S.C., Wold, L.E. (2012) Ataxia telangiectasia mutated kinase in the heart: currency for myocyte apoptosis. Pubmed Exp. Physiol. 97(4): 476.
- Guo, Z., Kozlov, S., Lavin, M.F., Person, M.D., Paull, T.T. (2010) ATM activation by oxidative stress. Science 330: 517-21.
- Halaby, M.J., et al (2008) ATM protein kinase mediates full activation of Akt and regulates glucose transporter 4 translocation by insulin in muscle cells. Cell Signal 20: 1555-1563.
- Halaby, M.J., Kastein, B.K., Yang, D.Q. (2013) Chloroquine stimulates glucose uptake and glycogen synthase in muscle cells through activation of Akt. Biochemical and Biophysical Research Communications 435: 708-713.
- Han, S., Liang, C.P., DeVries-Seimon, T., Ranalletta, M., Welch, C.L., et al (2006) Macrophage insulin receptor defi-ciency increases ER stress-induced apoptosis and necrotic core formation in advanced atherosclerotic lesions. Cell Metab. 3: 257-266.
- Hirani (2013) Hirani Medical Welness Center - www.drhirani.com/diabetes/difference-visceral-fat-subcutaneous-fat/, November 2015.

- Holt, K.H., Olson, A.L., Moye-Rowley, W.S., Pessin, J.E (1994) Phosphatidylinositol 3-kinase activation is mediated by high-affinity interactions between distinct domains within the p110 and p85 subunits. Mol. Cell. Biol. 14(1): 42-49.
- Huisamen B., Donthi, R.V., Lochner, A. (2001) Insulin in combination with vanadate stimulates glucose transport in isolated cardiomyocytes from obese Zucker rats. Cardiovascular Drugs Therapy 15:445-452.
- Huisamen, B., Genade, S., Lochner, A. (2008) Signalling pathways activated by glucagon-like peptide-1 (7-36) amide in the rat heart and their role in protection against ischaemia. Cardiovascular Journal of Africa 19 (2): 77-83.
- Inoue, G., Cheatham, B., Emkey, R., Kahn, C.R. (1998) Dynamics of insulin signalling in 3T3–L1 adipocytes. Differential compartmentalization and trafficking of insulin receptor substrate (IRS)-1 and IRS-2. J. Biol. Chem. 273: 11548-11555.
- International Diabetes Federation (2014) – www.idf.org, May 2015.
- Kim, F., Pham, M., Luttrell, I., Bannerman, D.D., Tupper, J., et al (2007) Toll-like receptor-4 mediates vascular inflammation and insulin resistance in diet-induced obesity. Circ. Res. 100: 1589-1596.
- Kim, S.T., Lim, D.S., Canman, C.E., Kastan, M.B. (1999) Substrate specificities and identification of putative substrates of ATM kinase family members. J. Biol. Chem. 274: 37538-37543.
- Kiriazis, H., Kranias, E.G. (2000) Genetically engineered models with alterations in cardiac membrane calcium-handling proteins. Annu. Rev. Physiol. 62: 321-351.
- Kivimäki, M., Nyberg, S.T., Batty, G.D., Fransson, E.I., Heikkilä, K., et al (2012) "Job strain as a risk factor for coronary heart disease: a collaborative meta-analysis of individual participant data". Lancet 380(9852): 1491-1497.
- Klip, A., Sun, Y., Chiu, T.T., Foley, K.P. (2014) Signal transduction meets vesicle traffic: the software and hardware of GLUT4 translocation. American Journal of Physiology 306(10): C879-C886.
- Klippel, A., Escobedo, J.A., Hirano, M., Williams, L.T. (1994) The interaction of small domains between the subunits of phosphatidylinositol 3-kinase determines enzyme activity. Mol. Cell Biol. 14(4): 2675-2685.
- Koves, T.R., Ussher, J.R., Noland, R.C., Slentz, D., Mosedale, M., et al (2008) Mitochondrial overload and incomplete fatty acid oxidation contribute to skeletal muscle insulin resistance. Cell Metabolism 1: 45-56.
- Kozlov, S.V., Graham, M.E., Jakob, B., Tobias, F., Kijas, A.W., et al (2011) Autophosphorylation and ATM Activation. The Journal of Biological Chemistry 286: 9107-9119.

- Krajewski, W.A. (2005) Alterations in the internucleosomal DNA helical twist in chromatin of human erythroleukemia cells in vivo influences the chromatin higher-order folding. FEBS Letters 361: 149-152.
- Kruit, J.K. (2008) ATM, an unexpected new target in metabolic syndrome. Clinical Genetics 73: 227–228.
- Kubota, T., Kubota, N., Kumagai, H., et al (2011) Impaired insulin signaling in endothelial cells reduces insulin-induced glucose uptake by skeletal muscle. Cell Metab. 13: 294-307.
- Kulkarni, R.N., Winnay, J.N., Daniel, M., Brüning, J.C., Flier, S.N., et al (1999) Altered function of insulin receptor substrate-1-deficient mouse islets and cultured b-cell lines. J. Clin. Invest. 104: R69-R75.
- Laemmli (1970) Cleavage of structural proteins during the assembly of the head of bacteriophage T4. Nature 227: 680-685
- Laustsen, P.G., Russell, S.J., Cui, L., Entingh-Pearsall, A., Holzenberger, M., et al (2007) Essential role of insulin and insulin-like growth factor 1 receptor signaling in cardiac development and function. Mol. Cell Biol. 27: 1649-1664.
- Lavan, B.E., Fantin, V.R., Chang, E.T., Lane, W.S., Keller, S.R., et al (1997) A novel 160-kDa phosphotyrosine protein in insulin-treated embryonic kidney cells is a new member of the insulin receptor substrate family. J. Biol. Chem. 272: 21403-21407.
- Lavan, B.E., Lane, W.S., Lienhard, G.E. (1997) The 60-kDa phosphotyrosine protein in insulin-treated adipocytes is a new member of the insulin receptor substrate family. J. Biol. Chem. 272: 11439-11443.
- Lazar, D.F., Saltiel A.R. (2006) Lipid phosphatases as drug discovery targets for type 2 diabetes. Nat. Rev. Drug Discov. 5: 333-342.
- Lefebvre, V., Mechin, M.C., Louckx, M.P., Rider, M.H., Hue, L. (1996) Signalling pathway involved in the activation of heart 6-phosphofructo-2-kinase by insulin. J. Biol. Chem. 271: 22289-22292.
- Li, J., Han, Y.R., Plummer, M.R., et al (2009) Cytoplasmic ATM in neurons modulates synaptic function. Curr. Biol. 19: 2091-2096.
- Lim, D.S., et al (1998) ATM binds to beta-adaptin in cytoplasmic vesicles. Proc. Natl. Acad. Sci. U.S.A. 95: 10146-10151.
- Livestrong (2013, 2015) - www.livestrong.com, May 2015.
- Lowry, O.H., Rosebrough, N.J., Farr, A.L., Randall, R.J (1951) Protein measurement with the Folin phenol reagent. J. Biol. Chem. 193: 265-275.
- Luiken, J.J., Koonen, D.P., Willems, J., Zorzano, A., Becker, C., et al (2002) Insulin stimulates long-chain fatty acid utilization by rat cardiac cardiomyocytes through cellular redistribution of FAT/CD36. Diabetes 51: 3113-3119.

- Matsuoka, S., Ballif, B.A., Smogorzewska, A., McDonald, E.R., Hurov, K.E., et al (2007) ATM and ATR substrate analysis reveals extensive protein networks responsive to DNA damage. Science 316: 1160-1166.
- Mayo Clinic Health - www.mayoclinic.org, May 2015.
- Mazumder, P.K., O'Neill, B.T., Roberts, M.W., Buchanan, J., Yun, U.J., et al (2004) Impaired cardiac efficiency and increased fatty acid oxidation in insulin-resistant ob/ob mouse hearts. Diabetes 53: 2366-2374.
- McDonagh, T.A. (2011) Oxford textbook of heart failure. Oxford: Oxford University Press: 3 ISBN 9780199577729.
- Mercer, J.R., Cheng, K.K., Figg, N., Gorenne, I., Mahmoudi, M., et al (2010) DNA damage links mitochondrial dysfunction to atherosclerosis and the metabolic syndrome. Circ. Res. 107: 1021-1031.
- Middelbeek, R.J.W., Chambers, M.A., Tantiwong, P., Treebak, J.T., An, D., et al (2013) Insulin stimulation regulates AS160 and TBC1D1 phosphorylation sites in human skeletal muscle. Nutrition & Diabetes 3: 74.
- Moore, K.J., Tabas, I. (2011) Macrophages in the pathogenesis of atherosclerosis. Cell. 145: 341-355.
- Morrow, J. (2003) Is a oxidative stress a connection between obesity and atherosclerosis. Arterioscler. Tromb. Vasc. Biol. 23: 368–370.
- Mouton, V., Vertommen, D., Bertrand, L., Hue, L., Rider, M.H. (2007) Evaluation of the role of protein kinase Czeta in insulin-induced heart 6-phosphofructo-2-kinase activation. Cell Signal 19: 52-61.
- Muir, A.F *(*1967*)* The effects of divalent cations on the ultrastructure of the perfused rat heart*.* J. Anat. 101*:* 239-261*.*
- Nadler, A.T., Stoehr, J.P., Rabaglia, M.E., Schueler, K.L., Birnbaum, M.J., et al (2001) Normal Akt/PKB with reduced PI3K activation in insulin-resistant mice. AJP-Endocrinol. Metab. 281: 1249-1254.
- Nakae, J., Kitamura, T., Silver, D.L., Accili, D. (2001) "The forkhead transcription factor Foxo1 (Fkhr) confers insulin sensitivity onto glucose-6-phosphatase expression"*.* J. Clin. Invest. 108(9): 1359-1367.
- Nathan, D.M., Buse, J.B., Davidson, M.B., et al (2009) Medical management of hyperglycaemia in type 2 diabetes: a consensus algorithm for the initiation and adjustment of therapy. A consensus statement from the American Diabetes Association and the European Association for the Study of Diabetes. Diabetologia 52: 17-30.
- National Ataxia Foundation - www.ataxia.org, November 2014.
- National Clinical Guideline Centre (2010) - www.ncgc.ac.uk, May 2015.

- National Institute of Diabetes and Digestive and Kidney Diseases - http://www.niddk.nih.gov, January 2016.
- Nature (2015) - www.nature.com, May 2015.
- Norman, B.H., Shih, C., Toth, J.E., Ray, J.E., Dodge, J.A., et al (1996) Studies on the Mechanism of Phosphatidylinositol 3-Kinase Inhibition by Wortmannin and Related Analogs. Journal of Medicinal Chemistry 39(5): 1106-1111.
- Ogihara, T., Shin, B.C., Anai, M., Katagiri, H., Inukai, K., et al (1997) Insulin receptor substrate (IRS)-2 is dephosphorylated more rapidly than IRS-1 via its association with phosphatidylinositol 3-kinase in skeletal muscle cells. J. Biol. Chem. 272: 12868-12873.
- Ojuka, E.O., Nolte, L.A., Holloszy, J.O. (2000) Increased expression of GLUT-4 and hexokinase in rat epitrochlearis muscles exposed to AICAR in vitro. J. Appl. Physiol. 88: 1072-1075.
- Oka, A., Takashima, S. (1998) Expression of the ataxia-telangiectasia gene (ATM) product in human cerebellar neurons during development. Neurosci. Lett. 252: 195-198.
- Owen, M.R., Doran, E., Halestrap, A.P. (2000) Evidence that metformin exerts its anti-diabetic effects through inhibition of complex 1 of the mitochondrial respiratory chain. Biochem. J348: 607-614.
- Paulus, W.J., Tschöpe, C., Sanderson, J.E., et al (2007) How to diagnose diastolic heart failure: a consensus statement on the diagnosis of heart failure with normal left ventricular ejection fraction by the Heart Failure and Echocardiography Associations of the European Society of Cardiology. Eur. Heart J28: 2539-2550.
- Pellegrini, M., Celeste, A., Didilippantonio, S., et al (2006) Autophosphorylation at serine 1987 is dispensable for murine ATM activation in vivo. Nature 443: 222-225.
- Peretz, S., et al (2001) ATM-dependent expression of the insulin-like growth factor-I receptor in a pathway regulating radiation response. Proc. Natl. Acad. Sci. U.S.A. 98: 1676-1681.
- Pessin, J.E., Saltiel, A.R. (2000) Signaling pathways in insulin action: molecular targets of insulin resistance. J. Clin. Invest. 106(2): 165-169
- Pharmacelsus (2003-2015) - http://www.pharmacelsus.de/ic50/, May 2015.
- Pickavance, L.C., Tadayyon, M., Widdowson, P.S., Buckingham, R.E., Wilding, J.P.H. (1999) Therapeutic index for rosiglitazone in dietary obese rats: separation of efficacy and haemodilution. Brit. J. Pharmacol.128:1570-1576.
- Picture - www.medchemexpress.com, May 2015.
- Piper, H.M. (2000) The calcium paradox revisited: An artefact of great heuristic value. Oxford University Press, European Society of cardiology.

- Pozuelo, R.M., Peggie M., Wong, B.H., Morrice, N., MacKintosh, C. (2003) 14-3-3s regulate fructose-2,6-bisphosphate levels by binding to PKB-phosphorylated cardiac fructose-2,6-bisphosphate kinase/phosphatase. EMBO J22: 3514-3523.
- Qu, B.H., Karas, M., Koval, A., Leroith, D. (1999) Insulin receptor substrate 4 enhances insulin-like growth factor-I-induced cell proliferation. J. Biol. Chem. 274: 31179-31184.
- Rains, J.L., Jain, S.K. (2011) Oxidative stress, insulin signalling, and diabetes. Free Radical Biology and Medicine 50 (5): 567-575.
- Rask-Madsen, C., Domínguez, H., Ihlemann, N., Hermann, T., Køber, L., et al (2003) Tumor necrosis factor-alpha inhibits insulin's stimulating effect on glucose uptake and endothelium-dependent vasodilation in humans. Circulation 108: 1815-1821.
- Rask-Madsen, C., Kahn, C.R. (2012) Tissue–Specific Insulin Signaling, Metabolic Syndrome, and Cardiovascular Disease. Arterioscler. Thromb. Vasc. Biol. 32(9): 2052-2059.
- Rask-Madsen, C., Li, Q., Freund, B., et al (2010) Loss of insulin signaling in vascular endothelial cells accelerates atherosclerosis in apolipoprotein E null mice. Cell Metab. 11: 379–389.
- Rider, M.H., Hue, L. (1984) Activation of rat heart phosphofructokinase-2 by insulin in vivo. FEBS Lett. 176: 484-488.
- Robertson, S. (2014) What is Fibrosis? - News Medical
- Rondinone, C.M., Wang, L.M., Lonnroth, P., Wesslau, C., Pierce, J.H., et al (1997) Insulin receptor substrate (IRS) 1 is reduced and IRS-2 is the main docking protein for phosphatidylinositol 3-kinase in adipocytes from subjects with non-insulin-dependent diabetes mellitus. Proc. Natl. Acad. Sci. U.S.A 94: 4171-4175.
- Rubler, S., Dlugash, J., Yuceoglu, Y.Z., Kumral, T., Branwood, A.W., et al (1972) New type of cardiomyopathy associated with diabetic glomerulosclerosis. Am. J. Cardiol. 30: 595-602.
- Ruiz-Alcaraz, A.J., Liu, H-K., Cuthbertson, D.J., McManus, E.J., Akhtar, S., et al (2005) A novel regulation of IRS1 (insulin receptor substrate-1) expression following short term insulin administration. Biochem. J. 392: 345–352.
- Salie, R., Huisamen, B., Lochner, A. (2014) High carbohydrate and high fat diets protect the heart against ischaemia/reperfusion injury. Cardiovasc. Diabetol. 13: 109.
- Sarkaria, J.N., Tibbetts, R.S., Busby, E.C., Kennedy, A.P., Hill, D.E., et al (1998) Inhibition of phosphoinositide 3-kinase related kinases by the radiosensitizing agent wortmannin. Cancer Res. 58(19): 4375-4382.
- Sawka-Verhelle, D., Tartare-Deckert, S., White, M.F., van Obberghen, E. (1996) Insulin receptor substrate-2 binds to the insulin receptor through its phosphotyrosine-binding

domain and through a newly identified domain comprising amino acid 591-786. J. Biol. Chem. 271: 5980-5983.

- Schalch, D.S., et al (1970) An unusual form of diabetes mellitus in ataxia telangiectasia. N. Engl. J. Med. 282: 1396-1402.
- Scheid, M.P., Woodgett, J.R. (2003) Unravelling the activation mechanisms of protein kinase B/Akt. Signal Transduction 546(1): 108-112.
- Schneider, J.G., et al (2006) ATM-dependent suppression of stress signalling reduces vascular disease in metabolic syndrome. Cell Metab. 4: 377-389.
- Sciacchitano, S., Taylor, S.I. (1997) Cloning, tissue expression, and chromosomal localization of the mouse IRS-3 gene. Endocrinology 138: 4931-4940.
- Sesti, G., Federici, M., Hribal, M.L., Lauro, D., Sbraccia, P., et al (2001) Defects of the insulin receptor substrate (IRS) system in human metabolic disorders. FASEB journal 18: 2099-2111.
- Shackelford, D.B., Shaw, R.J. (2009) The LKB1-AMPK pathway: metabolism and growth control in tumour suppression. Nature Reviews Cancer 9: 563-575.
- Shiloh, Y., Kastan, M.B. (2001) ATM: genome stability, neuronal development, and cancer cross paths. Adv. Cancer Res. 83: 209-254.
- Shuppin, G.T., Pons, S., Hugl, S., Aiello, L.P., King, G.L., et al (1998) A specific increased expression of Insulin Receptor Substrate 2 in pancreatic b-cell lines is involved in mediating serum-stimulated-cell growth. Diabetes 47: 1074-1085.
- Singh, V.N. (2014) eMedicine Health - www. emedicine helath.com, April 2015.
- Smith-Hall, J., Pons, S., Patti, M.E., Burks, D.J., Yenush, L., et al (1997) The 60 kDa insulin receptor substrate functions like an IRS protein (pp60IRS3) in adipose cells. Biochemistry 36: 8304-8310.
- Sogo, J.M., Ness, P.J., Widnmer, R.M., Parish, R.W., Koller, T.H. (1984) Psoralen-crosslinking DNA as a probe for the structure of active nucleolar chromatin. J. Mol. Biol. 178: 897-919.
- Su, Y., Swift, M. (2000) Mortality rates among carriers of ataxia-telangiectasia mutant alleles. Ann. Intern. Med. 133: 770-778.
- Sun, X. J., Wang, L.M., Zhang, Y., Yenush, L., Myers, M.G., et al (1995) Role of IRS-2 in insulin and cytokine signalling. Nature (London) 377: 173-177.
- Sun, X.J., Pons, S., Wang, L.M., Zhang, Y., Yenush, L., et al (1997) The IRS-2 gene on murine chromosome 8 encodes a unique signalling adapter for insulin and cytokine action. Mol. Endocrinol. 11: 251-262.

- Sun, X.J., Rothenberg, P., Kahn, C.R., Backer, J.M., Araki, E., et al (1991) Structure of the insulin receptor substrate IRS-1 defines a unique signal transduction protein. Nature (London) 352: 73-77.
- Swift M., Chase, C. (1983) Cancer and cardiac deaths in obligatory ataxiatelangiectasia heterozygotes. Lancet. 321: 1049-1050.
- The New Health Advisor (2015) - http://www.newhealthadvisor.com/Normal-Insulin-Levels.html, May 2015.
- Trachanas, K., Sideris, S., Aggeli, C., Poulidakis, E., Gatzoulis, K. (2014) Diabetic Cardiomyopathy: From Pathophysiology to Treatment. Hellenic J. Cardiol. 55: 411-421.
- Tsuchiya, K., Tanaka, J., Shuiqing, Y., Welch, C.L., DePinho, R.A., et al (2012) FoxOs integrate pleiotropic actions of insulin in vascular endothelium to protect mice from atherosclerosis. Cell Metab. 15: 372-381.
- Tsuruzoe, K., Emkey, R., Kriauciunas, K.M., Ueki, K., Kahn, C.R. (2001) Insulin receptor substrate 3 (IRS-3) and IRS-4 impair IRS-1- and IRS-2-mediated signalling. Mol. Cell. Biol. 21: 26-38.
- Type 2 Diabetes - www.diabetes.co.uk, May 2015.
- Uchida, T., Myers, M.G., White, M.F. (2000) IRS-4 mediates protein kinase B signalling during insulin stimulation without promoting antiapoptosis. Mol. Cell. Biol. 20: 126-138.
- Valentin-Vega, Y.A., MacLean, K.H., Tait-Mulder, J., Steeves, M., Dorsey, F.C., et al (2012) Mitochondrial dysfunction in ataxia-telangiectasia. Journal of the American Society of Hematology 119(6): 1490-1499.
- van der Heide, L.P., Ramakers, G.M., Smidt, M.P. (2006) Insulin signalling in the central nervous system: learning to survive. Prog. Neurobiol. 79: 205-221.
- Vanhaesebroeck, B., et al (2001) Synthesis and function of 3-phosphorylated inositol lipids. Annu. Rev. Biochem. 70: 535-602.
- Vazquez-Martin A., Oliveras-Ferraros, C., Cufí, S., Martin-Castillo, B., Menendez, J.A. (2011) Telangiectasia Mutated (ATM)/Chk2-regulated DNA damage-like response. Cell Cycle 10(9): 1499-1501.
- Viniegra, J.G., et al (2005) Full activation of PKB/Akt in response to insulin or ionizing radiation is mediated through ATM. J. Biol. Chem. 280: 4029-4036.
- Virtue S., Vidal-Puig A. (2010) Adipose tissue expandability, lipotoxicity and the Metabolic Syndrome - An allostatic perspective. Biochim. Biophys. Acta.1801(3): 338-349.
- Wada, A., Yokoo, H., Yanagita, T., Kobayashi, H. (2005) New twist on neuronal insulin receptor signalling in health, disease, and therapeutics. J. Pharmacol. Sci. 99: 128-143.
- Wade, A. (2009) GSK-3 inhibitors and insulin receptor signalling in health, disease and therapeutics. Front Biosci. 14: 1558-1570.

- White, M.F. (1997) The insulin signalling system and the IRS proteins. Diabetologia 40: S2-S17.
- Wilcox, G. (2005) Insulin and Insulin Resistance. Clin. Biochem. Rev. 26: 19-39.
- World Health Organization - www. who.int/en/, January 2015.
- Wymann, M.P., Bulgarelli-Leva, G., Zvelebil, M.J., Pirola, L., Vanhaesebroeck, B., et al (1996) Wortmannin inactivates phosphoinositide 3-kinase by covalent modification of Lys-802, a residue involved in the phosphate transfer reaction. Mol. Cell Biol. 16(4):1722-33.
- Xu, P., Jacobs, A.R., Taylor, S.I. (1999) Interaction of insulin receptor substrate-3 with insulin receptor, insulin receptor-related receptor, insulin-like growth factor-1 receptor, and downstream signalling proteins. J. Biol. Chem. 274: 15262-15270.
- Yanagita, T., Nemoto, T., Satoh, S., Yoshikawa, N., Maruta, T., et al (2013) Neuronal Insulin Receptor Signaling: A Potential Target for the Treatment of Cognitive and Mood Disorders. InTech. 11: 264-287.
- Yang, D.Q., Halaby, M.J., Li, Y., Hibma, J.C., Burn, P. (2011) Cytoplasmic ATM protein kinase: an emerging therapeutic target for diabetes, cancer and neuronal degeneration. Elsevier 16: 7-8.
- Yang, D.Q., Kastan, M.B. (2000) Participation of ATM in insulin signalling through phosphorylation of eIF-4E-binding protein 1. Nat. Cell Biol. 2: 893–898.
- Yano, M., Ikeda, Y., Matsuzaki, M. (2005) Altered intracellular Ca^{2+} handling in heart failure. J. Clin. Invest. 115(3): 556-564.
- Yates, J.C., Dhalla, N.S. (1975) Structural and functional changes associated with failure and recovery of hearts of the perfusion with Ca^{2+}-free medium. J. Mol. Cell Cardiol. 7: 91-103.
- Ying, Z., Changfei, M., Jianzhong, W., Shuchun, L., Rong, M., et al (2014) Improved ataxia telangiectasia mutated kinase inhibitor KU60019 provides a promising treatment strategy for non-invasive breast cancer. Oncol. Lett. 8(5): 2043-2048.
- Zaha, V.G., Young, L.H. (2012) AMP-Activated Protein Kinase Regulation and Biological Actions in the Heart. American Heart Association. Circ. Res. 111: 800-814.
- Zhang, N., et al (1997) Isolation of full-length ATM cDNA and correction of the ataxia-telangiectasia cellular phenotype. Proc. Natl. Acad. Sci. U.S.A. 94: 8021-8026.
- Zhou, L., Chen, H., Xu, P., Cong, L.N., Sciacchitano, S., et al (1999) Action of insulin receptor substrate-3 (IRS-3) and IRS-4 to stimulate translocation of GLUT4 in rat adipose cells. Mol. Endocrinol. 13: 505-514.
- Zimmerman, A.N., Daems, W., Hülsmann, W.C., et al *(*1967*)* Morphological changes of heart muscle caused by successive perfusion with calcium-free and calcium-containing solutions (calcium paradox) Cardiovasc. Res. 1: 201-209.

- Zvelebil, M.J., MacDougall, L., Leevers, S., Volinia S., Vanhaesebroeck B., et al (1996) Structural and functional diversity of phosphoinositide 3-kinases. Philos. Trans. R. Soc. Lond-Biol. Sci. 351: 217-223.